AUG 7 1957

OF MICH

AUG 6 1957

PHYSICS
LIBRARY

Journal of Research

of the National Bureau of Standards

AUGUST 1957

VOLUME 59 NUMBER 2

U. S. DEPARTMENT OF COMMERCE
Sinclair Weeks, Secretary
NATIONAL BUREAU OF STANDARDS
A. V. Astin, Director

AUGUST • 1957
VOLUME • 59
NUMBER • 2

JOURNAL OF RESEARCH

of the

NATIONAL BUREAU OF STANDARDS

The National Bureau of Standards

Functions and Activities

The functions of the National Bureau of Standards are set forth in the Act of Congress, March 3, 1901, as amended by Congress in Public Law 619, 1950. These include the development and maintenance of the national standards of measurement and the provision of means and methods for making measurements consistent with these standards; the determination of physical constants and properties of materials; the development of methods and instruments for testing materials, devices, and structures; advisory services to Government Agencies on scientific and technical problems; invention and development of devices to serve special needs of the Government; and the development of standard practices, codes, and specifications. The work includes basic and applied research, development, engineering, instrumentation, testing, evaluation, calibration services, and various consultation and information services. A major portion of the Bureau's work is performed for other Government Agencies, particularly the Department of Defense and the Atomic Energy Commission. The scope of activities is suggested by the listing of divisions and sections on the inside of the back cover.

Publications

The results of the Bureau's work take the form of either actual equipment and devices or published papers. These papers appear either in the Bureau's own series of publications or in the journals of professional and scientific societies. The Bureau itself publishes three monthly periodicals, available from the Government Printing Office: The Journal of Research, which presents complete papers reporting technical investigations; the Technical News Bulletin, which presents summary and preliminary reports on work in progress; and Basic Radio Propagation Predictions, which provides data for determining the best frequencies to use for radio communications throughout the world. There are also five series of nonperiodical publications: The Applied Mathematics Series, Circulars, Handbooks, Building Materials and Structures Reports, and Miscellaneous Publications.

Information on the Bureau's publications can be found in NBS Circular 460, Publications of the National Bureau of Standards ($1.25) and its Supplement ($0.75), available from the Superintendent of Documents, Government Printing Office, Washington 25, D. C.

Order all publications from the Superintendent of Documents
U. S. Government Printing Office, Washington 25, D. C.

Use of funds for printing this publication approved by the Director of the Bureau of the Budget (May 14, 1956)

Journal of Research of the National Bureau of Standards Vol. 59, No. 2, August 1957 Research Paper 2773

A Problem in Self-Heating of a Spherical Body

S. M. Genensky*

An analytic steady-state solution is developed for a spherical body in which heat is generated according to a first-order unimolecular-reaction law, and lost at the surface in accordance with Newton's law of cooling. The temperature within the sphere depends chiefly on the radial distance from the center, but also on the ambient temperature, the surface heat-loss coefficient, and the material properties, which are assumed constant.

1. Introduction

The analysis described was pursued in connection with an investigation into the self-heating of fibrous materials carried on at the National Bureau of Standards.[1]

Comparison of the results of this analysis with the experimental results indicated that the assumption of a single first-order unimolecular reaction was an oversimplification for the material investigated experimentally. However, the analysis serves to indicate the relative importance of the various parameters entering into the problem, and may be helpful in indicating the kind of data that would be of greatest use in further investigations in which the assumptions may be applicable.

A homogeneous sphere of radius B is generating heat, under steady-state conditions, in accordance with a first-order unimolecular-reaction law, $Ae^{-(E/RT)}$, and losing heat from its surface to an atmosphere at constant temperature, T_a, according to Newton's law of cooling. The temperature of the sphere, $T(r)$, is independent of time and depends upon the radial distance, r, from the center of the sphere. Within the sphere, transfer of heat by means other than conduction is considered negligible. The thermal conductivity, k; gas constant, R; rate of reaction-frequency product, A; and activation energy, E, of the material of the sphere are assumed to be known constants, as are the temperature, T_0, and gradient $dT/dr=0$, at the center of the sphere. The problem is to find the surface temperature of the sphere, T_B, at $r=B$, and the heat-transfer coefficient, h, between the surface of the sphere and a surrounding atmosphere.

2. Analysis

Mathematically the problem becomes

$$k\left[\frac{d^2T}{dr^2}+\frac{2}{r}\frac{dT}{dr}\right]+Ae^{-\frac{E}{RT}}=0 \qquad (0<r<B), \tag{1}$$

$$T=T_0 \quad \text{at} \quad r=0, \tag{2}$$

$$\frac{dT}{dr}=0 \quad \text{at} \quad r=0, \tag{3}$$

$$k\left(\frac{dT}{dr}\right)_{r=B}=-h[T_B-T_a]. \tag{4}$$

Let

$$\eta=\frac{r}{B}, \quad V(\eta)=\frac{R}{E}T(\eta), \quad \text{and} \quad C=\frac{ARB^2}{Ek}.$$

Then eq (1) to (4) become

$$\frac{d^2V}{d\eta^2}+\frac{2}{\eta}\frac{dV}{d\eta}+Ce^{-\frac{1}{V}}=0 \qquad (0<\eta<1), \tag{5}$$

$$V=V_0=\frac{RT_0}{E} \quad \text{at} \quad \eta=0, \tag{6}$$

$$\frac{dV}{d\eta}=0 \quad \text{at} \quad \eta=0, \tag{7}$$

$$k\left(\frac{dV}{d\eta}\right)_{\eta=1}=-\frac{BhR}{E}[T_B-T_a]. \tag{8}$$

It is further assumed that (a) the temperature gradient within the sphere exists and is continuous throughout the interval $0\leq\eta\leq1$, and (b) that the absolute value of the difference between $T(\eta)$, $0\leq\eta\leq1$, and T_0 is small in comparison to T_0. Under these restrictions, a technique presented by Chambre [2] proves useful to observe that

$$\frac{1}{V}=\frac{1}{V_0-\Delta V}=\frac{1}{V_0}\left[1/\left(1-\frac{\Delta V}{V_0}\right)\right]=\frac{1}{V_0}\sum_{i=0}^{\infty}\left(\frac{\Delta V}{V_0}\right)^i, \tag{9}$$

where $\Delta V=V_0-V$. Now, because $|\Delta V/V_0|<1$, the series converges, and for a sufficiently large positive integer, N, $(1/V_0)\sum_{i=0}^{N}(\Delta V/V_0)^i$ is a very good approximation to $1/V$.

Therefore, (5) may be written approximately as

$$\frac{d^2V}{d\eta^2}+\frac{2}{\eta}\frac{dV}{d\eta}+Ce^{-\frac{1}{V_0}\sum_{i=0}^{N}\left(\frac{\Delta V}{V_0}\right)^i}=0 \qquad (0<\eta<1). \tag{10}$$

*Present address: Brown University, Providence, R. I.

[1] N. D. Mitchell, New light on self-ignition, Natl. Fire Protect. Assoc. Quart. (October 1951).

[2] P. L. Chambré, On the solution of the Poisson-Boltzman equation with application to the theory of thermal explosions, J. Chem. Phys. **20**, 1795 (1952).

Now

$$\sum_{i=0}^{N}\left(\frac{\Delta V}{V_0}\right)^i=\sum_{i=0}^{N}\left(1-\frac{V}{V_0}\right)^i=(N+1)-\boldsymbol{B}_1V+\boldsymbol{B}_2V^2 -\ldots+(-1)^N\boldsymbol{B}_NV^N,$$

where

$$\boldsymbol{B}_k=\sum_{n=0}^{N}\frac{n!}{(n-k)!k!V_0^k},\qquad k=1,2,\ldots,N,$$

and in the special case $V=V_0$

$$(N+1)-\boldsymbol{B}_1V+\boldsymbol{B}_2V^2-\ldots+(-1)^N\boldsymbol{B}_NV^N=1 \qquad N=0,1,2,\ldots.$$

Therefore, (10) may be written

$$\frac{d^2V}{d\eta^2}+\frac{2}{\eta}\frac{dV}{d\eta}+Ce^{-\frac{N+1}{V_0}}e^{\frac{1}{V_0}[\boldsymbol{B}_1V-\boldsymbol{B}_2V^2+\ldots-(-1)^N\boldsymbol{B}_NV^N]}=0. \tag{11}$$

Because (11) is analytic and regular except at $\eta=0$, and further as $dV/d\eta=0$ at $\eta=0$, the solution of (11) may be written in the form

$$V=V(\eta)=\sum_{i=0}^{\infty}a_i\eta^i \qquad (0\leq\eta\leq1). \tag{12}$$

Recalling (6), eq (12) at $\eta=0$ yields

$$V_0=V(0)=\frac{T_0R}{E}=a_0, \tag{13}$$

and further differentiating (12) once and considering (7), it is found that

$$a_1=0. \tag{14}$$

Differentiating (12) twice, substituting these first two derivatives into eq (11) and rearranging terms:

$$\sum_{i=2}^{\infty}(i^2+i)a_i\eta^{i-2}=-De^{\frac{1}{V_0}[\boldsymbol{B}_1V-\boldsymbol{B}_2V^2+\ldots-(-1)^N\boldsymbol{B}_NV^N]}, \tag{15}$$

where $D=Ce^{-\frac{N+1}{V_0}}$ and the a_i are given by

$$a_i=-\frac{1}{(i^2+i)}\frac{1}{(i-2)!}\frac{d^{i-2}\left[De^{\frac{1}{V_0}(\boldsymbol{B}_1V-\boldsymbol{B}_2V^2+\ldots-(-1)^N\boldsymbol{B}_NV^N)}\right]}{d\eta^{i-2}} \tag{16}$$

for $\eta=0$, and $i=2,3,4,\ldots$.

Using the coefficients obtained from (13), (14), and (16) and substituting them into eq (12), V can be computed for $0\leq\eta\leq1$.

In particular, for $\eta=1$, eq (12) gives the dimensionless surface temperature $V(1)$, and thus recalling that $T(\eta)=(E/R)V(\eta)$, the surface temperature, $T(1)$, which equals T_B, is easily found. Differentiating eq (12) once and evaluating this derivative at $\eta=1$, h can then be found by solving eq (8), for all the other factors involved in this equation are either given or have been computed.

The first six nonzero coefficients have been evaluated and are

$$a_0=V_0$$

$$a_2=-\frac{C}{6}e^{-\frac{1}{V_0}}$$

$$a_4=\frac{C^2}{120V_0^2}e^{-\frac{2}{V_0}}$$

$$a_6=\frac{C^3}{1008V_0^3}\left[\frac{8}{15}\frac{C}{V_0}-\frac{2}{3}\right]e^{-\frac{3}{V_0}}$$

$$a_8=\frac{C^4}{51840V_0^4}\left[\frac{122C^2}{63V_0^2}-\frac{122C}{21V_0}+\frac{10}{3}\right]e^{-\frac{4}{V_0}}$$

$$a_{10}=\frac{C^5}{4435200V_0^5}\left[\frac{5032C^3}{405V_0^3}-\frac{8428C^2}{135V_0^2}+\frac{1486C}{27V_0}-\frac{560}{9}\right]e^{-\frac{5}{V_0}}$$

Observe that a_{2i-1} ($i=1,2,3,\ldots$) are zero. This follows from $a_1=0$ and the spherical symmetry of the problem.

Figure 1 is a plot of $V(1)$, as a function of C and $1/V_0$, where C was allowed to vary over the range $10^{-1}\leq C\leq10^{19}$ and $1/V_0$ took on selected values in the range $5\leq1/V_0\leq100$. The points were obtained by using

$$V(\eta)=\sum_{i=0}^{10}a_i\eta^i \tag{17}$$

over its range of applicability for the values of C and $1/V_0$ within the above limits.

In the foregoing, it has been assumed that the temperature at the center of the sphere T_0 is known, and also that the physical condition indicated by eq (8) is satisfied.

The more common steady-state problem of finding the temperature at the center of a sphere that generates heat according to a first-order unimolecular reaction law and loses heat according to Newton's law of cooling may be solved by using the analysis described above. In this case, E, R, k, A, h, T_a, T_B, and B are assumed known.

If the sphere being considered really satisfies the assumptions of the problem, then its temperature must satisfy eq (1). Because eq (1) is of the second order, only two boundary conditions can be preassigned. Further, because the temperature at the center of the sphere must remain finite, one of these preassigned boundary conditions must be $dT/dr=0$ at $r=0$. This leaves but one free boundary condition. However, at the surface of the sphere both

$$\left(\frac{dT}{dr}\right)_{r=B}=-\frac{h}{k}[T_B-T_a] \tag{18}$$

and

$$T=T_B \quad \text{at} \quad r=B \tag{19}$$

must be satisfied; and because only one of these two

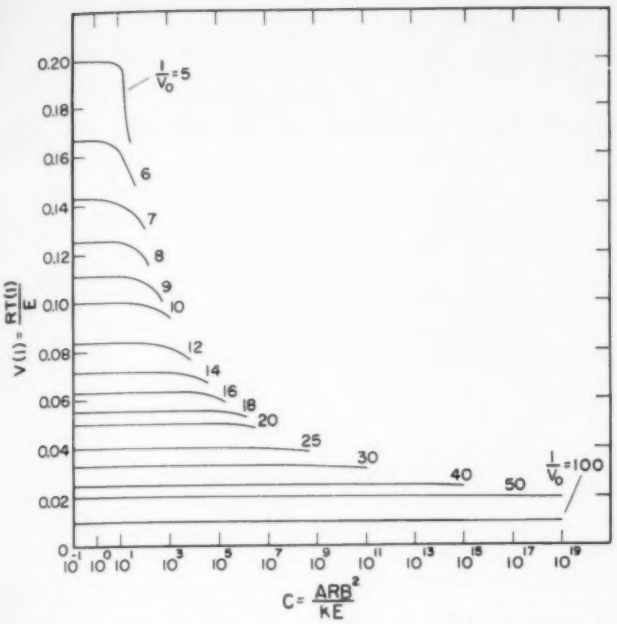

FIGURE 1. *V (1) as a function of C for selected values of* $1/V_0$.

boundary conditions may be formally assigned, it must be assumed that the other is consistent with the problem. Therefore, figure 1, which represents eq (17), may be used to solve this problem. Because R, E, k, A, and B are known, both C and $V(1)$ (recall that $T_B = EV(1)/R$) can be computed. Thus, by using figure 1, $1/V_0$ may be found by interpolation, provided the point $(C, V(1))$ under consideration lies within the region of applicability of eq (17), as indicated above. Because the center temperature of the sphere is T_0, that is EV_0/R, the problem is solved.

Here no use was made of condition (18), and as mentioned earlier, this condition must be satisfied independently, if the assumptions made are fulfilled. Thus the degree of consistency between conditions (18) and (19) serves as an indication of the applicability of the assumptions made in this analysis.

WASHINGTON, March 19, 1954.

Journal of Research of the National Bureau of Standards Vol. 59, No. 2, August 1957 Research Paper 2774

Properties of Arsenic Sulfide Glass[1]

Francis W. Glaze, Douglas H. Blackburn, Jerome S. Osmalov,[2] Donald Hubbard, and Mason H. Black[3]

Samples of arsenic sulfide glass were investigated to determine their chemical and physical properties. Among the properties reported are the hygroscopicity, chemical durability, hydrogen electrode function, expansivity, elastic moduli, modulus of rupture, hardness, transmittance, and indices of refraction.

The main interest in arsenic sulfide glass, for the present, is for its transmittance in the infrared. It is transparent to infrared energy out to approximately 13 microns. Although its physical properties are inferior to those of ordinary silicate glasses, they are superior to those of some of the available materials used in infrared optics.

1. Introduction

Arsenic sulfide (As_2S_3) glass, although reported in 1870 [1],[4] has received consideration only in recent years for its desirable spectral transparency to infrared radiation. It has a usable transmittance of radiant energy out to 12.0 or 12.5 μ, depending on thickness [2,3].

The present investigation was undertaken to determine the chemical and physical properties of this glass and also to obtain pertinent information as to its suitability for use as an element of an optical system when exposed to the atmosphere.

Much of the material contained in this paper has been the subject of a report to the U. S. Air Force [4].

2. Preparation of the Glass

The arsenic sulfide glass for most of the tests was made in the apparatus shown in figure 1.[5] The arsenic and sulfur, in stoichiometric ratio of 2 to 3 plus a 0.25 percent excess of sulfur, were allowed to react in the reaction tube in an atmosphere of nitrogen, and then the arsenic sulfide was distilled at approximately 735° C into the accumulator. A typical time-temperature schedule for a 5,000-g batch of arsenic sulfide is given in table 1. A slug of glass, chilled by means of a stream of nitrogen impinging on the outlet tube, retained the distillate in the accumulator. Nitrogen was used throughout this operation to prevent oxidation. When the distillation was completed, the glass in the accumulator was stirred to homogenize it. Heat was then applied to the outlet tube, the stirrer was stopped, and the first slug of glass was caught in the tube suspended from the bottom of the molding oven. The mold was then quickly moved into place and

[1] This work was supported first by the Department of the Navy, Bureau of Ships, and later by the United States Air Force, Wright Air Development Center, Materials Laboratory.

[2] Present address, Eastman Kodak Co., Rochester, N. Y.

[3] Deceased.

[4] Figures in brackets indicate the literature references at the end of this paper.

[5] A patent has been applied for on this one-step procedure for making arsenic sulfide glass.

TABLE 1. *Arsenic sulfide production run*

(Operation sheet)

Time	Melt		Condenser	Accumulator		Outlet tube	Collecting oven—		Remarks
	Top	Bottom		Top	Bottom		Top	Bottom	
	°C	°C	°C	°C	°C	°C	°C	°C	
8:00	(a)	(a)	(a)	(a)	(a)	(a)	(a)	(a)	Current on.
9:00	495	450	325	330	270	65	.....	.....	
9:30	600	585	345	420	355	100	.....	.....	
10:00	715	695	425	490	425	160	.....	.....	
10:30	735	725	440	540	480	245	145	140	
11:00	735	740	490	570	520	300	225	220	Stirrer on (approximately 240 rpm).
11:30	760	725	420	585	555	320	255	250	Distillation completed.
12:00	.....	.....	.....	565	540	325	255	250	
12:30	.....	.....	.....	560	540	325	260	255	
1:00	.....	.....	.....	560	540	320	265	260	Cut stirring speed to approximately 180 rpm.
1:30	.....	.....	.....	545	525	325	265	260	
2:00	.....	.....	.....	525	505	325	265	255	
2:30	.....	.....	.....	515	490	320	260	255	Cut stirring speed to approximately 120 rpm.
3:00	.....	.....	.....	515	490	320	260	250	
3:30	.....	.....	.....	515	490	325	260	250	
4:00	.....	.....	.....	475	450	320	260	250	Cast.

[a] Room temperature.

the slab cast. After flow practically ceased (about 3 min), a glass plate was placed over the mold and the mold and contents moved to an annealing oven at 185° C. It was held at this temperature for 12 to 16 hr and then slowly cooled to room temperature. For pieces weighing 2.0 to 2.5 kg, the whole annealing operation took 3½ to 3⅔ days. No attempt was made to control the atmosphere in the annealing oven.

Although the apparatus shown in figure 1 permitted the use of either technical-grade or distilled arsenic without appreciably altering the quality of the glass, the large amount of residue left behind by the technical grade attacked the reaction tube, thereby shortening its life.

Some of the experiments were made on samples of glass obtained from a commercial source [6] and others on experimental melts prepared at the Bureau by the one-step process described above.

The large thermal expansivity of the As_2S_3 glass presented a distinct hazard to molding blanks successfully. The blanks, while being formed in Pyrex 7740 or Vycor, often stuck to the walls and bottom of the molds. Upon cooling, the differential expansion between the mold and specimen and the adhesion of the arsenic sulfide glass to the walls of the mold frequently resulted in severe fracture of both mold and specimen. This difficulty was overcome by lining the mold with aluminum foil, which eliminated sticking and allowed complete freedom of adjustment to the large dimensional changes that occur during cooling.

[6] The commercial samples were produced by the American Optical Co., Southbridge, Mass.

The transmittances of arsenic sulfide glasses made at the Bureau by similar procedures and of materials of comparable purity will agree within ±2 percent between 2 and 8 μ, except possibly in the region of the water absorption band at about 2.8 μ.

Nothing is known about the details of preparation of the commercial specimens. The commercial and experimental glasses are appreciably different in appearance and spectral transmittance in the visible and very near infrared as shown by data obtained with a Beckman quartz spectrometer, model DU (fig. 2).

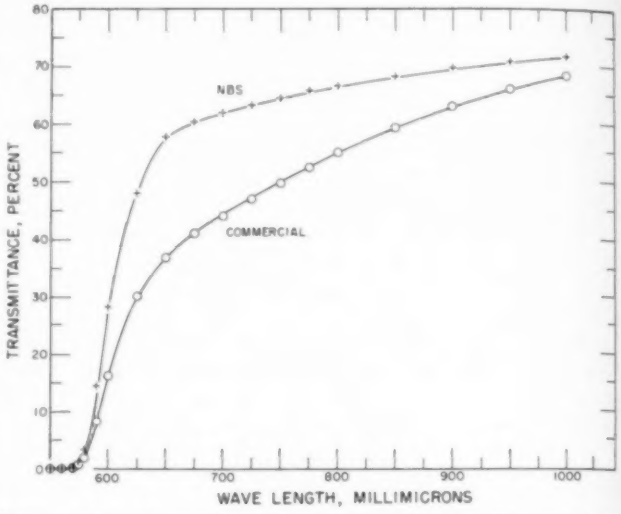

FIGURE 2. *Comparison of the spectral transmittance of two samples of arsenic sulfide glass from 500 to 1,000 mμ.*

Specimens 6 mm thick.

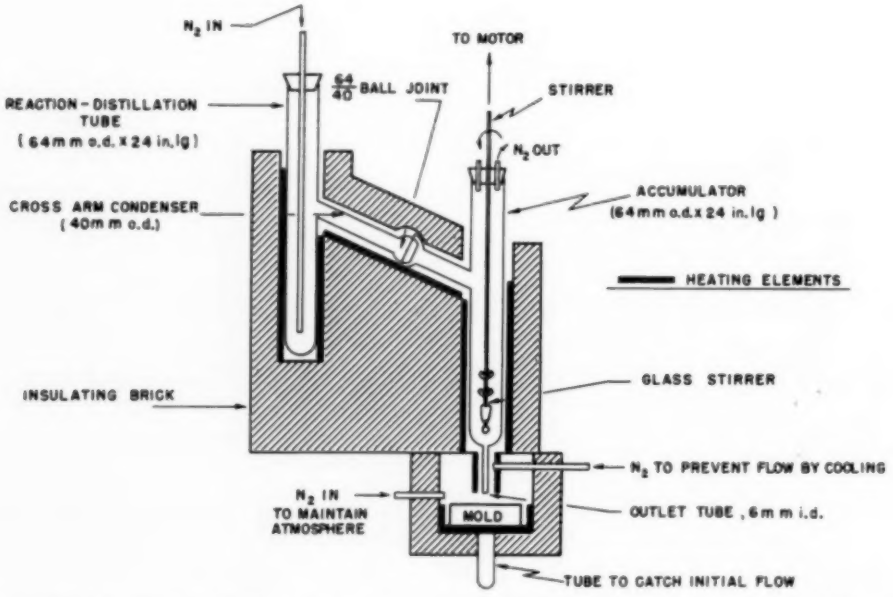

FIGURE 1. *Schematic drawing of the apparatus used in the production of arsenic sulfide glass.*

3. Chemical Properties

3.1. Hygroscopicity

The hygroscopicity and chemical-durability data were obtained by the powder and interferometer procedures described in earlier publications [5, 6]. In crushing and screening the powdered samples (approximately 1.5 g that passed a No. 150 Tyler standard sieve) for hygroscopicity determinations, the "fines" adhered conspicuously to the mortar, sieve, pan, walls of the hood, and the skin and clothing of the operator. Because the material is toxic, suitable precautions should be taken during this operation.

Figure 3, plotted from data given in table 2, shows the hygroscopicity curves (water sorbed versus hours of exposure to 98% relative humidity) for specimens of arsenic sulfide glass from two different sources, compared with those for fused SiO_2, Vycor, Pyrex 7740, a window glass, and Corning 015. These silicate glasses furnish a reference index covering a broad cross section of commercial usage. Although the results obtained on the two samples differ from each other, both are considerably less hygroscopic than Pyrex 7740. One of the samples even compares favorably with fused SiO_2 and Vycor, although this should not be interpreted as an indication of good chemical durability, as shown in figure 4

TABLE 2. *Hygroscopicity, voltage characteristics, and chemical durability of arsenic sulfide glasses compared with similar properties of typical commercial glasses.*

Glasses	Water sorbed		Voltage departure at pH—						Surface alteration, 6 hr, 80°C, at pH—					
	1 hr	2 hr	2	4.1	6.0	8.2	10.2	11.8	2	4.1	6.0	8.2	10.2	11.8
	mg/cm²	*mg/cm²*	*mv*	*mv*	*mv*	*mv*	*mv*	*mv*	*Fringes*	*Fringes*	*Fringes*	*Fringes*	*Fringes*	*Fringes*
Fused SiO_2	6.3	8	[a]	[a]	[a]	[a]	[a]	[a]	[b]ND	ND	ND	ND	[c]DA	½A
Vycor	8.1	10	[a]	[a]	[a]	[a]	[a]	[a]	ND	ND	ND	ND	AD	½+A
As_2S_3(NBS)	6	10	0	105	202	342	447	542	------	------	------	----------	------	------
	----	----	0	95	198	303	438	552	------	------	------	----------	------	------
	----	----	0	120	191	332	421	546	------	------	------	----------	------	------
As_2S_3(commercial)	13	19	----	----	----	----	----	----	[d]½S	½−S	¼−S	3A (variable)	114A	1152A
Pyrex 7740	16	28	0	77	165	288	----	----	ND	ND	ND	DA	¾−A	1¾A
Window	23	53	----	----	----	----	----	----	ND	ND	ND	ND	½0+A	1½−A
Corning 015	61	125	0	0	0	0	0	3	¾0−S	¾0−S	¾0−S	[e]SC	¼+A	2−A

[a] No definite pH response. [b] ND, not detectable. [c] A, attack. [d] S, swelling. [e] SC, surface cut.

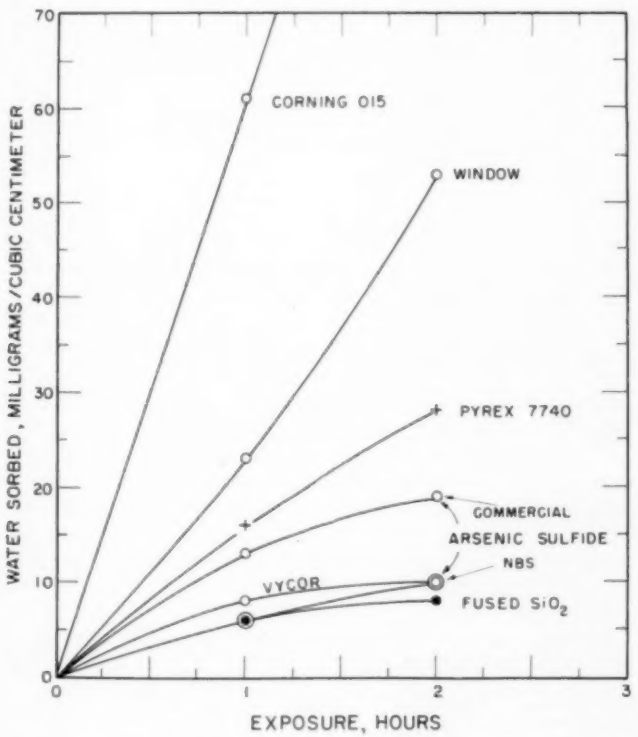

FIGURE 3. *Comparison of the hygroscopicity of two samples of arsenic sulfide glass with similar data for fused silica, Vycor, Pyrex 7740, window, and Corning 015 glasses.*

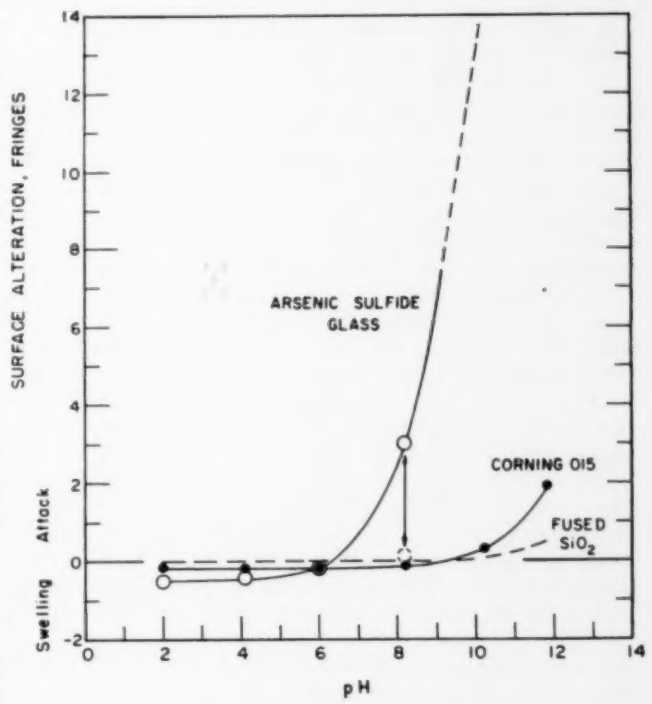

FIGURE 4. *Chemical durability of arsenic sulfide glass compared with similar data for Corning 015 glass and fused silica, over the range pH 2 to pH 11.8.*

Exposure, 6 hr at 80° C.

where fused silica and arsenic sulfide glasses are compared. The differences between these two As_2S_3 glasses, as shown by the hygroscopicity data, and which were also evident in the transmittance curves of figure 2, may be the result of impurities or variations in the arsenic-sulfur ratio.

3.2. Chemical Durability

a. Swelling and Attack

The chemical durability of the arsenic sulfide glass was reported as the surface alteration in interference fringes brought about by exposure of optically flat surfaces to various solutions under controlled conditions of temperature, time, and *p*H. Test solutions chosen were the Britton-Robinson universal buffers [7] over the range *p*H 2 to *p*H 11.8, hydrofluoric acid, and sulfuric acid.

There is general belief that the lower the hygroscopicity of a glass, the greater the ability of the glass surface to remain optically clear [8,9]. Judged on this basis from figure 3 and from the examination of polished samples which have been stored in the laboratory for approximately four years, both samples of As_2S_3 would be expected to maintain optically clear surfaces over a considerable period.

Although the above indicates that arsenic sulfide glass has satisfactory serviceability, it rates very low in chemical durability as judged from figure 4, plotted from data in table 2. In fact, it is inferior to the very hygroscopic, *p*H responsive Corning 015 glass. Among the most interesting features of the curve for the chemical durability of As_2S_3 glass, is the appreciable swelling in the acid range below *p*H 6. Experimentally, the data between *p*H 2 and *p*H 6 were readily reproducible. At *p*H 8, however, the attacks were variable, showing wide disagreement in results on duplicate samples ranging from difficultly detectable to large attack, as shown by the arrow in figure 4. Results in this region were highly dependent on just when the swollen layer sloughed off or dissolved. This is characteristic of glasses at *p*H values near which the surface alteration is passing through the transition from swelling to attack (approximately *p*H 7). The As_2S_3 glass exhibited swelling of 1/2 fringe (comparable with the swelling in acid buffer solutions) when exposed to distilled water for 6 hr at 80° C. At *p*H 11.8, the attack was so rapid that the exposure time had to be reduced to 1 min at room temperature. The value plotted was calculated on the assumption that the rate of attack doubles for each 10 deg C rise in temperature [6]. This rapid attack in alkaline solutions is in line with the high solubility of As_2S_3 in such solutions [10]. The swelling of the As_2S_3 glass in the *p*H range of 2 to 6 is similar to that observed on the Corning 015 glass.

Table 3 gives the results obtained by progressively increasing the concentration of electrolyte in the ambient solution by the use of H_2SO_4. Figure 5 shows the over-all curve for chemical durability obtained by splicing these results onto the data furnished by the Britton universal buffer mixtures. Below *p*H −1, the swelling is greatly repressed, with little or no surface alteration detectable in the majority of tests between *p*H −2.45 and *p*H −8.2.[7] However, 2 specimens (plotted as dashed lines in fig. 5) out of more than 15, showed vigorous attack in this "super acid" region. As similar attacks were obtained upon the addition of small amounts of ferric salts as an oxidizing agent,[8] it was concluded that residual amounts of the ferric compounds present from the polishing rouge were probably respon-

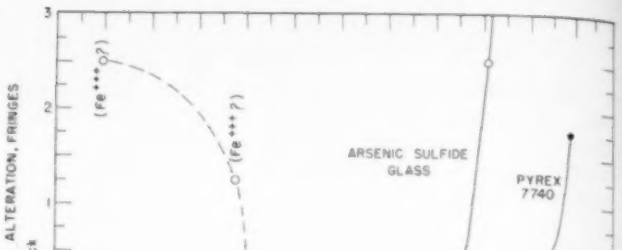

FIGURE 5. *Chemical durability-pH curve for arsenic sulfide glass compared with a similar curve for Pyrex 7740 glass over the range pH — 8.1 (concentrated H_2SO_4) to pH 11.8.* Exposure, 6 hr at 80° C.

TABLE 3. *Surface alterations of As_2S_3 glass in aqueous H_2SO_4*

H_2SO_4	H^+	Surface alteration, 6 hr at 80° C
Percent	*pH*	*Fringes*
H_2O		$\frac{1}{2}$S[a]
10	0.0	$\frac{1}{2}$S
25	0.62	$\frac{1}{2}$−S
50	−1.49	$\frac{1}{4}$+S
75	−2.45	ND[b], (1¼)[c]
80	−2.9	ND
85	−3.7	ND
90	−5	DA[d]
95	−8.1	DA, (2½)[c]
96+FeCl$_3$		2½+A

[a] S, Swelling. [b] ND, not detectable. [c] Spurious values caused by oxidation. [d] A, attack.

---

[7] Although such observed values as *p*H 8.2 cannot be rationalized in the Arrhenius sense, i. e. they cannot possibly represent hydrogen-ion concentration in moles per liter [11], nevertheless these activities as indicated by the hydrogen electrode : saturated KCl cell are accepted and plotted for convenience.

[8] Additional tests using HCl and $FeCl_3$ mixtures gave attacks of 4½ interference fringes.

sible for these exceptionally irregular results, i.e.,

$$S^{--}+2Fe^{+++}=S+2Fe^{++}.$$

The chemical-durability curve for Pyrex 7740 is included in figure 5 as a reference standard.

b. Arsenic Sulfide Glass in Hydrofluoric Acid

Silicate glasses are generally attacked vigorously by hydrofluoric acid with the formation of soluble products and volatile SiF_4. The chemical durability of arsenic sulfide glass in HF solutions is of interest because the glass contains no silica. Preliminary experiments showed no displacement of fringes or other detectable alteration of polished flats upon exposure to 48-percent HF for 6 hr at room temperature. At elevated temperatures, a perceptible swelling was observed after 1 hr of exposure. Figure 6 shows the results obtained upon exposing specimens to 48-percent HF at 80° C for various periods of time up to 6 hr. Swelling increased with time of exposure up to and including 4 hr, after which the swollen layer either became mechanically weak and sloughed off, or oxidized, forming soluble products. This attack, after 6 hr, was repeated on five different specimens, with similar results in each case.

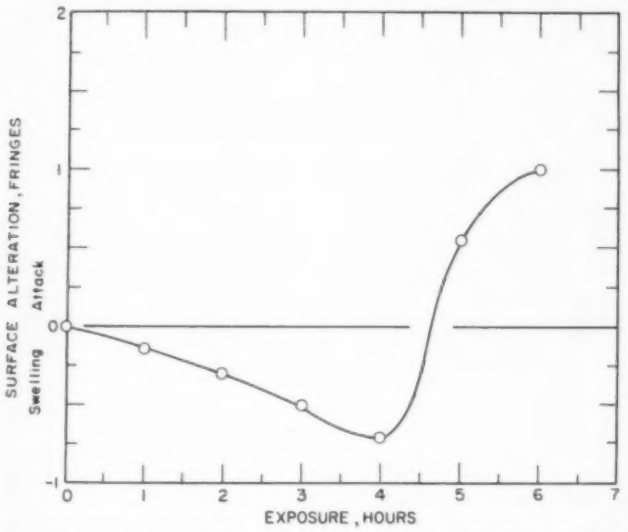

FIGURE 6. *Chemical durability of arsenic sulfide glass in* HF.
Expesure, 6 hr, to 48 percent HF at 80 C.

3.3. *p*H Response of Arsenic Sulfide Glass Electrodes

For studying the *p*H response, electrodes were prepared by coating an aluminum rod (approximately 2-mm diameter) with a film of the As_2S_3 glass. This was accomplished by dipping the rod into the molten glass, and withdrawing and cooling sufficiently quickly to prevent ignition of the arsenic sulfide in the air. Aluminum was used because it has approximately the same coefficient of expansion as the arsenic sulfide glass (23.8×10^{-6} and 23.7×10^{-6}/° C, respectively), and was the only material readily available for making successful electrodes of the Thompson metal-filled type [12]. This procedure was necessary because the conventional Cremer bulb type of electrode could not be blown [13].

All emf measurements were made at room temperature with a Beckman *p*H meter model G, using a calibrated glass electrode as the reference half cell.

At the time of preparation, these arsenic sulfide electrodes had resistance values greatly exceeding 1,000 meg, and were incapable of initiating or sustaining readable voltages on the electrometer, i. e., they behaved as an open circuit. The resistance upon exposure to aqueous solutions fell quickly to a few megohms, and the electrodes then behaved essentially as punctured electrodes. Their initial performance was in accord with the very low hygroscopicity of the arsenic sulfide glass, whereas the later electrical response was compatible with the excessive swelling exhibited by this glass in acid solutions between *p*H−2 and *p*H−6, and general overall poor chemical durability in the alkaline *p*H range.

Figure 7 and table 2 give the voltage departures (errors) obtained on three arsenic sulfide glass electrodes immediately after preparation, compared with the corresponding departures of a *p*H responsive glass (Corning 015) and the calomel half cell. The latter has no electrical response to hydrogen ions. From this comparison, it is obvious that the arsenic sulfide glass electrodes exhibited little or no response to hydrogen ion activity of aqueous solutions. This lack of *p*H response is in full accord with the low hygroscopicity and poor chemical durability of arsenic sulfide glass [10].

In order to establish that the data in figure 7 represent the performance of the arsenic sulfide, and not merely the characteristics of the aluminum electrical connector, the voltage characteristics of the bare aluminum rod were followed over the range *p*H 2 and *p*H 11.8. Figure 8 and tables 4 and 5 show a comparison of the electrode performance with the reported chemical durability of Al metal [11] and the *p*H range of precipitation of $Al(OH)_3$ [14]. The interesting feature of the voltage departure curve is the direction of drifts of the voltage below *p*H 4 and above *p*H 11. These drifts are toward increasing departure, indicating the electrode is being attacked as shown by the durability curve. Between *p*H 4 and *p*H 11, the aluminum electrode tended to indicate the H-ion concentration, with a steady reading appearing near *p*H 8. The latter point should be near the *p*H of minimum solubility of Al metal in the buffers used. Inspection of these data suffices to establish that the voltage departure recorded for the glass electrodes in figure 7 is characteristic of arsenic sulfide glass and not of aluminum.

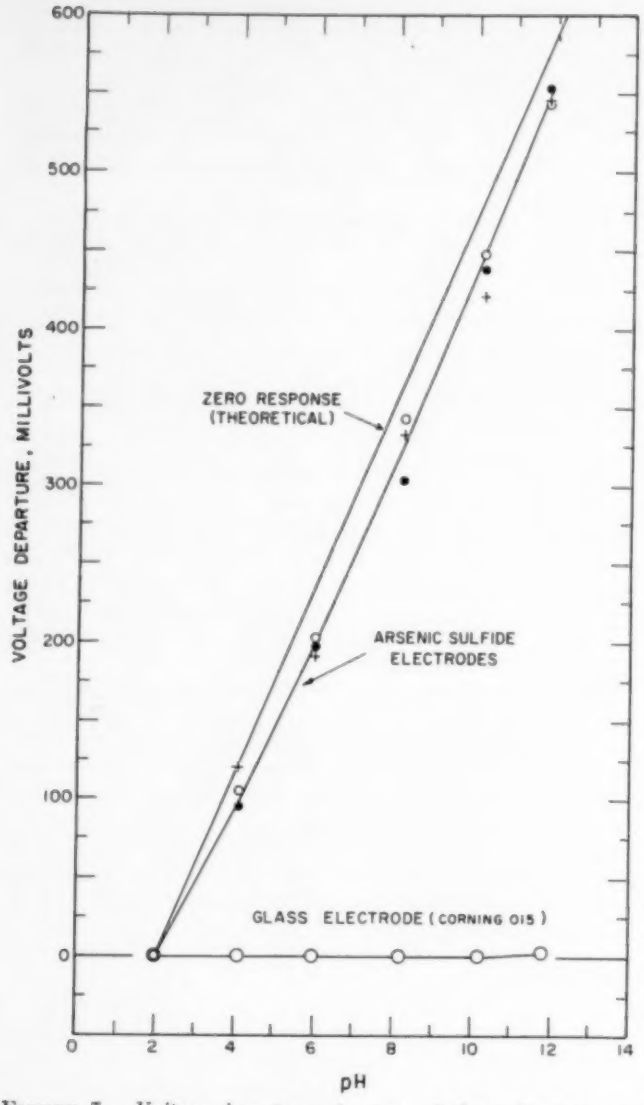

FIGURE 7. *Voltage departures (errors) of electrodes prepared from arsenic sulfide glass.*

(For comparison purposes, a curve is shown for an electrode having no hydrogen electrode function and for a glass electrode of Corning 015 glass, possessing approximately full *p*H response).

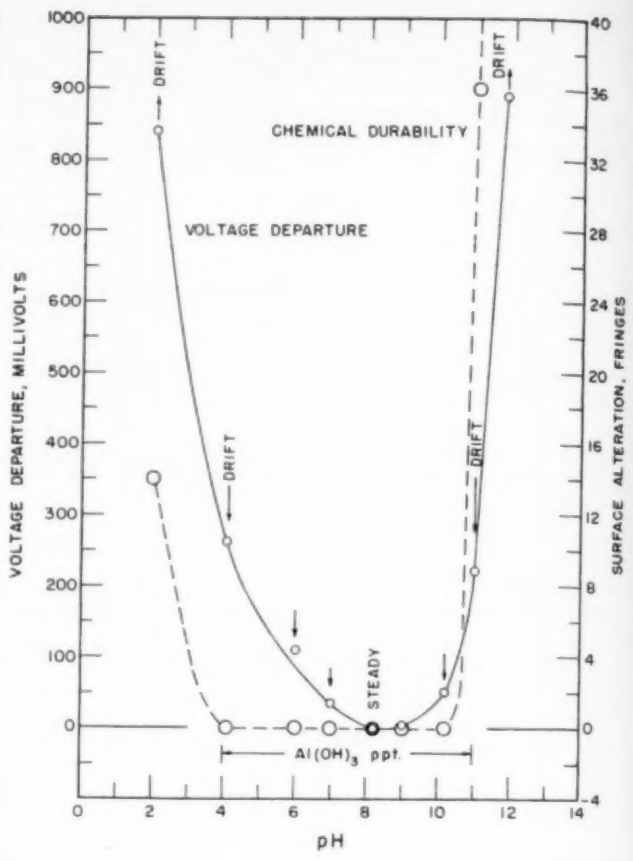

FIGURE 8. *Voltage departure of an aluminum electrode over the range pH 2 to pH 11.8.*

(For comparison purposes a curve is shown for the chemical durability of metallic aluminum, and also the *p*H range over which $Al(OH)_3$ is precipitated is indicated). It is of interest to note the significance of this voltage drift curve in connection with the quantitative precipitation and successful filtration of $Al(OH)_3$ from $Al(NO_3)_3$ by ammonia. [Clement Duval, Inorganic Thermogravimetric Analysis, p. 107, Elsevier Publishing Company, New York (1953)]. Precipitation is complete at *p*H 7.8. Immediate filtration at room temperature is possible. Imbibed water is driven off at 130° C and ignition to constant weight can be made at 475° C. Thus this procedure has two interesting features; ease of filtration and drying at low temperature.

TABLE 4. *Voltage characteristics of aluminum electrode, using the glass electrode as reference half cell*

Voltage departure at *p*H—								
2.0	4.1	6.0	7.0	8.2	9.0	10.2	11	11.8
mv 840 Drift Increase	*mv* 261 Drift Increase	*mv* 109 Drift Decrease	*mv* 34 Drift Decrease	*mv* 0 Steady	*mv* 6 Drift Decrease	*mv* 51 Drift Decrease	*mv* 221 Drift Decrease	*mv* 800 Drift Increase

TABLE 5. *Chemical durability of aluminum metal exposed to Britton buffers for 6 hr at 80° C*

Surface alteration at *p*H—								
2.0	4.1	6.0	7.0	8.2	9.0	10.2	11	11.8
Fringes 13A [a]	*Fringes* ND [b]	*Fringes* ND	*Fringes* ND	*Fringes* ND	*Fringes* ND	*Fringes* NDsc [c]	*Fringes* 36A	*Fringes* 390A

[a] A, attack. [b] ND, not detectable. [c] sc, surface cut.

4. Physical Properties

4.1. Thermal Expansion

Expansion data were obtained by means of the Saunders modification of the interferometer procedure for measuring dilation [15]. Figure 9 shows a typical curve for the thermal expansion from room temperature to the deformation point of arsenic sulfide glass. The coefficient of expansion of this glass, 23.7×10^{-6}/° C between 50° and 175° C, is over 7 times that for Pyrex 7740 (3.3×10^{-6}/° C), and approximately 2½ times that for common window and container glass.

4.2. Elastic Moduli

The elastic moduli were determined by the procedure used by Spinner [16]. Table 6 gives typical values for Young's and shear moduli and Poisson's ratio for annealed arsenic sulfide glass from 20° to 190° C. Both Young's and shear moduli decreased with increasing temperature, while Poisson's ratio increased. A graph of Young's and shear moduli versus temperature is given in figure 10.

Arsenic sulfide glass has a Young's modulus of 162 kilobars at room temperature (20° C), or approximately one-fourth that of ordinary glasses. This is very fortunate in respect to the thermal-shock resistance of this glass. The coefficient of thermal

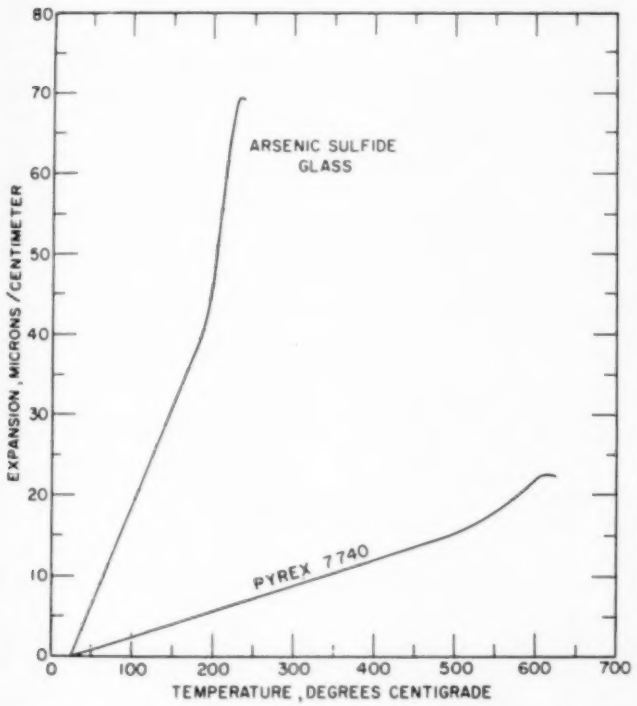

FIGURE 9. *Comparison of the thermal expansion curve for As_2S_3 with that of a thermal-shock-resistant glass (Pyrex 7740).*

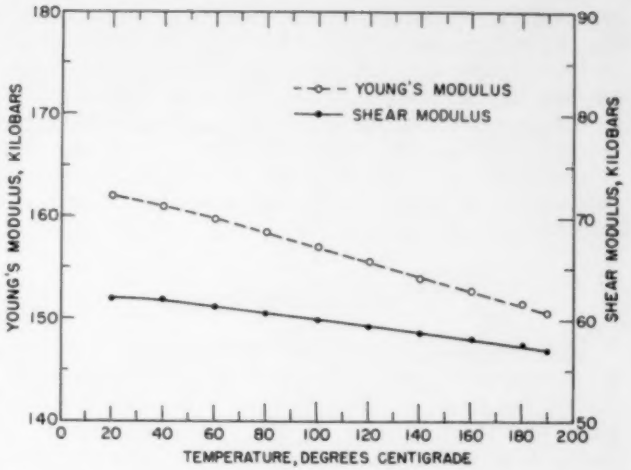

FIGURE 10. *Young's and shear moduli versus temperature for NBS arsenic sulfide glass.*

..○.., Young's modulus; —●—, shear modulus.

endurance, F, is defined by the expression,

$$F=\frac{P}{\alpha E}\sqrt{\frac{K}{sc}},$$

where P is the tensile strength, α the coefficient of expansion, E Young's modulus, K thermal conductivity, s the density, and c the specific heat [17]. The low Young's modulus helps to counteract, to a certain extent, the high coefficient of thermal expansion, because the coefficient of thermal endurance varies inversely with their product. In spite of the low Young's modulus, the thermal-shock resistance is low in comparison with the regular glasses of commerce.

TABLE 6. *Young's modulus, shear modulus, and Poisson's ratio versus temperature for arsenic sulfide glass*

Annealed sample of glass made at NBS [4].

Temperature	Young's modulus (E)	Shear modulus (G)	Poisson's ratio
° C	*Kilobars*	*Kilobars*	
20	162.0	62.0	0.306
40	160.8	61.9	.299
60	159.5	61.1	.305
80	158.1	60.5	.307
100	156.7	59.8	.310
120	155.2	59.2	.311
140	153.4	58.7	.307
160	152.3	58.1	.311
180	150.9	57.4	.314
190	149.9	57.0	.315

Although flat specimens of the As_2S_3 glass could only withstand quenching thermal shocks of less than 20° C, the same specimens could be placed on an aluminum plate at 300° C without breaking. Observations with the polariscope revealed that in the latter situation, both the upper and lower sur-

faces of the specimens were placed in compression. The large expansion of the hot lower surface caused the specimen to curl upward, placing the upper surface in compression. At the same time, as long as the main bulk of the slab remains below the deformation temperature, the lower surface was also held in compression. As soon as the deformation temperature is reached, the stresses are released and still no breakage can occur.

4.3. Modulus of Rupture

The modulus of rupture was determined on a transverse strength apparatus with midpoint loading. Values for annealed and "toughened" arsenic sulfide glass specimens made at the National Bureau of Standards are given in table 7. These measurements were made on specimens approximately 0.4 by 0.7 by 6.0 in. long, using a 4-in. span. The process used in "tempering" or "toughening" arsenic sulfide glass consisted of heating the specimens to 250° C, quenching them in oil at 130° C, and leaving the specimens to cool in the oil. As can be seen from the table, the "toughening" treatment increased the arithmetic mean of the modulus of rupture from 2,096 to 6,505 psi, or 3.1 times. Although the standard deviation was higher for the "toughened" samples (934 against 461 psi for the annealed samples), the coefficient of variation was less (14.36 to 21.99%).

TABLE 7. *Modulus of rupture of arsenic sulfide glass specimens made at the National Bureau of Standards (4-in. span)* [4]

Specimen	Modulus of rupture	
	Annealed	"Toughened"
	psi	*psi*
1	1,828	6,079
2	2,823	8,328
3	1,548	5,634
4	2,389	7,199
5	1,164	5,484
6	2,670	6,945
7	2,135	6,420
8	2,393	6,158
9	1,666	5,186
10	2,484	6,062
11	1,078	7,385
12	1,766	5,410
13	2,393	6,068
14	1,906	6,173
15	2,196	6,897
16	2,543	5,991
17	2,351	7,218
18	1,805	7,056
19	2,270	5,149
20	2,456	6,384
21	1,944	7,034
22	1,876	8,854
23	2,853	
24	1,815	
$\bar{X}$ (arithmetic mean)	2,096 psi	6,505 psi
σ (standard deviation)*	461 psi	934 psi
K (skewness)	−0.40	+0.70
v (coefficient of variation)	21.99%	14.36%

* This is the standard deviation of the individual values from the mean.

4.4. Hardness

The Knoop hardness of annealed arsenic sulfide glass was found to be 120 to 125. However, when these same samples were "toughened" and again tested, the Knoop hardness was only 100 to 111. The Knoop hardness of commercially annealed soda-lime glass is 520; that for lead glasses varies from 370 to 440, depending on the lead content [18].

4.5. Optical Properties

a. Transmittance

The infrared transmittance curve for two thicknesses of arsenic sulfide glass made at the National Bureau of Standards is shown in figure 11. These measurements were made by the Radiometry Section of the Bureau. Figure 12 shows the absorbance index and surface loss (one surface) calculated from the results plotted in figure 11 [19]. As can be seen, the maximum transmittance obtainable is about 70 percent because of the high reflection loss. This high loss is due to the high index of refraction, 2.4 in the infrared. Figure 13 gives an idea of the difference in transmittance between a sample made at the National Bureau of Standards and a commercial sample made by the American Optical Company. These same samples were then "toughened" and their transmittances again measured. A comparison of the transmittance curves before and after "toughening" indicated that the "toughening" process did not affect the transmittance in the infrared. Also, though there are differences between the transmittances of the two samples (NBS and commercial), the over-all transmittances of the two glasses are practically the same.

It will be noticed that there is appreciable difference between the transmittance curves in figures 11 and 13. The glass sample used for figure 11 resulted from a small melt (230 g of batch); the

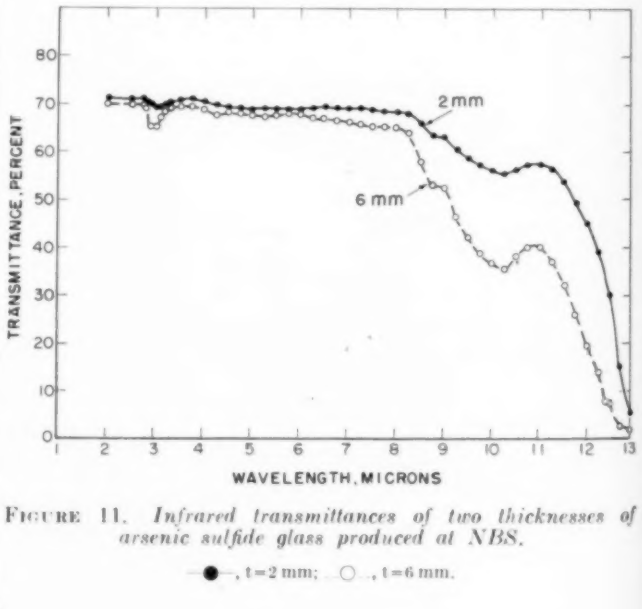

FIGURE 11. *Infrared transmittances of two thicknesses of arsenic sulfide glass produced at NBS.*

●, t=2 mm; ○, t=6 mm.

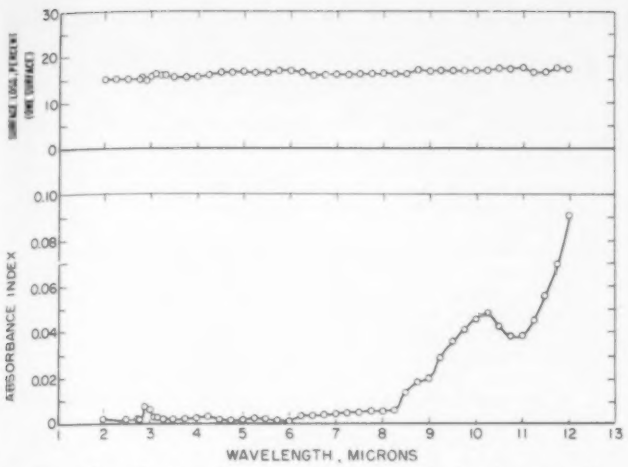

FIGURE 12. *Surface loss (one surface) and absorbance indices calculated from figure 11.*

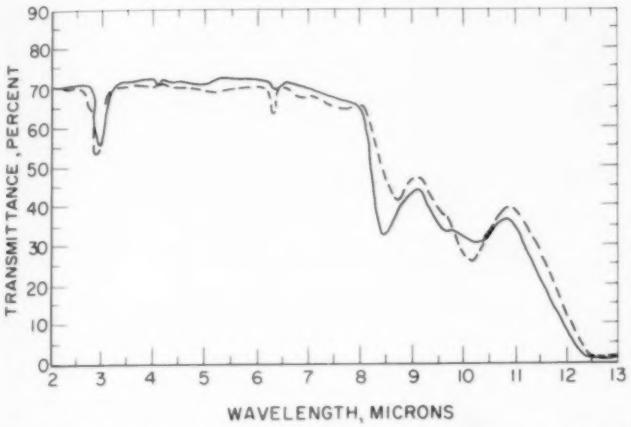

FIGURE 13. *Infrared transmittance curves for commercial and NBS arsenic sulfide glass. Annealed.*

———, commercial glass, t = 6.05 mm; – – – –, NBS glass, t = 6.00 mm.

sample used for figure 13 resulted from a large melt (5,000 g of batch) made in the one-step process described previously. Also, in the case of the small melt, doubly distilled arsenic was used; in the large melt, singly distilled arsenic was used. In the small melt, 1 ml of water was added to the batch to displace any residual air; in the large melt, none was added. The small melt was not cast, but was annealed in the reaction tube after homogenizing. The differences in the procedures enumerated above can easily account for the differences in the two transmittance curves.

b. Indices of Refraction

To our knowledge, only one measurement of the indices of refraction of arsenic sulfide glass in the infrared has been made. That measurement was made at the National Bureau of Standards, by the Optical Instruments Section, on a prism furnished by Walter A. Fraser, at that time working in the Research Laboratories of the American Optical Co., Stanford, Conn. The dispersion curve for this prism is shown in figure 14, plotted from the results given in table 8.

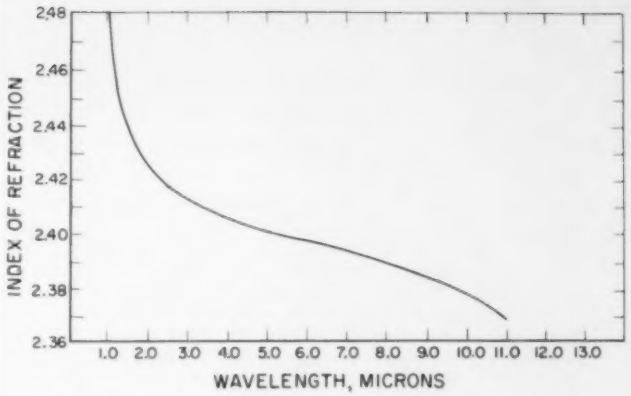

FIGURE 14. *Dispersion curve for arsenic sulfide glass.*

(This glass was produced by Walter A. Fraser while in the employ of the American Optical Co., Southbridge, Mass. Measurements were made at NBS.)

TABLE 8. *Index of refraction of a prism of arsenic sulfide glass produced by Walter A. Fraser while at the American Optical Co., Southbridge, Mass.*

Determinations made at NBS.

Wavelength (microns)	Index of refraction
0.579066	2.65822
.643847	2.59413
1.01398	2.47230
1.12866	2.45897
1.35703	2.44244
1.36728	2.44190
1.39506	2.44050
1.52952	2.43474
1.6932	2.42965
1.7092	2.42913
1.81307	2.42656
1.97009	2.42341
2.32542	2.41848
3.3033	2.41134
3.4188	2.41068
5.344	2.39900
6.238	2.39718
8.662	2.38734
9.724	2.38029
11.035	2.37055

5. Conclusions

The very low hygroscopicity exhibited by arsenic sulfide glass is a characteristic favorable to its use as an optical element. It is better than any other material of which we know, within its useful transmission range out to approximately 13 μ, for the optical elements of laboratory infrared instruments, for that reason. Infrared spectrometer cells made from it would be satisfactory for neutral or slightly acid organic liquids and water solutions. However, because of its low Knoop hardness, precautions should be taken to protect it when used in optical systems or as windows. It is also very easily attacked by alkaline and oxidizing materials.

The very high coefficient of expansion and low modulus of rupture tend to limit the thermal shock that can be withstood. Hence, caution must be exercised in molding procedures, mounting design, and service usage. The low value of Young's modulus, however, does, to a certain extent, counteract the effect of the high coefficient of expansion.

6. References

[1] C. Schultz-Sellack, Diathermansie einer Reihe von Stoffen für Wärme sehr geringer Brechbarkeit, Ann. Physik **139,** 182 (1870).

[2] Rudolf Frerichs, New optical glasses with good transparency in the infrared, J. Opt. Soc. Amer. **43,** 1153 (1953).

[3] W. A. Fraser and J. Jerger, Jr., Arsenic trisulfide: A new infrared transmitting glass, J. Opt. Soc. Amer. **43,** 322 A (1953); W. A. Fraser, A new triaxial system of infrared glasses, J. Opt. Soc. Amer. **43,** 823 A (1953); Servo Corporation of America, 20–20 Jericho Turnpike, New Hyde Park, N. Y., a leaflet entitled "Servofrax" (arsenic trisulfide glass); W. A. Fraser, Arsenic trisulfide glass and its applications, Proceedings of the conference on infrared optical materials, filters, and films, p. 25 (Held at the Engineer Research and Development Laboratories, Fort Belvoir, Va., 10 February 1955); and Francis W. Glaze, Transmittance of infrared energy by glasses, Bul. Am. Ceram. Soc. **34,** 291 (1955).

[4] F. W. Glaze, D. H. Blackburn, and W. Capps, Development of materials for transmitting infrared en rgy, WADC technical report 54–457, project No. 7350, Materials Laboratory, Wright Air Development Center, United States Air Force, Wright-Patterson Air Force Base, Ohio (March 1955).

[5] Donald Hubbard, Mason H. Black, Sylvanus F. Holley, and Gerald F. Rynders, Electrode function (*p*H response), hygroscopicity and chemical durability of soda-potash-silica glasses, J. Research NBS **46,** 168 (1951) RP2189.

[6] Donald Hubbard and Edgar H. Hamilton, Studies of the chemical durability of glass by an interferometer method, J. Research NBS **27,** 143 (1941) RP1409.

[7] H. T. S. Britton, Hydrogen ions (D. Van Nostrand Co., Inc., New York, N. Y., 1932).

[8] Donald Hubbard, Hygroscopicity of optical glasses as an indicator of serviceability, J. Research NBS **36,** 365 (1946) RP1706.

[9] George W. Morey, The properties of glass, p. 107 (Reinhold Publishing Corp., New York, N. Y. 1954).

[10] Herman F. Shermer, Gerald F. Rynders, Given W. Cleek, and Donald Hubbard, Atypical *p*H response of some nonsilicate glasses, J. Research NBS **52,** 251 (1954) RP2497.

[11] Robert G. Pike and Donald Hubbard, An interferometer procedure applied to the study of the chemical durability of silicates, enamels, and metals, J. Research NBS **50,** 87 (1953) RP2394.

[12] M. R. Thompson, A metal-connected glass electrode, BS J. Research **9,** 833 (1932) RP511.

[13] M. Cremer, On the causes of the electromotive properties of tissues and a discussion of polyphase electric cells, Z. Biol. **47,** 562 (1906).

[14] Lansing S. Wells, Reaction of water on calcium aluminate, BS J. Research **1,** table 15 (1928) RP34.

[15] James B. Saunders, Improved interferometric procedure with application to expansion measurements, J. Research NBS **23,** 179 (1939) RP1227.

[16] Sam Spinner, Elastic moduli of glasses by a dynamic method, J. Am. Ceram. Soc. **37,** 229 (1954).

[17] George W. Morey, The properties of glass, p. 351 (Reinhold Publishing Corp., New York, N. Y., 1954).

[18] Fay V. Tooley, Handbook of glass manufacture, p. 15. (Ogden Publishing Co., New York 36, N. Y., 1953).

[19] Jack M. Florence, Charles C. Allshouse, Francis W. Glaze, and Clarence H. Hahner, Absorption of near-infrared energy by certain glasses, J. Research NBS **45,** 121 (1950) RP2118.

Washington, November 9, 1956.

Journal of Research of the National Bureau of Standards Vol. 59, No. 2, August 1957 Research Paper 2775

Thermal Conductivity of Beryllium Oxide From 40° to 750° C

David A. Ditmars and Defoe C. Ginnings

The thermal conductivity of beryllium oxide has been measured by an absolute method from 40° to 750° C. The apparatus employed steady-state longitudinal heat flow along a rod of high-fired beryllium oxide, surrounded by a tube with matching temperature gradient to minimize radial heat loss. The estimated accuracy of the measurements is about 3 percent. However, the values of thermal conductivity of the ideal beryllium oxide crystal are probably considerably higher than the values given because of the lower density (87 percent theoretical) of the sample used.

1. Introduction

Not only is beryllium oxide useful as a moderator in the utilization of atomic energy, but it has an unusually high thermal conductivity, much higher than other nonmetals and even higher than most metals over a limited temperature range. At room temperature, its thermal conductivity is about that of aluminum, whereas its electrical conductivity is extremely low. It was the purpose of this investigation to measure the thermal conductivity of beryllium oxide in the high-temperature range.

2. Sample

The beryllium oxide was originally fabricated by the Norton Co. by hot-pressing. A rough sample was taken from this material and machined, at the Oak Ridge National Laboratory, to a cylindrical rod about 0.5 in. in diameter and 6 in. long. From information obtained on this material, together with that obtained from a spectrographic analysis, it seems likely that its impurities (other than carbon) were less than 0.2 percent. It is possible that carbon was present in larger amounts in the sample, although it was white, with only occasional dark inclusions. The sample was fired in the NBS Mineral Products Division at about 1,700° C and machined to the form of a true cylinder having a diameter of 0.4524 in. at room temperature and an average density of 2.62 g/cm^3 (87 percent of single crystal). The method of original fabrication by hot-pressing may have caused a variation in density in the sample of several percent.

3. Method and Apparatus

The method and apparatus have been described briefly in technical reports [1, 2].[1] The method used was absolute in that the results were obtained without comparison with another material. A longitudinal heat flow was used to establish a temperature gradient in the sample. From the measured values of heat flow, temperature gradient, and the cross section of the sample, the thermal conductivity of the sample was calculated. Longitudinal rather than radial heat flow was used in order to obtain a reasonable temperature gradient in a conveniently shaped sample. The temperature gradient on the sample was determined by measuring the temperatures along the sample. The longitudinal heat-flow method, as applied to relatively long samples, has the inherent disadvantage that radial heat losses to the surroundings may reduce the accuracy of the results. However, in this case, the conductivity of the BeO was so high that radial heat losses did not seriously limit the accuracy of the results.

A scale diagram of the essential parts of the apparatus is shown in figure 1. Measured electrical heat, introduced in the "sample heater" at the top of the sample (BeO), flowed down the sample and its "adapter" to a heat sink. The sample heater consisted of six small helices of No. 38 Nichrome wire located in holes in the top of the sample. The adapter was used here to position the sample, as well as to fill in the needed length, because the apparatus was built to accommodate samples longer than 6 in. Anhydrous boric oxide was used to give good thermal contact between the sample and adapter, and between the adapter and the sink. This compound has a very low vapor pressure and has excellent wetting properties, maintaining good thermal contact at temperatures far below its melting point. The sink was cooled with either water or air, depending on the temperature range, and was equipped with a heater and thermocouple so that it could be automatically kept at a constant temperature.

The temperatures along the sample were measured with three thermocouples (No. 36 AWG platinum-platinum-rhodium) having reference junctions at 0° C and principal junctions on the sample at the three levels shown in figure 1. In addition to these three absolute thermocouples, a differential thermocouple was also used to ascertain directly the temperature difference between the upper and lower levels on the sample. All of the thermocouples on the samples were made with junctions peened into small holes (about 0.6 mm in diameter and depth) in the cylindrical surface of the sample. In order that the temperature gradient measured on the sample would correspond to the electric heat put into the top of the sample, precautions were taken to minimize radial heat loss along the sample. For this purpose, the sample was surrounded by a "guard tube"

[1] Figures in brackets indicate the literature references at the end of this paper.

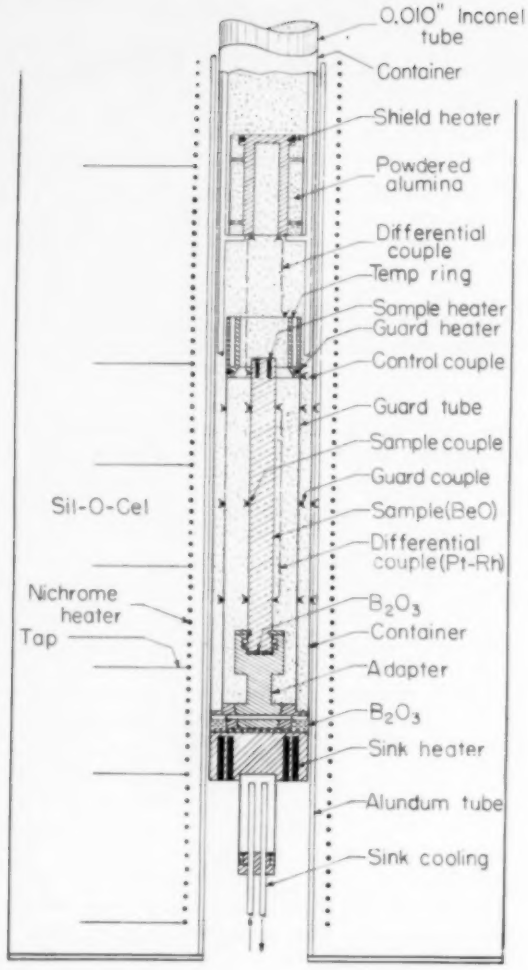

FIGURE 1. *Thermal-conductivity apparatus.*

(Inconel, 0.03-in. wall), with temperatures corresponding to those in the sample. Temperatures along the guard tube were measured with three platinum–platinum-rhodium thermocouples, with principal junctions attached to the guard tube at levels corresponding to those of the sample thermocouples. Three additional thermocouples, at the same levels on the guard tube but at different azimuths, were also provided. The top of the guard tube was heated by the "guard heater", and its temperature was controlled automatically, using the "control couple" close to the heater. Another heater with a control thermocouple (not shown in fig. 1) was provided at the bottom of the guard tube, but it was found unnecessary to use it when the furnace temperatures were suitably controlled. The top portion ("tempering ring") of the guard tube was made of thick nickel to which the electrical leads to the sample were thermally connected, so that it served as a tempering region for bringing the leads to the temperature of the top of the sample, and thus to reduce heat conduction along them. A "thermal shield" (nickel) and heater, placed above the sample and tempering ring, also served for this purpose and to prevent heat transfer upward through supports and insulation.

Although the apparatus shown in figure 1 has been used only for measuring the thermal conductivity of solids, it was designed so that it could be used also for high-conductivity liquids. For this application, the liquid would be contained in a thin-walled tube equipped with a suitable heater and a liquid expansion chamber extending up into the shield. To obtain the thermal conductivity of the liquid, it would be necessary to account for the thermal conduction in the container tube by making another experiment with the liquid replaced by a powder of very low and known thermal conductivity.

The whole assembly, supported by rods extending down to the bottom of the guard, was filled with fine aluminum oxide powder for insulation and enclosed in a 0.010-in. Inconel tube, which served to hold the powder. This tube, fitting closely in the "container" (0.035-in. Inconel tube) centered along the axis of the furnace, facilitated assembly. Thermocouple and heater leads were brought out from this container through an insulating seal at the top (not shown in fig. 1), so that the conductivity apparatus could either be evacuated or filled with argon. Because experiments with the apparatus had shown the electrical insulation to fail when it was evacuated at high temperatures, the apparatus was filled with argon after evacuation at moderately high temperatures to outgas the aluminum oxide. The thermal-conductivity apparatus was maintained at the chosen temperature by the surrounding furnace, which was equipped with numerous taps on the heater winding to give the desired vertical temperature gradients. Two automatic regulators, actuated by thermocouples in the furnace, were used to maintain constant temperatures.

4. Experimental Procedure

Two basic types of experiment were performed for each measurement of thermal conductivity. In the first type (called a *conductivity experiment*), the furnace temperature was controlled to the desired value, a known constant electric power was put into the sample heater, the temperatures of the guard and shield were adjusted to match those on the sample as closely as possible, and the sink temperature was adjusted to a constant value. After a steady state was obtained, several consecutive sets of observations of thermocouple emf and sample power were recorded. In the second type of experiment (called *calibration experiment*), no power was put into the sample heater, but in other ways, the experimental procedure was similar to the first. The purpose of this experiment was to correct for errors that did not depend on the power transmitted through the sample. Errors of this type are those due to differences, in thermocouples and those resulting from unknown heat leaks, which presumably were the same in both

types of experiments. Several other experiments were made to detect other errors and to determine their importance. Some of these experiments are described later.

Several hours were usually required to bring the various parts of the apparatus to the desired temperatures and to make sure that these temperatures were not changing significantly. The final data were usually obtained in a period of about 30 min, subsequent to an interval of about an hour during which the temperatures were observed to be constant. Automatic thermoregulators were used to control the temperatures of the furnace, guard, and sink.

5. Calculation of Results and Uncertainties

The conductivity values were calculated from the observed quantities by means of the equation

$$k=\frac{\dot{Q}\Delta X_0}{A_0(1+\alpha t_a)\Delta t},$$

where

k = thermal conductivity (watts cm^{-1} deg^{-1} C) at temperature t_a.
t_a = average temperature of sample between thermocouples.
$\dot{Q}$ = heat-flow rate (watts).
ΔX_0 = thermocouple spacing at 0° C (cm).
A_0 = cross-sectional area at 0° C (cm^2).
α = coefficient of linear thermal expansion (deg^{-1} C).
Δt = temperature difference (deg C) between thermocouples.

This equation is valid for steady-state longitudinal heat flow over a small temperature interval. The determination of these factors in the conductivity equation, together with a consideration of their uncertainties, will now be discussed individually. The uncertainties referred to in this report are the authors' estimates (based on their judgment) on the basis that the observed quantity would have about an equal chance of being within that limit as being outside it, and that the sign of the uncertainty is just as likely to be positive as negative.

5.1. Heat-Flow Rate ($\dot{Q}$)

a. Electric Power

Heat was generated by direct current in the sample heater, and power was measured in a conventional manner, using a potentiometer in conjunction with a high-resistance volt box to measure the potential drop across the heater, and a standard resistor in a current lead to measure the current. The errors in these electrical measurements were almost negligible. In measuring the potential drop across the heater, the potential terminals were located to evaluate properly the heat that went to the sample. Because the sample heater was made with very high resistance (relative to that of the heater leads), the uncertainty in the location of the potential terminals resulted in only about 0.1-percent uncertainty in the measured thermal conductivity.

b. Heat Flow From Sample to the Tempering Ring

In addition to the electric-power input to the top of the sample, it is necessary to consider the heat transfer between the sample and its surroundings. Because of the excess temperature of the sample heater, heat flowed along the heater leads to the tempering ring; the uncertainty in this heat flow (taken to be 50 percent of the correction) averaged about 0.24 percent of the total heat flow in the sample. In addition to this heat flow, there was the heat flow between the top part of the sample and the tempering ring. The evaluation of this was difficult because of the configuration and the temperature distribution on the top part of the sample where the sample heater was located. Using differential thermocouples, observations were made of the temperature difference between the isothermal tempering ring and a point on the top part of the sample. The location of this point was determined by calculation so that the net heat flow from the top of the sample to the tempering ring would be proportional to the emf of the differential thermocouple. The height of the top of the sample relative to the guard was made so that the bottom of the sample heater was at the same level as the bottom of the tempering ring. In the actual experiments, the tempering-ring temperature depended on the power in the guard heater and was indicated by the differential thermocouple to be 2 or 3 deg higher than the temperature of the sample, making necessary a correction for the resulting heat flow. It was found convenient to evaluate this correction experimentally by making two conductivity experiments in which only the tempering-ring temperature was changed and the furnace temperature adjusted to maintain the match between the guard and sample thermocouples. Using the resulting change in sample gradient, the data were corrected to correspond to no difference in temperature as indicated by the differential thermocouple. However, there still remained an uncertainty in heat flow due to some uncertainty in the proper location of the thermocouple junction on the sample head. It was estimated that the uncertainty in the heat flow between the sample and tempering ring, excluding heat flow along leads mentioned above, resulted in an uncertainty in measured conductivity averaging about 0.5 percent.

c. Heat Flow Down the Insulating Powder

Even when the guard temperatures matched sample temperatures, some of the heat input to the sample necessarily went to maintain some of the longitudinal heat flow in the insulating powder between the sample and guard. The conductivity of the aluminum oxide powder with argon gas was determined approximately by a few experiments as it was used in the apparatus. The temperature distribution in the insulation had been previously estimated with a resistance analog computer, setting up boundary conditions corresponding to the configuration and assumed temperatures of the sample and guard. It was estimated from these results

that when the thermocouple on the top part of the sample indicated the same temperature as the guard ring, the sample heater contributed only 16 percent of the total longitudinal heat flow in the powder, the remainder of the heat being furnished by the guard. Under this condition, about 0.2 percent of the heat of the sample heater flowed down through the insulating powder. The uncertainty of this correction was estimated to give less than 0.1-percent uncertainty in the measured thermal conductivity.

d. Heat Flow Between Sample and Guard

Because it was found impractical to match the sample and guard temperatures exactly during all conductivity experiments, experiments were made that permitted calculation of corrections for imperfect matching. For each guard thermocouple, two thermal-conductivity experiments were made, varying only the difference between that guard thermocouple and the corresponding thermocouple on the sample. From the resulting change in temperature gradient on the sample in these two experiments, it was possible to estimate a correction for small differences in matching guard and sample thermocouples. It was calculated that there was an uncertainty of about 50 percent in correcting for heat flow between the sample and the guard. This uncertainty resulted in an average uncertainty in measured conductivity of about 0.3 percent.

e. Heat Flow Into Heat Capacity of Sample

If the temperature of the sample were changing with time, some of the heat input would go to produce this change, and the temperature gradient on the sample would not correspond to the heat input at the top of the sample. In all experiments, the rate of temperature change was less than 0.8 deg C/hr, corresponding to an effect of 0.5 percent in the calculated value of conductivity. The average uncertainty in the correction for this was negligible.

5.2. Thermocouple Spacing (ΔX_0)

The distance between the principal junctions of the upper and middle sample thermocouples was 4.97 cm at 0° C, whereas the corresponding distance for the middle and lower thermocouples was 5.05 cm; this gives 10.02 cm for the distance between the extreme absolute thermocouples. The distance between junctions on the differential thermocouple was 10.01 cm. These distances, taken as the lengths between centers of the thermocouple holes, were measured to better than 0.01 cm with a traveling microscope, but because the thermocouples were peened into holes 0.06 cm in diameter, the possibility of nonuniform thermal contact makes a tolerance of 0.03 cm appear more realistic. This tolerance corresponds to 0.3-percent uncertainty in the 10-cm spacing between the sets of thermocouples used in the conductivity calculations. The effect of thermal expansion on both thermocouple spacing and cross-sectional area is lumped into the correction $(1+\alpha t_a)$, which is described later.

5.3. Cross-Sectional Area (A_0)

The sample was ground to have a uniform diameter of 0.4524 ± 0.0003 in., corresponding to a cross-sectional area of 1.038 cm^2. The uncertainty in this area was estimated to be less than 0.1 percent.

5.4. Thermal-Expansion Correction $(1+\alpha t_a)$

Thermal-expansion changes the thermocouple spacing by the factor $(1+\alpha t_a)$, and the cross-sectional area by the factor $(1+\alpha t_a)^2$, resulting in the $(1+\alpha t_a)$ term given in the conductivity equation. The coefficient of linear thermal expansion (α) has been determined by White and Schremp [3]. At the highest temperatures (747° C) of the conductivity experiments, the correction for expansion amounted to about 0.6 percent, with negligible uncertainty in the measured conductivity.

5.5. Temperature Difference (Δt)

The accurate measurement of the temperature difference on the sample was difficult, requiring a number of tests to eliminate or evaluate certain errors. As described in section 3, two different thermocouple systems were used to measure the temperature difference over the 10-cm length on the sample. The two independent thermocouple systems served to check on each other, usually agreeing on the measured temperature difference to better than 1 percent.

All temperatures were measured with platinum-platinum-rhodium thermocouples of No. 36 AWG wires. A sample thermocouple was calibrated at several points between 0° and 1,000° C in the Pyrometry Laboratory of the National Bureau of Standards. No significant difference was observed between the thermoelectric power of this sample and that given in the standard tables [4]. Even though the thermocouples were all made from wire off the same spools, it was possible that they had slightly different thermoelectric powers. Although these differences might not be serious for measurement of absolute temperatures, they could be significant for measurement of small temperature differences at high temperatures. These differences were automatically accounted for by the calibration experiments mentioned previously, in which no power was put into the sample heater. These calibration experiments gave differences in thermocouple readings, which increased regularly up to 470° C, and amounted to as much as 7 μv at this temperature. At temperatures approaching 750° C, the differences became both larger and more irregular, so that after each conductivity experiment, a calibration experiment was made to evaluate the differences.

In addition to the differences described above, the evaluation of Δt was uncertain because of the occasional effect of high humidity on the potentiometer used to measure the thermocouple emf. This effect was observed as a reading on the potentiometer, even when the potential across its terminals was

zero. When the value of Δt was observed, using the differential thermocouple, the value was subject to the full potentiometer uncertainty (about 2 μv) because only one reading was involved. When the value of Δt was determined by using the two absolute thermocouples, most of this potentiometer uncertainty was reduced (to about 0.5 μv) because the value of Δt was obtained from a difference of two readings. It is for this reason that the uncertainties in the value of Δt, using the differential thermocouple, were larger than the uncertainties when using the absolute thermocouples, averaging about 1.5 percent as compared to 0.4 percent. That the two thermocouple systems usually agreed to better than 1 percent is evidence that the error due to the humidity effect on the potentiometer was not excessive.

6. Results

The results of the individual thermal-conductivity measurements on beryllium oxide are given in table 1. Values of observed conductivity (k) are given as determined by using each of the thermocouple systems (absolute and differential) at the average temperature (t_a) of that portion of the sample measured by the thermocouples. At the lower temperatures, where the thermal conductivity of the beryllium oxide changes rapidly with temperature, small corrections to conductivity were made for the curvature of the conductivity-temperature function. In this table, the quantities given are corrected for all known errors. In the previous discussion, each uncertainty has been estimated by the authors on the basis that the observed quantity would have an equal chance of being within that limit as being outside that limit. These uncertainties have been combined (square root of the sum of the squares) and arbitrarily increased by over a factor of 2 to give more realistic values of estimated error listed in table 1.

Table 1 indicates that the results, using the absolute thermocouples, seem to be reliable to about 2 percent. The experiments under 60° C are not as accurate as the other experiments. This is due to the smaller temperature drop in the sample, first because the limitations of the heat sink made it necessary to use lower power, and second, because the thermal conductivity of the beryllium oxide was so high in this low-temperature range. The larger error estimated by using the differential thermocouple in this low-temperature region is due to the humidity trouble mentioned previously. No results are given for measurements with absolute thermocouples above 500° C because of failure of their electrical insulation.

A smooth function of thermal conductivity was obtained graphically from the observed values in table 1, giving greatest weight to those values having the smallest estimated errors. Table 2 gives smoothed values of the conductivity at even temperatures as obtained from the graph. Figure 2 gives the deviations of the results (obtained with the two different thermocouple systems) from the smooth

TABLE 1. *Experimental results*

Date (1954)	t_a	Power	Absolute thermocouples			Differential thermocouples		
			Δt	Observed k	Estimated error [a]	Δt	Observed k	Estimated error [a]
	°C	w	°C	w/cm-°C	%	°C	w/cm-°C	%
Aug. 25	38.2	0.8960	3.95	2.19	5.4	4.11	2.10	19.2
Aug. 26	46.2	1.4452	6.84	2.04	3.2	7.03	1.98	10.7
Aug. 25	52.6	1.8894	9.41	1.94	2.6	9.61	1.90	7.9
Aug. 27	59.7	2.3620	12.15	1.879	2.1	12.33	1.849	6.2
Aug. 24	85.8	3.3179	19.16	1.674	1.6	19.28	1.661	4.0
Oct. 8	86.2	3.8007	21.88	1.679	1.7	22.09	1.660	3.6
Sept. 29	86.9	3.6073	20.90	1.668	2.1	21.07	1.652	3.9
Sept. 23	87.3	3.6084	20.86	1.672	1.8	21.08	1.652	3.7
Sept. 30	87.3	3.6138	21.01	1.662	1.7	21.17	1.647	3.7
Aug. 31	91.4	2.5903	15.20	1.647	2.0	15.10	1.655	4.9
Sept. 1	123.8	2.4474	16.26	1.454	1.7	16.33	1.446	5.4
Sept. 15	153.0	2.4894	18.27	1.316	1.7	18.36	1.308	4.1
Sept. 2	153.4	2.4795	18.27	1.311	1.8	18.37	1.302	4.2
Oct. 11	202.0	3.9603	33.80	1.131	2.0	33.65	1.135	2.6
Aug. 23 [b]	202.1	3.8745	33.29	1.124	1.6	33.10	1.128	2.4
Aug. 18	241.5	3.7312	36.20	0.995	1.7	35.87	1.002	2.3
Aug. 19	241.4	3.7396	36.51	.989	2.2	36.19	0.996	2.7
Aug. 20 [b]	251.4	0.8739	8.95	.942	2.2	8.85	.952	6.5
Sept. 20	287.3	2.3441	25.93	.872	1.8	25.54	.884	2.8
Sept. 17	287.7	2.3378	25.87	.872	1.9	25.71	.876	2.9
Oct. 7	379.5	3.5169	48.12	.704	1.5	47.77	.709	2.0
Oct. 5	380.4	3.5378	48.64	.701	1.9	47.60	.715	2.3
Oct. 12	439.2	3.3054	51.83	.614	1.2	51.82	.614	1.7
Oct. 18	517.2	2.9239	.....	.....	.....	53.63	.524	2.7
Oct. 19	578.7	2.5664	.....	.....	.....	51.54	.478	3.5
Oct. 20	646.7	2.7048	.....	.....	.....	59.94	.433	2.4
Nov. 2	747.9	2.6370	.....	.....	.....	65.84	.384	4.3

[a] Estimated error is the authors' estimate, considering only the various uncertainties mentioned in the text.
[b] The results on August 20 and 23 represent averages of 2 experiments on each day.

function. At 50° C and below, the observed values deviate markedly from the smooth function, giving values at 40° C that are 4 percent different. These deviations are probably due to the very small temperature difference of 4° C in the sample, so that errors in the measurement of this temperature difference have greater influence on the result. Figure 2 also shows the results at 251° C to be about 3 percent lower than the other results. It seems probable that this departure is also due to the lower temperature difference on the sample resulting from the lower power; the power here was only one-fourth the power in the other experiments in this temperature range. If it is assumed that there existed an unknown constant absolute error in either heat flow or temperature difference, the deviations of about 3 percent in the low-power experiments would indicate that the experiments with the higher power might be in error by about 0.8 percent. Consequently, the authors believe that the over-all accuracy of the results is more likely to be about 3 percent instead of the 2 percent indicated by the estimated errors listed in table 1.

TABLE 2. *Thermal conductivity of* BeO (*density=2.62 g/cm³*)

(Smoothed values)

t	*k*	*t*	*k*
° C	*w/cm-° C*	*° C*	*w/cm-° C*
30	2.155	400	0.666
50	1.967	450	.598
100	1.581	500	.541
150	1.328	550	.498
200	1.131	600	.462
250	0.972	650	.433
300	.845	700	.406
350	.746	748	.384

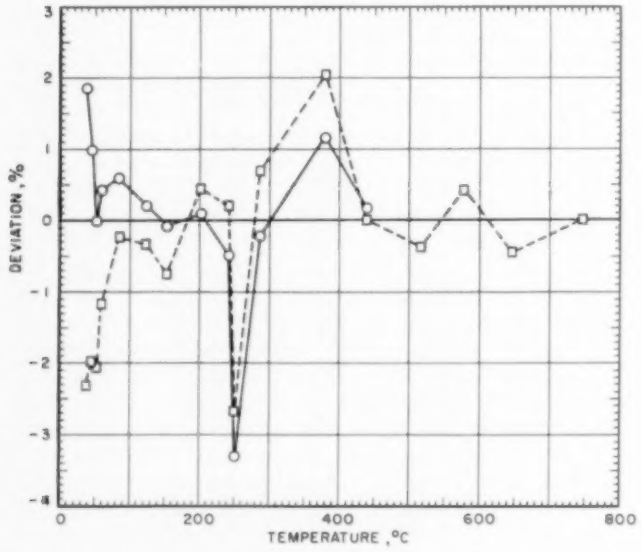

FIGURE 2. *Deviations of beryllium oxide thermal-conductivity data.*

Base line = NBS smoothed data.
○, NBS (absolute couples); □, NBS (differential couples).

No attempt has been made to correct the thermal-conductivity values for the NBS sample to correspond to zero porosity. Because the density of this sample was only 2.62 g/cm³ compared to about 3.0 for the ideal crystal, the thermal conductivity of the crystal should be significantly higher than the values given in table 2. From the investigation of Francl and Kingery [5], it would appear that the conductivity of the ideal crystal would be about 15 percent higher. However, the measurements of Powell [6] on beryllium oxide specimens (densities 1.85 to 2.82 g/cm³) would indicate a much larger correction. The authors feel that the correction for porosity is uncertain and that there are other factors beside porosity that also should be accounted for. One of these factors is the degree of bonding of the individual particles by the firing process.

7. Comparison With Other Results

Figure 3 gives a comparison of the results of the NBS measurements on BeO with the results of measurements at other laboratories on other samples. At the lower temperatures, the agreement with Scholes [7] is probably as good as the physical states of the two samples permit. Scholes used a sample having a density of about 2.97 g/cm³ as compared with the NBS sample having a density of 2.62. At higher temperatures, the results of Francl and Kingery [5] are consistently higher than the NBS results. They used a sample having a density of 2.86 g/cm³, but this would probably account for only a small part of the difference. The results of

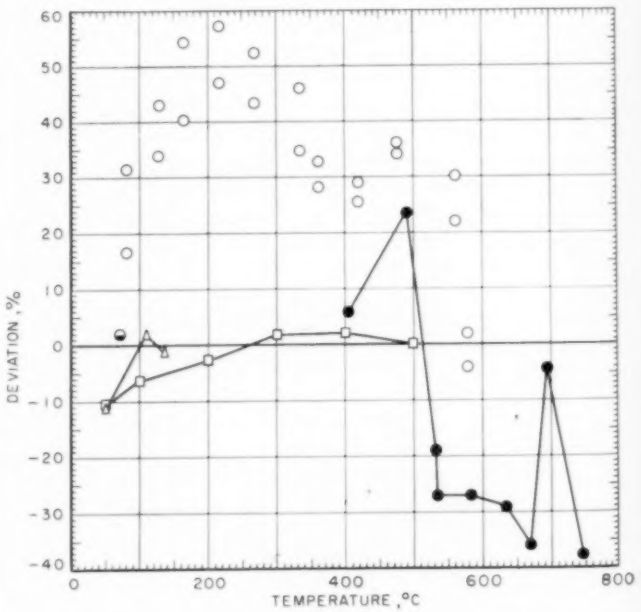

FIGURE 3. *Comparison of beryllium oxide thermal-conductivity data.*

Base line = NBS smoothed data.
△, Scholes (1950); ○, Francl and Kingery (1954); ●, Adams (1954); □, Powell (1954); ◒, Weeks and Seifert (1953).

Adams [8] are lower than the NBS results at higher temperatures, even though the samples had about the same densities (2.7 as compared to 2.62). Powell [6] measured the thermal conductivities of several samples of BeO having densities ranging from 1.85 to 2.82. His results, shown in figure 3, are interpolated for a density of 2.62 to compare with the NBS results; in general, the agreement is very good. Weeks and Seifert [9] determined the conductivity of a sample of BeO (density 3.0) at 70° C. Their agreement with the NBS value is probably better than the differences in the samples warrant.

The authors thank L. M. Doney, Oak Ridge National Laboratory, for furnishing the BeO sample used in this investigation, and S. M. Lang, National Bureau of Standards, for firing the sample at a high temperature.

The work described in this paper was sponsored by the Wright Air Development Center. The results that are given were taken from a report [2] submitted to that agency.

8. References

[1] E. D. West, D. A. Ditmars, and D. C. Ginnings, Technical Report 53–201, Part 5, to Wright Air Development Center (1954).
[2] D. A. Ditmars and D. C. Ginnings, Technical Report 53–201, Part 6 (1955).
[3] H. E. White and R. M. Schremp, J. Am. Ceram. Soc. **22,** 185 (1939).
[4] Reference tables for thermocouples, NBS Circular 506 (1951).
[5] J. Francl and W. D. Kingery, J. Am. Ceram. Soc. **37,** 80 (1954).
[6] R. W. Powell, Trans. Brit. Ceram. Soc. **53,** 389 (1954).
[7] W. A. Scholes, J. Am. Ceram. Soc. **33,** 111 (1950).
[8] Milton Adams, J. Am. Ceram. Soc. **37,** 74 (1954).
[9] J. L. Weeks and R. L. Seifert, Rev. Sci. Instr. **24,** 1054 (1953).

Washington, August 22, 1955.

Journal of Research of the National Bureau of Standards Vol. 59, No. 2, August 1957 Research Paper 2776

A Self-Balancing Direct-Current Bridge for Accurate Bolometric Power Measurements

Glenn F. Engen

Until recently, the most accurate microwave power measurements of the bolometric type have required the use of a manual d-c bridge. A self-balancing d-c bridge has been developed that preserves the inherent accuracy of the manual bridge, extends the dynamic range of operation, and greatly simplifies the operating procedure. A general description of the equipment and operating techniques is given, followed by a comprehensive survey of the sources of error accompanying the method and the accuracy achieved.

1. Introduction

A large amount of the research effort expended in the field of low level microwave power measurement in the past few years has been directed toward a determination of bolometer-mount efficiencies, or evaluation of the validity of the r-f–d-c substitution principle.[1,2,3,4] Until recently the only accessory instrument of sufficient accuracy to utilize the results of these investigations has been a manually operated d c Wheatstone bolometer bridge. The use of this device is, however, both tedious and time consuming; the dynamic range over which the desired accuracy is achieved is rather small, and the danger of barretter burnout due to a misstep on the part of the operator is ever present.

A self-balancing d-c bolometer bridge has been developed at the NBS Boulder Laboratories, which to a large measure relieves these problems, while preserving the accuracy and extending the dynamic range of operation. To date, the technique has been employed primarily with barretter-type elements, although on the basis of preliminary results, the technique should prove equally useful with thermistors.

2. Manual Bridge

One of the simplest forms of the manual bridge previously employed at the National Bureau of Standards is shown in figure 1. The r-f power [5] is given by

$$P_{rf}=\frac{r_0}{4}(i_1^2-i_2^2), \qquad (1)$$

where i_1 and i_2 are the total currents required to balance the bridge without and with r-f power present, respectively. A precision potentiometer-standard resistor combination is used to measure i_1 and i_2. If it is assumed that this measurement contains a random error of ± 0.005 percent, it can be shown that for a typical bolometer operating at 200 ohms and requiring 8.5 ma of bias ($i_1=17$ ma) the error in measuring P_{rf} may be as large as 0.02, 0.3, and 3 percent at the 10, 1, and 0.1 mw levels, respectively, if all other sources of error are neglected. The small difference between i_1 and i_2 at low levels accounts for the deterioration in accuracy. A variety of alternative techniques have been proposed and employed with some degree of success, but it is not within the scope of this paper to examine the manual technique in detail or to establish the maximum accuracy obtainable. In practice, this is often determined by the stability requirements imposed on the generator and measuring system by the time-consuming nature of the technique, rather than by more fundamental limitations.

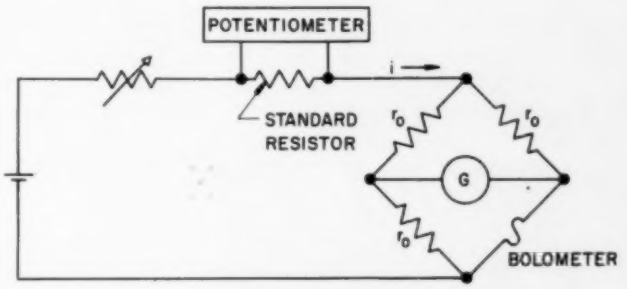

FIGURE 1. *Manual direct-current bolometer bridge.*

3. Self-Balancing Bridge

The self-balancing d-c bolometer bridge employs a d-c amplifier in a feedback loop to balance the bolometer bridge. The amplifier is connected in such a manner that the bridge unbalance signal is amplified to provide the bridge current (fig. 2). The use of this self-balancing circuit eliminates many of the time-consuming features of the technique, but the power-measurement problem is essentially the same. This problem, at low power levels, is basically one of trying to accurately measure a small change in a comparatively large d-c power.

[1] R. W. Beatty and Frank Reggia, An improved method of measuring efficiencies of ultra-high-frequency and microwave bolometer mounts, J. Research NBS **54**, 321 (1955) RP2594.
[2] A. C. Macpherson and D. M. Kerns, A microwave microcalorimeter, Rev. Sci. Instr. **26**, 27 (1955).
[3] H. J. Carlin and Max Sucher, Accuracy of bolometric power measurements, Proc. Inst. Radio Engrs. **40**, 1042 (Sept. 1952).
[4] D. M. Kerns, Determination of efficiency of microwave bolometer mounts from impedance data, J. Research NBS **42**, 579 (1949) RP1995.
[5] More correctly, "the retracted d-c power".

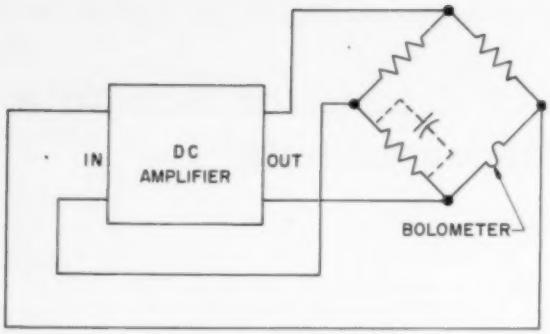

FIGURE 2. *Basic circuit of self-balancing bridge.*

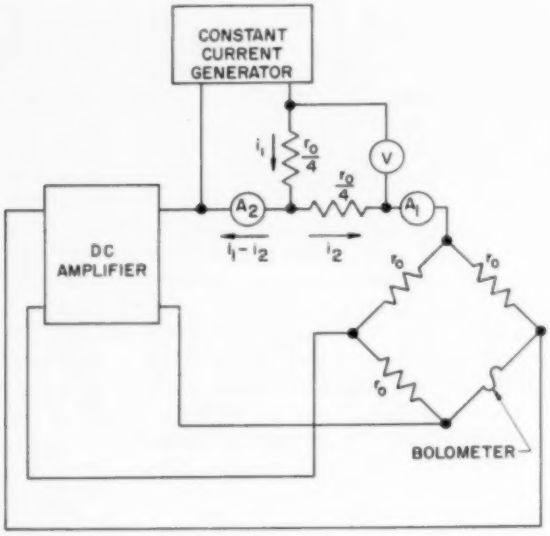

FIGURE 3. *Basic circuit for the determination of Δi and power.*

The formula for the r-f power may be rewritten

$$P_{rf}=\frac{r_0}{4}(i_1+i_2)(i_1-i_2) \tag{2}$$

$$=\frac{r_0}{4}(2i_1-\Delta i)\Delta i, \tag{3}$$

where $\Delta i=i_1-i_2$.

The difficult factor to measure accurately is Δi. A constant-current generator of high stability has been developed for use in conjunction with a differential current-measuring technique, which enables a direct and accurate determination of Δi. The circuit is illustrated in figure 3 and operates as follows: First, with no microwave power present in the bolometer, i_1 is determined by ammeter A_1, and the output of the constant-current generator is adjusted with the aid of ammeter A_2 to equal i_1 (ammeter A_2 reads zero). Then, with microwave power applied, A_2 will read Δi directly, and the power may be determined from eq (3). In practice, a potentiometer and standard resistor are employed in place of A_1 and A_2 to achieve high accuracy.

Alternatively, a voltmeter, V, connected as shown, will read $(r_0/4)\ (i_1+i_2)$, and the power is given by the product of V and A_2. These operations may also be combined in a single instrument of the dynamometer type to achieve a direct reading of the power.

The degree of success obtained with this technique is, of course, contingent upon the degree of stability achieved in the constant-current generator. In this case the change in generator output for a complete cutoff of bridge current is less than 1 part in 10^5, resulting in a negligible error from this source.

4. Performance

It is shown in a following section that the over-all accuracy in power measurement achieved, using a potentiometer to measure the current, is about 0.1 percent, whereas substitution of a suitable dynamometer to achieve direct reading is expected to yield an accuracy of about 0.3 percent. The instrument thus provides an increase in accuracy of 10 to 50 times that provided by the commercially avaiablel audiobridges. Other advantages over the tylpica audiobridge include: (1) Comparatively simple techniques are available for establishing, verifying, and monitoring the specified accuracy. (For example, the bridge balance may be monitored by a suitable galvanometer.) (2) The performance is, to a large degree, independent of the nominal deterioriation of the vacuum tubes and other electronic components. (3) The elimination of the audio bias power avoids its interaction with the pulse-repetition frequency in the measurement of pulse power.

At low power levels the r-f power is approximately proportional to Δi (eq 3), and the low-level performance may be displayed by recording this current with the r-f power alternately on and off. The system response to a 1-μw signal is given in figure 4.

Barring failure of the electronic components, the self-balancing operation eliminates the danger of bolometer burnout due to excessive bias current, whereas protection against an r-f overload may also

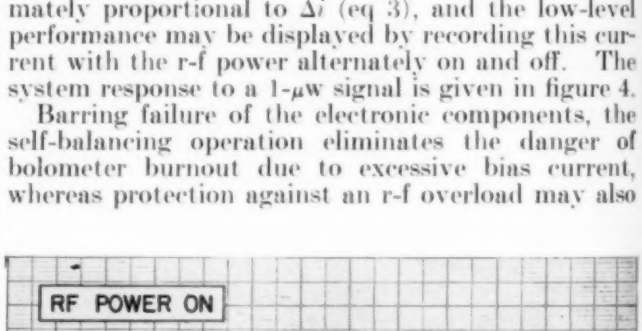

FIGURE 4. *Bridge response to a 1-microwatt signal.*
(Radiofrequency on and off for 1-minute intervals)

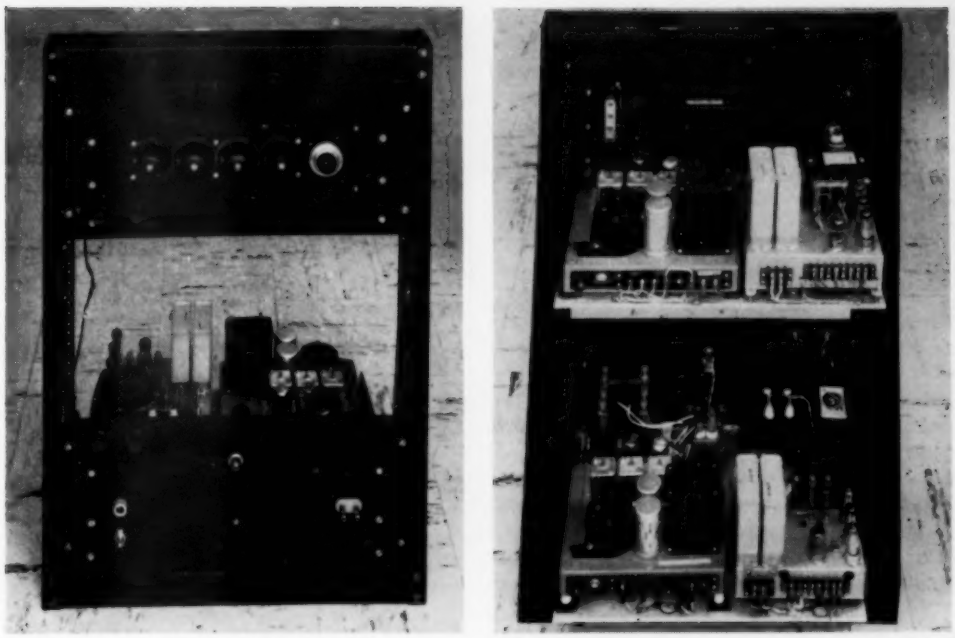

FIGURE 5. *Prototype model of self-balancing bridge, front and rear views.*

be provided through use of a suitable relay to turn off the r-f source when the power input to the bolometer exceeds a prescribed amount.

The d-c amplifier employed in this application is a commercially available instrument of exceptional gain, zero stability, and phase response, which was modified by the addition of a cathode follower to provide the required output current. The current amplification of the amplifier, as thus modified, is approximately 100,000. Compensation for the thermal lag of the bolometer is provided in the feedback loop by means of a condenser, as indicated in figure 2, but the achievement of stable operation with this large amplification is primarily a tribute to the amplifier phase response. The constant-current generator employs a second amplifier of the same type, which, with modification, maintains a constant-output current by reference against a mercury cell. A prototype model of this equipment is shown in figure 5.

5. Analysis of Errors

The practical problems involved in making an accurate determination of the power, using eq (1) to (3), have been noted. But use of these formulas implies that the bridge is exactly balanced, the bridge arms are equal to r_0, etc. It is shown in the appendix that a more complete expression for the power is

$$P_{rf}\simeq\frac{r_0}{4}(i_{b1}^2-i_{b2}^2)\left[1+Z-\frac{r_l}{r_0}+\frac{2e}{r_0(i_{b1}+i_{b2})}\left(1+\frac{8}{\gamma i_{b1}i_{b2}}\right)+\frac{16(1+g)}{\gamma i_{b2}(i_{b1}+i_{b2})}\left(\frac{1}{\alpha}-\frac{i_{g1}}{i_{b1}}\right)-\frac{2g}{(i_{b1}+i_{b2})}\left(\frac{i_{b1}}{\alpha}+i_{g2}\right)\right], \quad (4)$$

where

$\alpha=(i_{b1}-i_{b2})/(i_{g1}-i_{g2})$=current amplification of amplifier
Z=fractional deviation of the lower bridge arm from the value r_0
r_l=resistance of bolometer leads
e=thermal (or other) emf in amplifier input
i_b=total bridge current
i_g=amplifier input current
gr_0=amplifier input resistance
γ="ohms per watt" bolometer coefficient.

For a typical bolometer operating in the 0 to 10-mw region, the following values may be assigned:

$r_0=200$ ohms
$\gamma=4.5$ ohms/mw
$i_{b1}=17$ ma
$i_{b2}>8$ ma

Substituting these values in the above expression yields the result

$$P_{rf}\simeq\frac{r_0}{4}(i_{b1}^2-i_{b2}^2)\left[1+Z-\frac{r_l}{r_0}+5.6e+18(1+g)\left(\frac{1}{\alpha}-\frac{i_{g1}}{i_{b1}}\right)-80g\left(\frac{i_{b1}}{\alpha}+i_{g2}\right)\right],$$

where the last three terms in the bracket reflect the inability of the d-c amplifier to balance the bridge exactly.

The characteristics of the d-c amplifier employed in this application are such that the following values

obtain:

$g=1/4$ (amplifier input resistance 50 ohms)

$\alpha>10^5$ (current amplification)

$0<i_{g1}/i_{b1}<2\times10^{-5}$
$0<i_{g2}<10^{-7}$
$|e|<10^{-6}$
} (amplifier zero stability).

Substituting these values in the last three terms gives a value for their sum of about 0.0002.

The bolometer lead resistance can be measured with little effort and the correction applied, so the error from this source is negligible, whereas the value of $|Z|$ can ordinarily be held to 0.0001 or less.

Finally, it is possible to measure current by means of a precision potentiometer-standard resistor combination to an accuracy of a few parts in 10^4; thus the first factor in eq (4) may be determined by the technique discussed earlier to an accuracy of about 0.06 percent.

In summary, the total limits of error are as follows:

Deviation of bridge arms from value r_0	0.01 percent.
Failure of bridge to be exactly balanced	.02 percent.
Measurement of $i_{b1}+i_{b2}$	.03 percent.
Measurement of $i_{b1}-i_{b2}$	.03 percent.
Bolometer lead resistance	.00 percent.
Amplifier noise and instability (experimentally observed)	0.1 μw.
Total	.09 percent + 0.1 μw.

6. Appendix

From figure 6 the power may be expressed in the form

$$P_{rf}=\frac{r_0}{4}(i_{b1}^2-i_{b2}^2)+f(X,Y,Z,i_g,e,r_l) \tag{5}$$

where X, Y, and Z are the deviations of each of the bridge arms from the value r_0, i_g and e are the detector current and thermal (or other) emf, respectively, and r_l the resistance of the bolometer leads.

Assuming a knowledge of the bolometer resistance law, an exact expression for the second term could be derived, but the labor required suggests the following approximate treatment. By hypothesis, the variables $X \ldots r_l$ and $f(X \ldots r_l)$ are small, and $f(X \ldots r_l)$ may, to a good approximation, be written as the sum of the first-order corrections for each of these quantities, where the correction for each of the variables is determined with the other variables equal to zero.

Application of this technique to the circuit in figure 6 yields the following first-order expressions for the d-c power dissipated in the bolometer, and the bolometer resistance

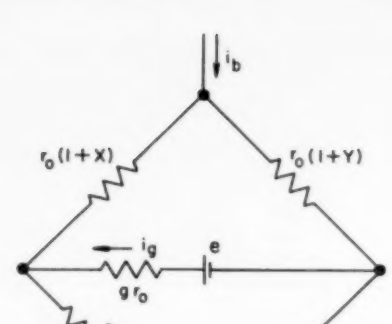

FIGURE 6. *Bridge circuit used in the evaluation of errors.*

$$P_{dc}\cong\frac{i_b^2 r_0}{4}\left[1+Z-\frac{r_l}{r_0}+\frac{2e}{r_0 i_b}-\frac{2gi_g}{i_b}\right], \tag{6}$$

$$r\cong r_0\left[1+x-y+Z-\frac{r_l}{r_0}+\frac{4e}{i_b r_o}-\frac{4(1+g)i_g}{i_b}\right]. \tag{7}$$

The failure of the expression for power to have a first-order dependence on X or Y is explained as follows: A prescribed, small value for X or Y will cause a first-order variation in bolometer resistance r, as indicated in eq (7), but also produces an unequal division of current in the two sides of the bridge. These two sources of error cancel to a first approximation. The only general requirement on the upper bridge arms is that they be equal, and if they have a nominal value of r_0, it can be shown that they may differ from each other by as much as 2 percent and produce an error in the power measurement of only 0.01 percent.

At a constant ambient temperature and assuming equivalence of d-c and r-f heating,[6] the power, P, dissipated in the bolometer will be a function of its resistance, r:

$$P=f(r).$$

Because the bolometer is nearly a square-law detector, one may in the neighborhood of an arbitrarily selected operating resistance r_0, write

$$P\cong P_0+\frac{\partial P}{\partial r}(r-r_0),$$

where P_0 is the power required to bring the bolometer to the resistance r_0 at the given ambient temperature, P is the sum of the d-c and r-f power, $P=P_{dc}+P_{rf}$, and $\partial P/\partial r$ is the reciprocal of the "ohms-per-watt"

[6] The r-f–d-c substitution error is assumed to be negligible in this discussion. For a treatment of this problem, see footnotes 2 and 3.

bolometer coefficient, i. e., $(\partial P/\partial r)=(1/\gamma)$. Then

$$P_{dc}+P_{rf}\cong P_0+\frac{1}{\gamma}(r-r_0).$$

P_0 may be determined by measurements in the absence of r-f power:

$$P_0\cong P_{dc}-\frac{1}{\gamma}(r_1-r_0),$$

where the subscript 1 has been used to indicate the value of quantities measured in the absence of r-f power, whereas the subscript 2 will indicate values with r-f present.

The formula for r-f power is then

$$P_{rf}=P_0-P_{dc}+\frac{1}{\gamma}(r_2-r_0)=P_{dc1}-P_{dc2}-\frac{1}{\gamma}(r_1-r_2). \quad (8)$$

In the given application, only i_g of the variables $X \ldots r_l$ has a functional dependence upon i_b, or is subject to change with the application of r-f power. Substituting eq (6) and (7) in eq (8) gives the desired result

$$P_{rf}\cong\frac{r_0}{4}(i_{b1}^2-i_{b2}^2)\left[1+Z-\frac{r_l}{r_0}+\frac{2e}{r_0(i_{b1}+i_{b2})}\left(1+\frac{8}{\gamma i_{b1}i_{b2}}\right)\right.$$
$$\left.+\frac{16(1+g)}{\gamma i_{b2}(i_{b1}+i_{b2})}\left(\frac{1}{\alpha}-\frac{i_{g1}}{i_{b1}}\right)-\frac{2g}{(i_{b1}+i_{b2})}\left(\frac{i_{b1}}{\alpha}+i_{g2}\right)\right],$$

where

$$\alpha=\frac{i_{b1}-i_{b2}}{i_{g1}-i_{g2}}.$$

The author extends his thanks to R. W. Beatty and John E. Lauer for their valuable criticisms and suggestions in the preparation of this paper, and to Ray R. Rumfelt for his assistance in the design and construction of this equipment.

Boulder, Colo., November 28, 1956.

Journal of Research of the National Bureau of Standards Vol. 59, No. 2, August 1957 Research Paper 2777

Some Observations on Hydrated Monocalcium Aluminate and Monostrontium Aluminate

Elmer T. Carlson

Monocalcium aluminate hydrate, probably having the composition $CaO \cdot Al_2O_3 \cdot 10H_2O$, was prepared by precipitation from calcium aluminate solutions at 1° C, and by hydration of pastes of monocalcium aluminate or aluminous cement. It was obtained as hexagonal prisms, very weakly birefringent, with mean index 1.471. Three molecules of water were expelled by drying over $CaCl_2$, without apparent change in crystal structure; however, the structure was destroyed by heating to 175° C. Monostrontium aluminate hydrate was obtained by analogous methods in the form of minute needles or prisms with mean index 1.478. The maximum degree of hydration was not successfully determined, as the compound underwent decomposition to $3SrO \cdot Al_2O_3 \cdot 6H_2O$ and gibbsite. X-ray diffraction powder patterns indicate a close similarity in structure between the monocalcium and monostrontium aluminate hydrates.

1. Introduction

The existence of a monocalcium aluminate hydrate has been, for many years, a matter of some uncertainty among investigators in the field of cement hydration. Over 20 years ago, Assarsson [1] [1] reported the preparation of a compound having the composition $CaO \cdot Al_2O_3 \cdot 10H_2O$. It was obtained in the form of a "gel" by the action of water on anhydrous calcium aluminates and aluminous cements. Although Assarsson gave an X-ray diffraction powder pattern for the material, this in itself was not conclusive evidence of the existence of a monocalcium aluminate hydrate. A number of other hydrated calcium aluminates give somewhat similar patterns, and the gel might conceivably have been a mixture of two or more phases.

More recently, Longuet [2] reported the preparation of a compound for which he indicated the formula $CaO \cdot Al_2O_3 \cdot 7H_2O$ as most probable. He also gave an X-ray diffraction pattern, differing in several respects from that given by Assarsson.

It has been pointed out in a previous paper [3] that the two patterns probably can be reconciled; also, that patterns agreeing in general with that of Longuet have been obtained at the Bureau on hydrated pastes of aluminous cements and of monocalcium aluminate. Because of the probable importance of this compound in the setting and hardening of aluminous cements, some additional work was undertaken in an attempt to obtain the hydrate in better crystallized form.

While this study was in progress, two additional important investigations bearing on the subject were reported in the literature. In the revised edition of "The Chemistry of Cement and Concrete" [4], Lea gives an X-ray diffraction pattern obtained by H. G. Midgley for $CaO \cdot Al_2O_3 \cdot 10H_2O$. The pattern agrees fairly well with the more abbreviated patterns given by both Assarsson and Longuet. Farran [5] developed a novel technique for the study of crystal formation at the interface between cement and aggregate, and by this means obtained crystals of a monocalcium aluminate hydrate large enough for a determination of optical properties and shape. The crystals grew from a paste of aluminous cement, and the hydration product contained small amounts of one or more other phases. Farran also published an X-ray pattern for his preparation.

The existence of a monocalcium aluminate hydrate thus seems established. Because of the close relationship between calcium and strontium, it was considered of interest to determine whether a monostrontium aluminate hydrate also can be prepared.

2. Apparatus and Procedure

From the work of Assarsson [1] it appeared likely that formation of the monocalcium aluminate hydrate would be favored by low temperature; consequently, in the present study, most of the reaction mixtures were held near the freezing point. A household refrigerator, equipped with a special control unit and a blower, was used as a cold cabinet. The temperature ranged between 0° and 2° C.

Supersaturated solutions were prepared by shaking synthetic anhydrous monocalcium aluminate with water, filtering, and diluting the filtrate with distilled water or lime water as required. The solutions were kept in polyethylene bottles. A similar procedure was used in the study of the strontium analog.

The solutions were allowed to stand in the cold cabinet until precipitation was essentially complete, which in one case required several months. The precipitate was then separated by filtration with the aid of an aspirator and a suction train to minimize contamination by atmospheric carbon dioxide. Washing was omitted, because the solutions were extremely dilute, and the resulting contamination was negligible.

In addition to the experiments based on precipitation from supersaturated solutions, a few were conducted with pastes made from the anhydrous aluminates with small amounts of water.

[1] Figures in brackets indicate the literature references at the end of this paper.

3. Results and Discussion

3.1. Monocalcium Aluminate Hydrate

Data pertaining to three preparations of monocalcium aluminate hydrate are given in table 1. The precipitate in No. 1 was so finely divided that it formed a flocculent suspension that failed to settle out completely. Under the light microscope it appeared amorphous, but its crystalline character was revealed by the electron microscope, as well as by X-ray diffraction. Figure 1 is an electron micrograph of this preparation. Other areas in the field showed some poorly defined matted fibers, possibly of amorphous hydrated alumina, and a very few hexagonal plates, much larger in size, were also noted. Neither of these phases is visible in figure 1. The X-ray diffraction pattern was similar to those reported by other investigators [1, 2, 4, 5] for monocalcium aluminate hydrate. No additional diffraction lines were observed.

The precipitate from solution 2 formed aggregates of fine crystals, which settled rather rapidly after the mixture was shaken. When first examined microscopically, 11 days after the reaction mixture was prepared, the precipitate was well formed. There was no visible change in it at 74 days, when it was filtered off. The crystals apparently were isotropic, with a refractive index about 1.47. The index was observed to vary with the degree of drying. Under the electron microscope the preparation appeared to consist of aggregates of prismatic crystals, much larger than those of preparation 1. Some of the prisms showed terminal pyramids. A few hexagonal plates were also observed. The X-ray diffraction pattern was similar to that of the first preparation, but the intensities were stronger. A very weak line corresponding to the strongest reflection of $2CaO \cdot Al_2O_3 \cdot 8H_2O$ was also observed.

Preparation 3 was initially much more dilute than the others. Gibbsite was added to the solution, in the amount of 1 g for 1 liter, to hasten the precipitation, because it was supposed at the time that gibbsite would be the stable phase in this area. Precipitation was negligible during the first month, but after 6 months a new solid phase was observed, mixed with the gibbsite. It consisted of short hexagonal prisms with terminal pyramids (see fig. 2), occurring singly or in clusters. Also, in many cases, it appeared as a chainlike aggregate of crystals, which appeared to have grown around a long, slender needle. When viewed in contact with the solution in which they were grown, the prisms showed extremely low birefringence. The index of refraction of the prisms agreed with that of preparation 2, and the X-ray diffraction patterns showed that they were the same phase. The nature of the needles is unknown; they had the same index of refraction as the prisms, but showed slightly higher birefringence. A few of the needles may be observed in figure 2. The prismatic crystals are similar in appearance to those described by Farran, except that Farran's crystals are, in comparison, much shorter in the direction of the prism axis.

In addition to gibbsite and monocalcium aluminate hydrate, another phase was present in minor amount in preparation 3. It consisted of large hexagonal plates, and was at first assumed to be $2CaO \cdot Al_2O_3 \cdot 8H_2O$. The X-ray diffraction pattern, however, showed no trace of the dicalcium compound. It did contain three weak lines that could be attributed to tetracalcium aluminate hydrate, along with strong patterns of monocalcium aluminate hydrate and gibbsite. The appearance of tetracalcium aluminate in this region of the system, however, would be contrary to expectations based on earlier work at 21° C [6].

The molar oxide ratio, CaO/Al_2O_3, in preparation 1, determined by chemical analysis, was 1.04. In preparation 2 it was 1.01. Greater weight is attached to the latter value, because this preparation was microscopically almost homogeneous. The only observable impurity was dicalcium aluminate hydrate, present in amount estimated at less than 5 percent. Preparation 3 was not analyzed, as there were three solid phases present; also, the amount of material available was very small. Additional gibbsite may have been precipitated (as was originally expected), in which case it would be indistinguishable from that initially added. Hence, the oxide ratio 0.57, calculated from the change in concentration of the solution, does not even approximately represent the composition of any one solid phase.

Accepting the oxide ratio as 1 to 1, there remains the question of the amount of water of hydration.

TABLE 1. *Data pertaining to preparation of* $CaO \cdot Al_2O_3 \cdot 10H_2O$ *from calcium aluminate solutions at approximately 1° C*

Preparation	Initial concentration of solution		Duration of storage	Solid phases present at end of storage	Final concentration of solution		Molar ratio in precipitate CaO/Al_2O_3	Appearance of precipitate
	CaO	Al_2O_3			CaO	Al_2O_3		
	g/liter	*g/liter*	*Days*		*g/liter*	*g/liter*		
1	0.833	1.278	34	$CaO \cdot Al_2O_3 \cdot 10H_2O$; very few hexagonal plates; probably some amorphous hydrated Al_2O_3.	0.198	0.148	1.04	Gelatinous.
2	.879	1.150	74	$CaO \cdot Al_2O_3 \cdot 10H_2O$; trace of $2CaO \cdot Al_2O_3 \cdot 8H_2O$.	.300	.104	1.01	Finely crystalline aggregates.
3 [a]	.327	0.466	210	Gibbsite; $CaO \cdot Al_2O_3 \cdot 10H_2O$; hexagonal plates in minor amount.	.229	.152	0.57 [b]	Aggregates and separate crystals.

[a] Gibbsite added (1 g in 1 liter). [b] Calculated from change in concentration of the solution.

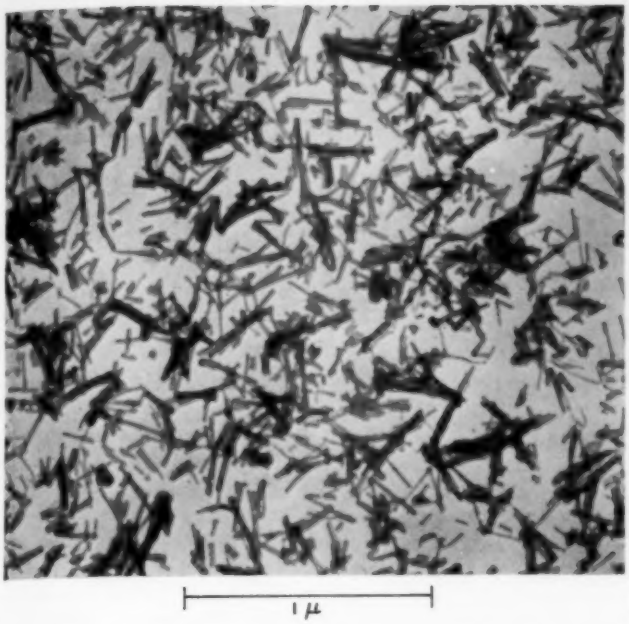

FIGURE 1. *Electron micrograph of monocalcium aluminate hydrate (preparation 1).*

Magnification 32,500 diameters.

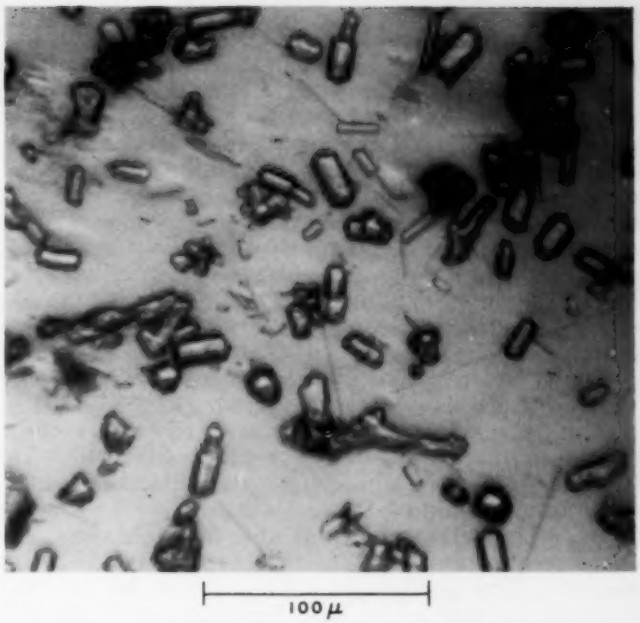

FIGURE 2. *Photomicrograph of monocalcium aluminate hydrate (preparation 3).*

Magnification 300 diameters.

Assarsson [1] concluded from his analyses that the hydrate contained 10 molecules of water. Longuet [2] reported approximately 7 molecules of water in his preparations after drying at 45-percent relative humidity.

In the present study, preparation 2, after standing in a desiccator over $CaCl_2$ for 3 months, had an ignition loss equivalent to 7.13 moles of H_2O per mole of Al_2O_3. When placed over a saturated solution of $CaSO_4$ at room temperature (relative humidity assumed to be 98%) it rapidly took up water until the ratio of H_2O to Al_2O_3 reached 9.9 at the end of 2 days, remaining essentially constant thereafter. A similar preparation confined over saturated NH_4Cl (relative humidity about 79%) attained a ratio $H_2O/Al_2O_3=9.8$. The results of these experiments strongly suggest that the fully hydrated compound has the composition $CaO{\cdot}Al_2O_3{\cdot}10H_2O$. (This formula, though not definitely established, is used in this report to designate the compound.)

Three of the molecules of water apparently are very loosely bound, as they can be removed by drying over $CaCl_2$.

Monocalcium aluminate hydrate was also prepared by mixing anhydrous monocalcium aluminate with a little water and storing the paste in the cold cabinet for 10 days. The X-ray diffraction pattern indicated the presence of $CaO{\cdot}Al_2O_3{\cdot}10H_2O$, with smaller amounts of $2CaO{\cdot}Al_2O_3{\cdot}8H_2O$ and unhydrated $CaO{\cdot}Al_2O_3$. Under similar conditions, a white aluminous cement, consisting essentially of Al_2O_3 and CaO, likewise, was partially hydrated to monocalcium aluminate hydrate.

It has been shown that monocalcium aluminate hydrate may be prepared at approximately 1° C. There is evidence that it may also form at slightly higher temperatures. Farran's preparations were made at 15° C, whereas Midgley (as reported by Lea [4]) obtained $CaO{\cdot}Al_2O_3{\cdot}10H_2O$ at 1° and 20° C, but not at 25° C. In the present study, a few experiments with pastes led to the formation of monocalcium aluminate hydrate at 25° C. Thus, when monocalcium aluminate paste was hydrated at 25° C for 10 days, the X-ray diffraction pattern indicated the presence of monocalcium aluminate hydrate, together with a somewhat greater amount of dicalcium aluminate hydrate. As reported in a previous paper [3], similar experiments with the pastes of three aluminous cements at 24° C also gave evidence of the formation of monocalcium aluminate hydrate. These experiments have since been extended to include a white aluminous cement, known to consist largely of monocalcium aluminate and corundum. On curing for 7 days at 25° C, the cement was partly hydrated to $CaO{\cdot}Al_2O_3{\cdot}10H_2O$ and a smaller amount of $2CaO{\cdot}Al_2O_3{\cdot}8H_2O$.

From the foregoing discussion, it is evident that monocalcium aluminate hydrate can be formed at temperatures as high as 25° C. In view of this fact, it is rather surprising that Wells, Clarke, and McMurdie [6], in their study of the system $CaO-Al_2O_3-H_2O$ at 21° C, failed to observe any such compound. Perhaps the explanation may be found in the difference in experimental conditions. The experiments of Wells et al. were performed not with pastes but with relatively large volumes of solutions.

There is evidence that in some earlier work of Wells [7], monocalcium aluminate hydrate was obtained at least once by precipitation from solution

at room temperature. The actual temperature, unfortunately, was not recorded. The solution was an aqueous extract of an aluminous cement. The crystals obtained were well formed and similar in appearance to those shown in figure 2. Another precipitated phase (presumably hydrated alumina) was also present; hence the composition of the crystals could not be determined. The following optical properties were recorded: $\omega=1.477$; $\epsilon=1.492$; uniaxial positive. Apparently the phase was not observed again, although the study [3] included a large number of similar experiments. It is reasonable to assume, however, that the unknown crystals found by Wells were $CaO{\cdot}Al_2O_3{\cdot}10H_2O$.

The completely hydrated crystals obtained in the present study had a refractive index of 1.471, with birefringence too faint to measure. After the crystals had been dried to a water content equivalent to $CaO{\cdot}Al_2O_3{\cdot}7H_2O$, the birefringence was stronger, and the minimum and maximum indices were 1.477 and 1.480. The birefringence is still much lower than that reported by Wells for the crystals described in the preceding paragraph. No explanation for the discrepancy can be offered, because the degree of drying of Wells' crystals is unknown. Farran [5] reported the indices, $\omega=1.489 \pm 0.002$, $\epsilon=1.507 \pm 0.002$, but here again the amount of preliminary drying was not stated.

Although the optical properties of the monocalcium aluminate hydrate were measurably affected by the degree of drying, no significant change was observed in the X-ray diffraction pattern. The pattern given in table 2 is for the material rehydrated to the decahydrate stage. The pattern for the material dried to the heptahydrate stage showed lines agreeing closely with those in the table, with no apparent trend in either direction. The pattern in table 2 is in excellent agreement with that obtained by Midgley, as reported by Lea [4]. The difference between corresponding *d*-spacings does not exceed 0.02 A, except for the first line, for which the measurement error is necessarily high. Also, a few lines are reported as doublets in one pattern and as singlets in the other; and a very few weak lines are present in one pattern and not in the other. Good general correlation is also observed between these patterns and those of Assarsson [1], Longuet [2], and Farran [5], if allowance is made for the lines due to other phases present. Nevertheless, a few discrepancies are worthy of mention. The pattern given by Assarsson fails to show a spacing near 14 A, although the patterns reported by the other investigators show a strong line in this region. Limitations of the earlier X-ray equipment may account for this difference. The largest spacing reported by Assarsson was 7.68 A, whereas the line closest to this in the other patterns ranges in position from 7.16 to 7.3 A. No explanation for this discrepancy can be advanced at present. In other respects, the pattern of Assarsson agrees well with that given in table 2. Farran's pattern is likewise in agreement, except that a few of the weaker lines are absent. Longuet's pattern shows the same series of lines, but for some reason they are all displaced toward higher *d*-spacings in comparison with the other patterns.

TABLE 2. *X-ray powder diffraction patterns of* $CaO{\cdot}Al_2O_3{\cdot}10H_2O$ *and* $SrO{\cdot}Al_2O_3{\cdot}nH_2O$[a]

$CaO{\cdot}Al_2O_3{\cdot}10H_2O$		$SrO{\cdot}Al_2O_3{\cdot}nH_2O$[b]		$CaO{\cdot}Al_2O_3{\cdot}10H_2O$		$SrO{\cdot}Al_2O_3{\cdot}nH_2O$[b]	
d	*I*[c]	*d*	*I*	*d*	*I*[c]	*d*	*I*
A		A		A		A	
14.2	90	14.7	100	2.18	7	2.22	29
7.16	100	7.27	95	2.17	7	.....	.....
5.37	8	5.43	9	2.11	7	2.14	20
4.73	10	4.86	28	2.07	5	2.11	23
4.51	4	4.61	8	2.03	1	.....	.....
4.16	4	4.23	6	1.969	2	2.02	23
3.96	2	4.04	5	1.945	6	1.97	21
3.70	7	3.74	15	1.927	1	.....	.....
3.56	13	3.65	90	1.879	2	1.91	10
3.26	7	3.35	33	1.836	3	1.88	15
3.10	6	3.14	15	1.786	3	1.84	8
3.03	2	.....	.....	1.757	2	.....	.....
2.91	7	2.98	45	1.713	2	1.74	10
2.86	8	2.91	31	1.698	1	.....	.....
2.70	5	2.75	20	1.650	3	1.68	7
2.56	11	2.62	52	1.637	1	.....	.....
2.48	6	2.53	5	1.630	1	.....	.....
2.46	6	2.48	8	1.604	4	1.64	8
2.37	8	2.43	10	1.555	1	.....	.....
2.34	6	2.38	14	1.524	1	.....	.....
2.30	1	2.33	15	1.472	1	.....	.....
2.27	11	2.30	23	1.388	3	1.42	6

[a] Obtained on a Geiger-counter diffractometer, using copper Kα radiation.
[b] $n=8.4$ in sample used for determination of X-ray pattern. n may range from 7 to 10.
[c] d = interplanar spacing; I = relative intensity.

3.2. Monostrontium Aluminate Hydrate

In an earlier paper [8] on the strontium aluminates, it was reported that only the cubic tristrontium aluminate hydrate was formed by the various methods employed in that study. However, none of the experiments had been conducted below room temperature. It was, therefore, considered of interest to carry out some additional reactions in the cold cabinet.

In one experiment, anhydrous monostrontium aluminate was prepared by heating a mixture of strontium carbonate and alumina at 1,460° C, followed by fusion in an oxygen blast. A small amount of the material was ground and placed in a vial with just enough water to moisten it. It was then stored in the cold cabinet for 10 days. An X-ray pattern of the hardened mass showed a series of lines very similar to the pattern of monocalcium aluminate hydrate. Lines of unhydrated $SrO{\cdot}Al_2O_3$ were also present.

In another experiment, the new hydrate was prepared by a precipitation method analogous to that used for the calcium aluminate hydrate. For this purpose, anhydrous monostrontium aluminate was first prepared by heating a mixture of the hydrated oxides at 1,400° C. Combination was not complete, but further heating was avoided because increased crystal size would tend to lower the rate of solution. The product was ground, shaken with water, and filtered, and the filtrate was stored in a glass flask in the cold cabinet. The data relevant to two such experiments are given in table 3.

Because of the extreme fineness of the precipitate, the optical properties could not be accurately

TABLE 3. *Data pertaining to preparation of* $SrO \cdot Al_2O_3 \cdot 10H_2O$ *from strontium aluminate solutions at approximately 1° C*

Preparation	Initial concentration of solution		Duration of storage	Solid phase present at end of storage	Molar ratio SrO/Al_2O_3 in preparation	Appearance of precipitate
	SrO	Al_2O_3				
	g/liter	*g/liter*	*Days*			
1	4.43	2.62	14	$SrO \cdot Al_2O_3 \cdot 10H_2O$.	1.69	Needles.
2	6.92	5.66	2	$SrO \cdot Al_2O_3 \cdot 10H_2O$.	0.98	Slender prisms about 3 μ long.

determined. The crystals were acicular and slightly birefringent, with a mean index of refraction about 1.478.

The water content was determined by methods similar to those used for the calcium compound. After exposure to high humidity (over saturated $Ca(OH)_2$ solution) at 1° C, the H_2O/Al_2O_3 ratio was 9.9, whereas in material dried over $CaCl_2$ the ratio was 6.9. Thus, the strontium and the calcium compounds appear to be analogous in their response to humidity changes. However, it was found necessary to keep the strontium aluminate hydrate in the cold cabinet while exposing it to the higher humidity, because it decomposed at room temperature. The products of decomposition, identified by microscopic and X-ray methods, were $3SrO \cdot Al_2O_3 \cdot 6H_2O$ and gibbsite ($Al_2O_3 \cdot 3H_2O$).

The X–ray pattern given for the strontium aluminate hydrate in table 2 was obtained on a portion of preparation 1, which had been dried to a water content of about 8.4 moles per mole of $SrO \cdot Al_2O_3$. Because of the acicular habit of the crystals, the relative intensities indicated may be somewhat affected by orientation. The similarity between the patterns of the strontium and calcium aluminate hydrates is readily apparent.

The question may be asked whether barium might also form a monoaluminate hydrate analogous to those of calcium and strontium. In an earlier paper [9] a barium aluminate hydrate, $BaO \cdot Al_2O_3 \cdot 7H_2O$, was described. The amount of water of hydration is the same as that of the monocalcium and monostrontium aluminate hydrates dried over $CaCl_2$. However, the barium compound differs from those of calcium and strontium in crystal habit, indices of refraction, and birefringence, and gives a distinctly different X-ray pattern. It seems clear, therefore, that $BaO \cdot Al_2O_3 \cdot 7H_2O$ is not an analog of the monocalcium and monostrontium aluminate hydrates.

4. Summary

Monocalcium aluminate hydrate, probably having the composition $CaO \cdot Al_2O_3 \cdot 10H_2O$, was prepared by precipitation from calcium aluminate solutions at approximately 1° C, and by hydration of pastes of monocalcium aluminate and of aluminous cement at 1° and 25° C. Under conditions favorable for slow crystal growth, this hydrate crystallized as hexagonal prisms with terminal pyramids. They were very weakly birefringent, with a mean refractive index of 1.471. Drying over calcium chloride reduced the water of hydration to $7H_2O$, and the indices and birefringence increased, but the X-ray pattern was apparently unchanged.

An analogous monostrontium aluminate hydrate was prepared by similar methods, but it was obtained only as minute needles or prisms. Like the calcium analog, it probably crystallizes with 10 molecules of H_2O, 3 of which may be removed by drying over calcium chloride. The mean index of refraction is about 1.478. When placed in a humid atmosphere at room temperature it decomposed, with the formation of $3SrO \cdot Al_2O_3 \cdot 6H_2O$ and $Al_2O_3 \cdot 3H_2O$ (gibbsite).

X-ray powder diffraction patterns are given for both monocalcium aluminate hydrate and monostrontium aluminate hydrate. The similarity between the two is readily apparent.

The author acknowledges with thanks the assistance of several members of the Constitution and Microstructure Section of the Bureau, who prepared the X-ray diffraction patterns and the electron and photomicrographs.

5. References

[1] G. Assarsson, Sveriges Geol. Undersokn. **27** Ser. C, No. 379, **22** (1933).
[2] P. Longuet, Symposium Chem. Cements, p. 328 (London, 1952).
[3] L. S. Wells and E. T. Carlson, J. Research NBS **57,** 335 (1956) RP2723.
[4] F. M. Lea, The chemistry of cement and concrete, ch. IX and appendix III (St. Martin's Press, Inc., New York, N. Y. 1956).
[5] J. Farran, Rev. matériaux construction et trav. publ., C. No. 490–491, 155; No. 492, 191 (1956).
[6] L. S. Wells, W. F. Clarke and H. F. McMurdie, J. Research NBS **30,** 367 (1943) RP1539.
[7] L. S. Wells (unpublished data, 1929).
[8] E. T. Carlson, J. Research NBS **54,** 329 (1955) RP2595.
[9] E. T. Carlson and L. S. Wells, J. Research NBS **41,** 103 (1948) RP1908.

WASHINGTON, January 31, 1957.

426700—57——3

Journal of Research of the National Bureau of Standards Vol. 59, No. 2, August 1957 Research Paper 2778

Turbidity and Viscosity Measurements on Some Cationic Detergents in Water and in Sodium Chloride Solutions

Lawrence M. Kushner, Willard D. Hubbard, and Rebecca A. Parker

Light-scattering and viscosity measurements were made on solutions of three cationic detergents in distilled water and in various solutions of sodium chloride. The detergents were dodecylamine hydrochloride, dodecyltrimethylammonium chloride, and tetradecyltrimethylammonium chloride. The first of these was investigated at 30° C and the others at 23° C. The micellar weight and the intrinsic viscosity of the micelles of each detergent were calculated, and the dependence of these quantities on the concentration of sodium chloride is discussed.

1. Introduction

The anionic detergent sodium dodecyl sulfate has been the subject of a number of physical chemical investigations. Studies have been made on dilute aqueous solutions of the detergent with respect to light scattering [1, 2],[1] viscosity [3], and electrophoresis [4]. As a result, the micellar behavior of the material has been well characterized.

A particularly interesting feature of these investigations is the marked dependence of the physical property being measured (turbidity, viscosity, etc.) on the quantity of simple electrolyte in the solutions. In the case of light-scattering measurements, it is found that the addition of sodium chloride up to a concentration of about 0.05 to 0.06 M causes a large increase in the turbidity of the solutions. Accordingly, the micellar weight calculated from the data by the method of Debye [5] or Mysels [6] increases rapidly with increasing salt concentration in this range. The relative viscosity of the solutions decreases markedly in the presence of similar concentrations of simple electrolyte. This is reflected in the intrinsic viscosity which decreases rapidly in precisely the same range.

This paper describes the results of turbidity and viscosity measurements made on solutions of three cationic detergents in distilled water and in solutions of sodium chloride. Dodecylamine hydrochloride was chosen because its surface active ion is the positively charged analog of the dodecyl sulfate ion. Because of the poor solubility of the primary amine hydrochloride in salt solutions, measurements were also made on a comparable quaternary salt, dodecyltrimethylammonium chloride. Tetradecyltrimethylammonium chloride was investigated to give an indication of the effect of increasing the chain length of the hydrophobic portion of the surface active ion.

[1] Figures in brackets indicate the literature references at the end of this paper.

2. Experimental Procedure

2.1. Materials

Dodecylamine hydrochloride was prepared from dodecylamine in the following manner. Fifty grams of dodecylamine (Armour & Co.) was dissolved in anhydrous benzene. Gaseous hydrogen chloride was bubbled through the solution until a slight excess, as indicated by a methyl redspot test, had been added. The solution was cooled to approximately 0° C, and the dodecylamine hydrochloride crystals were filtered off at that temperature. The material was then recrystallized twice in the same manner from benzene and finally dried overnight in a vacuum oven at 60° C. As a check on the purity of the salt, the specific conductance of a 0.01354-N aqueous solution was determined at 30° C. A value of 13.62×10^{-4} ohm^{-1} was obtained. This is to be compared with the value 13.64×10^{-4} ohm^{-1} given by Armour & Co. The chloride content was determined to be 15.96 percent. The theoretical value is 15.99 percent.

Subsequent measurements of the turbidity of aqueous solutions of the dodecylamine hydrochloride indicated the presence of traces of a water-insoluble impurity, suspected to be benzene. Two recrystallizations of the salt from cold methyl alcohol eliminated the contaminant.

Dodecyltrimethylammonium chloride and tetradecyltrimethylammonium chloride were obtained as the quaternary salts from Armour & Co. Both were purified by precipitating them from solutions of ethanol by the addition of anhydrous ethyl ether. The resulting slurry was cooled as before, and the crystals were removed by filtration. They were then dried under vacuum at room temperature.

2.2. Refractive Index

Measurements of the refractive-index increments ($\Delta n/\Delta c$) of the three detergents in distilled water and

TABLE 1. *Light-scattering and viscosity data for solutions of dodecylamine hydrochloride, dodecyltrimethylammonium chloride, and tetradecyltrimethylammonium chloride in distilled water and in solutions of sodium chloride*

(cp=centipoise; [η]=intrinsic viscosity; $\Delta n/\Delta c$=refractive index increment; CMC=critical micelle concentration; [Z]=intrinsic dissymmetry).

DODECYLAMINE HYDROCHLORIDE (30° C)

Solvent	Concentration	Density	Viscosity	[η]	Concentration	Turbidity	$\Delta n/\Delta c$	Micellar weight
	g/dl	*g/ml*	*cp*		*g/ml×10²*	*cm⁻¹×10⁵*	*ml/g*	
Distilled H_2O CMC=0.323 g/dl	0	0.99565	0.7975	0.064	0	4.76	0.161	17,800
	0.100	.99556	.....		0.089	5.00		
	.200	.99548	.....		.222	4.95		
	.300	.99539	.8000		.295	5.33		
	.400	.99531	.8095		.343	6.95		
	.500	.99523	.8148		.363	7.81		
	.600	.99515	.8189		.400	12.23		
	.800	.99498	.8327		.439	15.28		
	1.000	.99482	.8466		.505	20.42		
	1.100	.99473	.8519		.561	24.18		
	1.200	.99465	.8562		.680	31.42		
	.....	.....	.....		.800	38.70		
	.....	.....	.....		.907	40.08		
	.....	.....	.....		.927	40.89		
	.....	.....	.....		1.027	43.03		
	.....	.....	.....		1.188	45.17		
	.....	.....	.....		1.428	48.60		
	.....	.....	.....		1.648	51.31		
0.01−*M* NaCl CMC=0.272 g/dl	.....	.....	.....	.....	0	4.90	0.160	21,700
					0.075	5.14		
					.121	5.09		
					.190	5.47		
					.218	5.38		
					.275	5.95		
					.320	12.00		
					.410	21.13		
					.510	29.04		
					.610	34.84		
					.735	40.41		
					.815	43.32		
					1.015	49.46		
					1.215	54.36		
0.02−*M* NaCl CMC=0.227 g/dl	0	0.99646	0.7990	0.048	0	4.76	0.160	24,100
	0.100	.99638	.....		0.123	5.24		
	.200	.99630	.8037		.268	12.42		
	.300	.99621	.8075		.300	17.37		
	.400	.99613	.8118		.400	30.5		
	.500	.99605	.8161		.500	40.1		
	.600	.99596	.8205		.600	48.1		
	.800	.99580	.8298		.700	55.2		
	1.000	.99563	.8397		.800	61.4		
	.....	.....	.....		.900	66.6		
	.....	.....	.....		1.000	71.9		
	.....	.....	.....		1.100	76.6		
	.....	.....	.....		1.250	83.3		
0.04−*M* NaCl CMC=0.165 g/dl	0	0.99725	0.8006	0.039	0	5.24	0.160	28,200
	0.100	.99717	.8048		0.103	5.38		
	.200	.99709	.8051		.187	10.57		
	.300	.99702	.8089		.200	12.99		
	.400	.99694	.8114		.300	30.5		
	.500	.99686	.8159		.400	45.2		
	.600	.99678	.8199		.500	58.5		
	.800	.99663	.8287		.600	70.8		
	1.000	.99647	.8393		.700	81.6		
	.....	.....	.....		.800	91.7		
	.....	.....	.....		.900	101.2		
	.....	.....	.....		1.000	110.4		
	.....	.....	.....		1.100	120.0		
	.....	.....	.....		1.200	129.0		
	.....	.....	.....		1.250	133.8		
0.06−*M* NaCl CMC=0.145 g/dl	0	0.99807	0.8021	0.034	0	5.24	0.160	34,000
	0.100	.99798	.8091		0.101	5.24		
	.200	.99789	.8071		.200	20.8		
	.300	.99780	.8104		.300	42.8		
	.400	.99771	.8136		.400	62.8		
	.500	.99762	.8186		.500	80.4		
	.600	.99752	.8226		.650	105.7		
	.800	.99734	.8304		.750	121.9		
	1.000	.99716	.8399		.800	129.5		
	.....	.....	.....		.900	145		
	.....	.....	.....		1.000	158		
	.....	.....	.....		1.050	165		
	.....	.....	.....		1.100	171		
	.....	.....	.....		1.250	191		

in the sodium chloride solutions were made with a differential refractometer similar to that described by P. P. Debye [7]. All measurements were made at 23° C, using blue light (436 mμ). The refractive-index increments determined are given in table 1.

2.3. Turbidity

Measurements of turbidity were made in semi-octagonal cells in an absolute light-scattering photometer [8]. Semioctagonal cells were used so that determinations of dissymmetry, Z (the ratio of the

TABLE 1. *Light-scattering and viscosity data for solutions of dodecylamine hydrochloride, dodecyltrimethylammonium chloride, and tetradecyltrimethylammonium chloride in distilled water and in solutions of sodium chloride*—Continued

(cp=centipoise; $[\eta]$=intrinsic viscosity; $\Delta n/\Delta c$=refractive index increment; CMC=critical micelle concentration; $[Z]$=intrinsic dissymmetry)

Solvent	Concentration	Density	Viscosity	$[\eta]$	Concentration	Turbidity	$\Delta n/\Delta c$	Micellar weight
	g/dl	*g/ml*	*cp*		*g/ml*×10²	*cm*⁻¹×10⁵	*ml/g*	
0.08-*M* NaCl CMC=0.118 g/dl	0	0.99890	0.8036	0.038	0	5.24	0.160	51,100
	0.100	.99881	.8057		0.037	5.14		
	.200	.99873	.8085		.097	5.28		
	.300	.99864	.8124		.155	17.47		
	.400	.99855	.8165		.200	32.8		
	.500	.99846	.8207		.300	67.8		
	.600	.99838	.8254		.340	81.4		
	.800	.99820	.8355		.461	122		
	1.000	.99803	.8479		.612	167		
					.794	222		
					.926	261		
					1.000	283		
0.10-*M* NaCl CMC=0.109 g/dl	0	0.99972	0.8049	0.044	0	5.42	0.160	85,500
	0.100	.99964	.8069		0.099	5.47		
	.200	.99955	.8094		.150	31.9		
	.300	.99946	.8148		.315	127.6		
	.400	.99938	.8202		.385	167		
	.500	.99929	.8260		.490	225		
	.600	.99921	.8327		.585	284		
	.800	.99904	.8484		.755	381		
	1.000	.99887	.8789		.880	454		
					.970	506		
					1.000	524		
0.15-*M* NaCl CMC=0.101 g/dl	0	1.00178	0.8090	0.060	0	5.38	0.160	231,000
	0.100	1.00169	.8108		0.050	5.47		
	.200	1.00159	.8167		.074	5.52		
	.300	1.00149	.8261		.107	11.57		
	.400	1.00139	.8384		.130	47.6		
	.500	1.00130	.8528		.205	162.8		
	.600	1.00120	.8694		.330	353		
	.800	1.00101	.9101		.480	558		
	1.000	1.00081	.9638		.592	700		
					.780	919		
					.916	1076		
					1.000	1176		
0.20-*M* NaCl CMC=0.093 g/dl	0	1.00367	0.8129	0.15	0	5.52	0.160	655,000
	0.100	1.00359	.8167		0.050	5.52		
	.200	1.00350	.8350		.107	61.9		
	.300	1.00342	.8610		.171	346		
	.400	1.00333	.8966		.281	743		
	.500	1.00324	.9401		.408	1257		
	.600	1.00316	.9909		.667	1950		
	.800	1.00298	1.1204		.769	2220		
	1.000	1.00281	1.2965		.901	2550		
					1.000	2750		
0.25-*M* NaCl CMC=0.093 g/dl	0	1.00580	0.8156	0.33	$[Z]\simeq 1.20$		-------	~1,125,000
	0.100	1.00570	.8270					
	.200	1.00559	.8670					
	.300	1.00548	.9230					
	.400	1.00537	1.0000					
	.600	1.00516	1.2701					
	.800	1.00494	1.7631					
0.30-*M* NaCl CMC=0.085 g/dl	0	1.00785	0.8201	0.45	$[Z]\simeq 1.40$		-------	~1,800,000
	0.100	1.00772	.8384					
	.200	1.00758	.9102					
	.300	1.00745	1.0446					
	.400	1.00731	1.2909					
	.500	1.00717	1.6907					
DODECYLTRIMETHYLAMMONIUM CHLORIDE (23° C)								
Distilled H_2O CMC=0.570 g/dl	0	0.99754	0.9323	0.040	0.183	5.47	0.156	9,900
	0.404	.99703	.9491		.225	5.62		
	.508	.99703	.9515		.427	5.66		
	.607	.99698	.9546		.478	5.71		
	.708	.99687	.9588		.545	5.71		
	.800	.99678	.9631		.620	8.81		
	1.013	.99655	.9744		.709	13.09		
	1.202	.99636	.9853		.793	16.66		
	1.402	.99615	.9974		.955	21.75		
					1.092	25.09		
					1.197	26.89		

scattered intensity at 45° to that at 135°), could be made as a check on the cleanliness of the solutions. The solvents, distilled water or solutions of sodium chloride, were easily obtained with no dissymmetry by filtering two or three times through ultrafine fritted glass or porcelain filters. Solutions of increasing concentration were prepared by the addition of a known weight of detergent crystals to clean solvent or solution already in the light-scattering cell. After the detergent crystals had dissolved, the solution was filtered a number of times until the dissymmetry was at an acceptably low level. Except for dodecyl-

TABLE 1. *Light-scattering and viscosity data for solutions of dodecylamine hydrochloride, dodecyltrimethylammonium chloride, and tetradecyltrimethylammonium chloride in distilled water and in solutions of sodium chloride*—Continued

(cp=centipoise; [η]=intrinsic viscosity; $\Delta n/\Delta c$=refractive index increment; CMC=critical micelle concentration; [Z]=intrinsic dissymmetry).

Solvent	Concentration	Density	Viscosity	[η]	Concentration	Turbidity	$\Delta n/\Delta c$	Micellar weight
	g/dl	*g/ml*	*cp*		*g/ml*×10²	*cm*⁻¹×10⁵	*ml/g*	
0.02-*M* NaCl CMC=0.420 g/dl	0	0.99825	0.9329	0.040	0	4.81	0.156	10,200
	0.360	.99791	.9471		0.390	5.52		
	.400	.99789	.9483		.431	6.24		
	.600	.99774	.9556		.478	9.14		
	.800	.99755	.9647		.583	15.4		
	1.000	.99737	.9743		.737	22.8		
	1.200	.99717	.9839		.935	30.9		
	1.400	.99698	.9937		1.139	37.8		
	.....	.....	.....		1.249	41.4		
0.04-*M* NaCl CMC=0.310 g/dl	0	0.99914	0.9349	0.035	0	4.81	0.156	11,000
	.250	.99882	.9452		0.179	5.43		
	.300	.99880	.9466		.323	6.52		
	.400	.99874	.9491		.373	9.71		
	.600	.99855	.9571		.478	17.1		
	.800	.99836	.9653		.638	27.0		
	1.000	.99817	.9744		.765	34.3		
	1.200	.99799	.9831		.890	41.2		
	1.400	.99780	.9923		1.084	50.9		
0.10-*M* NaCl CMC=0.190 g/dl	0	1.00149	0.9399	0.035	0	5.05	0.155	16,400
	0.150	1.00134	.9459		0.144	5.24		
	.200	1.00130	.9476		.204	6.71		
	.400	1.00113	.9540		.251	11.4		
	.600	1.00096	.9621		.342	20.3		
	.800	1.00079	.9697		.445	29.5		
	1.000	1.00062	.9779		.550	38.2		
	1.200	1.00045	.9859		.738	50.8		
	.....	.....	.....		.926	62.9		
	.....	.....	.....		1.048	71.1		
TETRADECYLTRIMETHYLAMMONIUM CHLORIDE (23° C)								
Distilled H_2O CMC=0.120 g/dl	0	0.99754	0.9323	0.061	0	4.81	0.157	10,100
	0.100	.99743	.9355		0.044	5.00		
	.200	.99732	.9396		.143	6.47		
	.300	.99721	.9466		.194	9.43		
	.400	.99710	.9554		.334	14.9		
	.600	.99688	.9732		.431	17.8		
	.800	.99666	.9933		.513	19.2		
	1.000	.99644	1.0121		.616	20.8		
0.02-*M* NaCl CMC=0.070 g/dl	0	0.99825	0.9329	0.042	0	4.81	0.157	21,800
	0.100	.99815	.9367		0.054	5.14		
	.200	.99806	.9406		.105	10.1		
	.300	.99797	.9451		.166	17.0		
	.400	.99787	.9501		.220	22.7		
	.600	.99769	.9605		.282	28.3		
	.800	.99750	.9712		.344	32.6		
	1.000	.99731	.9820		.407	37.2		
	.....	.....	.....		.498	42.7		
	.....	.....	.....		.565	45.2		
0.04-*M* NaCl CMC=0.040 g/dl	0	0.99914	0.9349	0.040	0	4.72	0.157	22,200
	0.100	.99904	.9379		0.043	5.52		
	.200	.99894	.9422		.095	12.5		
	.300	.99884	.9464		.154	20.3		
	.400	.99874	.9502		.229	29.5		
	.600	.99854	.9592		.308	38.3		
	.800	.99834	.9687		.401	47.1		
	1.000	.99813	.9786		.493	55.0		
	.....	.....	.....		.585	63.3		
	.....	.....	.....		.680	69.3		
0.10-*M* NaCl CMC=0.030 g/dl	0	1.00149	0.9399	0.040	0	4.90	0.157	25,500
	0.100	1.00142	.9438		0.054	9.76		
	.200	1.00133	.9464		.112	18.8		
	.300	1.00124	.9509		.178	28.7		
	.400	1.00115	.9546		.255	39.4		
	.600	1.00098	.9616		.329	50.6		
	.800	1.00080	.9698		.409	61.3		
	1.000	1.00062	.9779		.496	72.1		
	.....	.....	.....		.602	84.7		
	.....	.....	.....		.692	93.4		

amine hydrochloride in the presence of high concentrations of sodium chloride, a small dissymmetry, generally 1.05 or less, was observed. In the case of dodecylamine hydrochloride, the dissymmetries observed are caused by the presence of very large micellar structures and are of significance. This is discussed further in a later section.

Because of the low solubility of dodecylamine hydrochloride in salt solutions at 23° C, the turbidity measurements on it were made at 30° C. All other turbidity measurements were made at 23° C. The 436-mμ line of a mercury-arc lamp was used throughout.

2.4. Viscosity

The experimental details and necessary corrections to be applied to the measured efflux time have been described previously [3]. The only change in procedure was the use of smaller pycnometers for the density determinations [9]. The measurements on the dodecylamine hydrochloride solutions were made at 30° C. All others were made at 23° C.

3. Results and Discussion

All of the pertinent experimental data are given in table 1. Typical plots of turbidity and viscosity as a function of detergent concentration at various concentrations of sodium chloride are shown in figures 1 and 2. The pronounced effect of the addition of sodium chloride is evident in both figures.

In order to evaluate the micellar weight from the turbidity data, and the intrinsic viscosity of the micelles from the viscosity data, it is necessary to evaluate the critical micelle concentration of the detergent in each of the solvents used. Debye [5] has shown that this can be obtained conveniently from the dependence of the turbidity on concentration (cf. fig. 1). The detergent concentration at which the turbidity begins to increase rapidly clearly represents the concentration at which aggregation of the individual detergent molecules or ions into micelles is beginning to occur to a significant extent. These concentrations, as obtained from the turbidity data, have been chosen as the critical micelle concentration, and are given in table 1. The dependence of the critical micelle concentration of each detergent on the amount of sodium chloride present is shown in figure 3. The data reported by Corrin and Harkins (dye titration method) [10] for dodecylamine hydrochloride at 26±2° C are also shown. It is seen that the quaternary dodecylammonium chloride has a much larger critical micelle concentration than does the corresponding primary amine salt. This is simply another manifestation of the greater degree of ionization of the quaternary salt. The addition of two CH_2 groups to the long hydrocarbon chain of the surface active ion, as in tetradecyltrimethylammonium chloride, increases the hydrophobic nature of the ion and results in a lower critical micelle concentration.

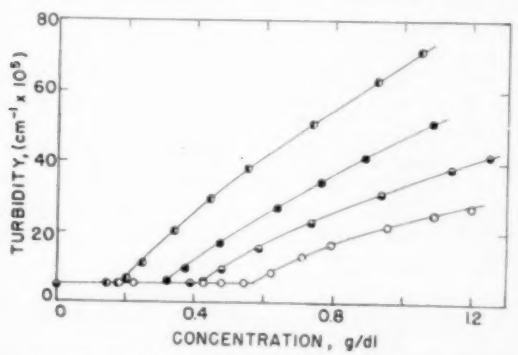

FIGURE 1. *Dependence of the turbidity on the concentration of dodecyltrimethylammonium chloride in water (○) and in various sodium chloride solutions.*

◒, 0.02 *M*; ●, 0.04 *M*; ◐, 0.10 *M*.

The intrinsic viscosity of the micelles was obtained from plots of the experimental data according to eq (1).

$$\frac{(\eta_{rel}-1)}{C_m}=[\eta]+AC_m. \qquad (1)$$

$[\eta]$ is the intrinsic viscosity. C_m is the concentration of micelles in grams per deciliter and is assumed to be equal to the total concentration of detergent

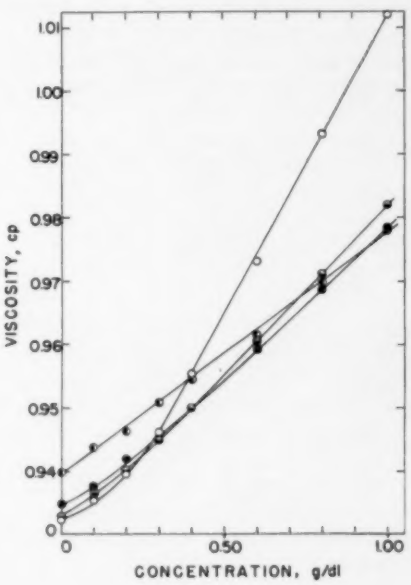

FIGURE 2. *Dependence of the viscosity on the concentration of tetradecyltrimethylammonium chloride in water (○) and in various sodium chloride solutions.*

◒, 0.02 *M*; ●, 0.04 *M*; ◐, 0.10 *M*.

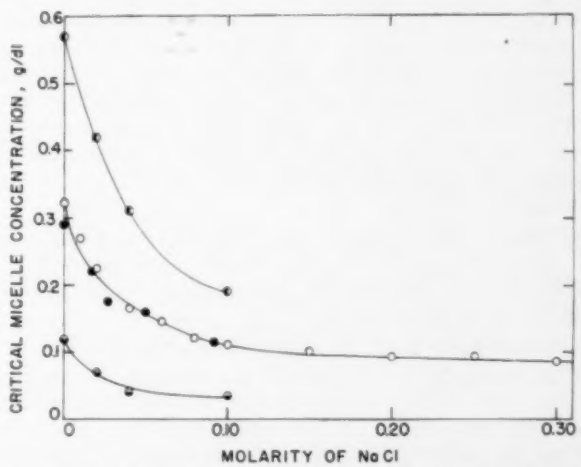

FIGURE 3. *Dependence of the critical micelle concentration of dodecyltrimethylammonium chloride (◐), dodecylamine hydrochloride (○), and tetradecyltrimethylammonium chloride (◒) on the concentration of sodium chloride in aqueous solutions.*

●, data of Corrin and Harkins [10] for dodecylamine hydrochloride at 26° C.

minus the critical micelle concentration. η_{rel} is the viscosity of a solution of concentration C_m relative to the viscosity at the critical micelle concentration (i. e., at $C_m=0$). The constant A is related to hydrodynamic interactions in the solution. The relationship between $[\eta]$ and a shape factor, K, for suspended particles of density d, is

$$[\eta]=\frac{K}{100d}. \tag{2}$$

For spherical particles, $K=2.5$. Values of K as a function of axial ratio for oblate and prolate spheroids of revolution have been calculated by Mehl, Oncley, and Simha [11].

Calculation of the micellar weights from the light-scattering data was done with the simple Debye equation

$$H\frac{C_m}{\tau}=\frac{1}{M}+2BC_m, \tag{3}$$

where

$$H=\frac{32\pi^3}{3}\cdot\frac{n_0^2(\Delta n/\Delta c)^2}{\lambda^4 N}. \tag{4}$$

Once again C_m is the concentration of micelles, although this time in grams per milliliter. M is the micellar weight. B is an interaction constant; its significance in solutions of charged colloidal particles has been discussed [12]. τ is the turbidity due to the presence of micelles. It is the observed turbidity of a solution minus the turbidity at the critical micelle concentration. The refractive index of the solvent is n_0. $(\Delta n/\Delta c)$ is the refractive-index increment of the solutions. λ is the vacuum wavelength of the light used, 436 mμ. N is Avogadro's number.

In the case of dodecylamine hydrochloride at sodium chloride concentrations above 0.20 M, the micelles are large enough to scatter asymmetrically. This means that the scattered intensity observed at 90° is not indicative of the turbidity of the solutions and that the micellar weight calculated therefrom is in error. Because no dissymmetry corrections were applied, turbidities for these systems are not given in table 1. An estimation of the intrinsic dissymmetry has been made, and these values are given. The micellar weights listed are approximations calculated from the data as if there were no dissymmetry effects.

Plots of the intrinsic viscosity and micellar weight as a function of sodium chloride concentration for each of the detergents investigated are given in figures 4, 5, and 6.

Considering both M and $[\eta]$ over the total range of sodium chloride concentrations covered, each of the three detergents investigated shows different behavior. However, considering only the dependence of $[\eta]$ on sodium chloride concentration up to about 0.05 M, the three detergents behave similarly, i. e., the intrinsic viscosity decreases as sodium chloride is added. This is the same behavior as that exhibited by sodium dodecyl sulfate, and reflects the diminution

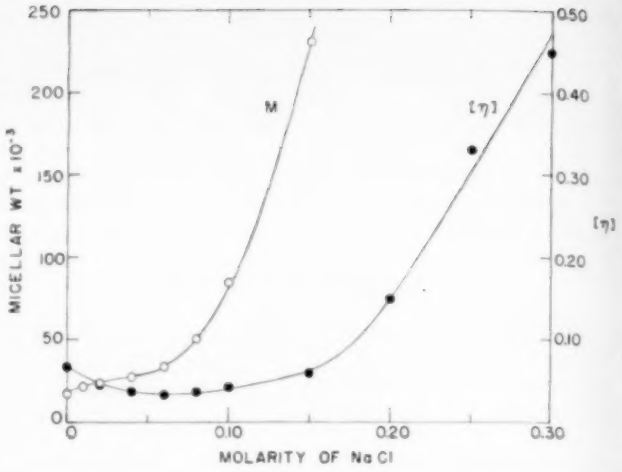

FIGURE 4. *Dependence of the micellar weight (○) and intrinsic viscosity (●) of dodecylamine hydrochloride micelles on the concentration of sodium chloride in aqueous solutions.*

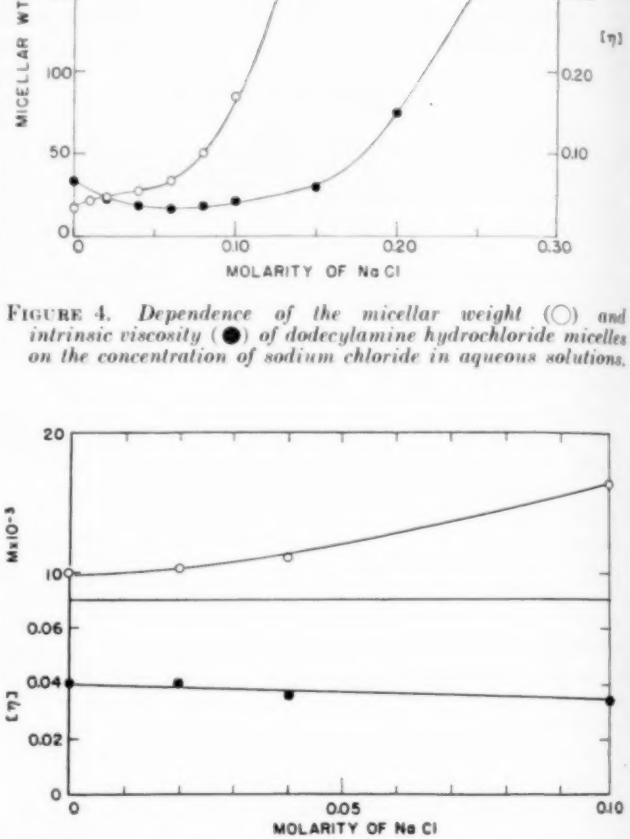

FIGURE 5. *Dependence of the micellar weight (○) and intrinsic viscosity (●) of dodecyltrimethylammonium chloride micelles on the concentration of sodium chloride in aqueous solutions.*

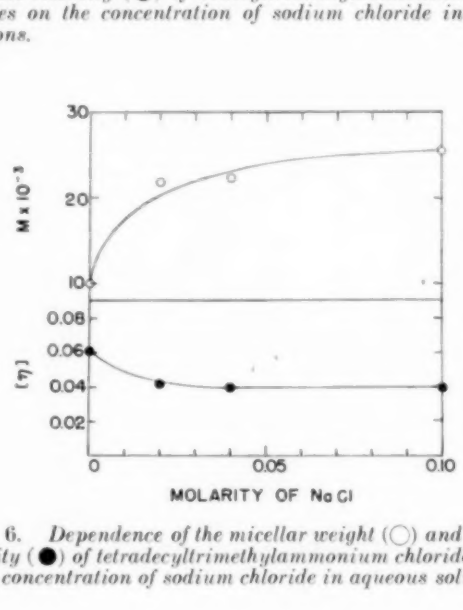

FIGURE 6. *Dependence of the micellar weight (○) and intrinsic viscosity (●) of tetradecyltrimethylammonium chloride micelles on the concentration of sodium chloride in aqueous solutions.*

of electroviscous effects caused by the high degree of ionization of the micelles.[2]

At a concentration of about 0.05 M sodium chloride, the electroviscous effect appears to be virtually eliminated. An interesting result is that the electroviscous effect for dodecyltrimethylammonium chloride is substantially less than that for dodecylamine hydrochloride or tetradecyltrimethylammonium chloride. The inference is that the micelles of dodecyltrimethylammonium chloride carry a lower charge than the micelles of the other two detergents. However, no explanation for this can be given at this time.

The minimum value of $[\eta]$, 0.033 to 0.040, obtained with all of the cationic detergents is to be compared with the value 0.035 obtained with sodium dodecyl sulfate. All of these values are consistent with the concept of spherical hydrocarbon micelles having a density of about 0.75 g/ml. According to eq 2, $[\eta]$ for such micelles would be about 0.033. The differences among the intrinsic viscosities observed may reflect a difference in the density of the micelles in each case.

At higher concentrations of sodium chloride (up to 0.1 M) the intrinsic viscosities of the two quaternary salts remain constant in spite of the increasing micellar weight. This merely serves to emphasize that small micelles (those containing about 50 to 150 detergent molecules), regardless of their precise shape, will of necessity have axial ratios close to unity and will behave hydrodynamically as spheres. The growth of the micelles on the addition of neutral electrolyte has been interpreted [5] as resulting from a reduction in the work necessary to bring together the ionic heads of the detergent molecules when a micelle is formed.

With dodecylamine hydrochloride the addition of sodium chloride beyond 0.05 M results in rapid growth of the micelles. This is made evident not only by the micellar weight but also by the intrinsic viscosity, which increases greatly. Once again it is evident that the light-scattering method is much more sensitive for measuring the growth of the micelles than is the viscosity method, particularly up to micellar weights of about 250,000. The high values of $[\eta]$ that are obtained as M increases are additional evidence for the high asymmetry of large micelles. The quantitative correlation between micelle dimensions calculated from the viscosity data and from the light-scattering data is poor. For example, at a sodium chloride concentration of 0.3 M, $[\eta]=0.45$, and the intrinsic dissymmetry is close to 1.40. Taking a rodlike micelle as being the most likely [13], one calculates from the intrinsic dissymmetry [14] a length of about 1177 A. Approximating the rod to an elongated ellipsoid of revolution whose minor axis is equal to the extended length of a dodecylamine hydrochloride molecule, 20 A, one calculates [11] a length of 720 A from $[\eta]$. It must be mentioned, however, that for this system both Z and $(\eta_{rel}-1)/C_m$ are rapidly changing functions of C_m as $C_m \to 0$. Hence the probable errors in both the intrinsic dissymmetry, $[Z]$, and in the intrinsic viscosity, $[\eta]$, are quite large (± 10 to 15% would not be unreasonable). In addition, with such large asymmetric micelles, one must consider the possibility of non-Newtonian flow. This was not investigated.

The rapidly increasing size of the dodecylamine hydrochloride micelles is probably the first step in the salting-out process. On standing at 23° C, visible crystals were observed in 0.5-percent solutions of the detergent in a 0.04-M sodium chloride solution. At 30° C it was possible to prepare 1-percent solutions of the detergent in sodium chloride solutions as concentrated as 0.30 M, but at higher salt concentrations it was insoluble. The quaternary salts, being inherently more soluble, show no such effects in this range of sodium chloride concentrations.

In the case of tetradecyltrimethylammonium chloride in distilled water, because it has a low critical micelle concentration, it was thought that it might be possible to observe dissymmetries of less than unity, as discussed by Doty and Steiner [14]. Such effects should exist, being the result of external interference arising from the nonrandom fluctuations in concentration of the highly charged micelles. However, dissymmetries of less than unity were not observed. Apparently, even in this case, in which the shielding electrolyte is unaggregated detergent at its critical micelle concentration (0.0043 M), shielding is sufficiently good to permit random fluctuations, at least up to $C_m \simeq 1$ g/dl.

[2] For a brief discussion of the electroviscous effect, see Colloid science, edited by H. R. Kruyt, vol. I, p. 348 (Elsevier Publishing Co., New York, N. Y., 1952).

4. References

[1] J. N. Phillips and K. J. Mysels, J. Phys. Chem. **59,** 325 (1955).
[2] L. M. Kushner and W. D. Hubbard, J. Colloid Sci. **10,** 428 (1955).
[3] L. M. Kushner, B. C. Duncan, and J. I. Hoffman, J. Research NBS **49,** 85 (1952) RP2346.
[4] D. Stigter and K. J. Mysels, J. Phys. Chem. **59,** 45 (1955).
[5] P. Debye, Ann. N. Y. Acad. Sci. **51,** Art. 4, 575 (1949).
[6] K. J. Mysels, J. Phys. Chem. **58,** 303 (1954).
[7] P. P. Debye, J. Appl. Phys. **17,** 392 (1946).
[8] L. M. Kushner, J. Opt. Soc. Am. **44,** 155 (1954).
[9] H. M. Smith and cooperators, Anal. Chem. **22,** 1452 (1950).
[10] M. L. Corrin and W. D. Harkins, J. Am. Chem. Soc. **69,** 683 (1947).
[11] J. Mehl, J. Oncley, and R. Simha, Science **92,** 132 (1940).
[12] P. Doty and J. T. Edsall, Advances in protein chemistry, vol. VI (Academic Press Inc., New York, N. Y., 1951).
[13] P. Debye and E. W. Anacker, J. Phys. & Colloid Chem. **55,** 644 (1951).
[14] P. Doty and R. F. Steiner, J. Chem. Phys. **20,** 85 (1952).

WASHINGTON, D. C., December 6, 1956.

Journal of Research of the National Bureau of Standards Vol. 59, No. 2, August 1957 Research Paper 2779

Relative Stress-Optical Coefficients of Some National Bureau of Standards Optical Glasses [1]

Roy M. Waxler and Albert Napolitano

The relative stress-optical coefficients of 27 optical glasses made at the National Bureau of Standards have been determined. The glasses were loaded in compression, and the amount of birefringence was measured with a polarimeter, using a quarter-wave plate compensator. The stress-optical coefficients determined for the crown glasses ranged between +2.95 and +1.82 brewsters. For the flint glasses, a regular variation of the stress-optical coefficient with weight percent of lead oxide was found with values ranging from +3.18 to −1.16 brewsters.

1. Introduction

The double refraction produced in isotropic solids by the application of stress was discovered by Brewster [1] [2] who, incidentally, used glass for the greater part of his experiments. From Brewster's early work, the theory of photoelasticity has been developed [2] and is the basis of a recognized method of stress analysis for isotropic transparent solids.

For a given material, the relationship between the optical-path difference and the applied stress is

$$r = Ctd. \tag{1}$$

C is called the relative stress-optical coefficient and is characteristic of the type of glass under investigation. The above equation holds true for both compression and tension [3], and it is presumed to be valid up to the breaking stress of glass [4]. When r, the retardation, is expressed in angstroms; t, the stress, in bars; and d, the thickness, in millimeters, the resulting coefficient, C, is measured in brewsters.

The effect of the chemical composition of glass on the photoelastic effect was first investigated by Pockels [5], who came to the conclusion that an increase of lead oxide, or decrease of boric oxide, always lowers the relative stress-optical coefficient. In compression most glasses act as uniaxial negative crystals, but Pockels succeeded in observing a reversal of this effect for very heavy lead silicate glasses. The effect of the composition was more accurately studied by Filon [6] and Adams and Williamson [7], who reached the same general conclusions.

In more recent work, Vedam [8] measured the elastic and photoelastic properties of 18 optical glasses, and Schaefer and Nassenstein [9] made a very extensive study of these properties for 154 optical glasses produced by Schott & Co. Unfortunately, the compositions of the glasses measured by Vedam are given only to a rough approximation, and these data are not mentioned in the paper of Schaefer and Nassenstein.

As the relative stress-optical coefficient relates the stress exerted upon a glass to the optical-path difference produced, a knowledge of this coefficient permits one to carry out a stress analysis of a glass specimen on the basis of the optical evidence of the existing strain. Furthermore, Lillie and Ritland [10] have shown that a knowledge of this coefficient for optical glasses is needed in order to develop fine annealing schedules that will keep the amount of birefringence within prescribed limits. In the course of developing annealing schedules for large optical elements, it was felt desirable to evaluate these coefficients for several glasses made at the Bureau. Because these are similar to commercial types of optical glasses, the results are offered for their potential interest to glass technologists.

2. Optical System

In most investigations of the relative stress-optical coefficient, the stressed specimen is placed in a 45-deg position between crossed nicols. A Babinet compensator, also placed between the crossed nicols and at the same angle as the specimen, is used to measure the optical-path difference. However, the use of a quarter-wave plate as a compensator affords greater accuracy, and was used in this investigation [11]. With this arrangement, the polarizer is set at a 45-deg position with respect to the principal directions of the stressed specimen, and the elliptically polarized light emerging from the glass is restored to a linear polarization by a properly oriented quarter-wave plate. The quarter-wave plate and stressed glass in combination then have the same effect as an optically active material that rotates the plane of polarization of the incident light. The angular difference in the extinction positions of the analyzer may be noted if the analyzing nicol is mounted in a graduated circular scale. The amount of rotation is equal to one-half the phase angle, and may be used to measure the optical-path difference in the birefringent glass.

The optical arrangement and loading device used in this investigation are shown in figure 1. The light source consisted of a laboratory sodium arc lamp. The light was collimated and filtered through a glass cell 15 mm in length that contained a 6-percent solu-

[1] This work was sponsored by the Air Research and Development Command, U. S. Air Force under Contract No. AF 18 (600)-139.

[2] Figures in brackets indicate the literature references at the end of this paper.

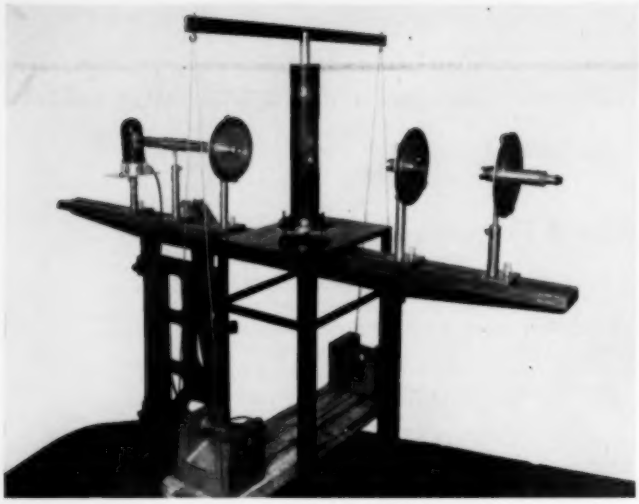

FIGURE 1. *Optical system and loading device for determining the stress-optical coefficient of glasses.*

tion of potassium dichromate. The wavelength was then taken as the mean of the two sodium D lines, or 5893 A.

The polarizer, quarter-wave plate, and analyzer were each mounted in a brass tube 3¼ in. long and 1¼ in. in diameter. Nicol prisms were used for polarizer and analyzer, and the quarter-wave plate was a Babinet compensator adjusted to give the proper retardation.

The circles for measuring the amount of rotation were 8½ in. in diameter and graduated to 0.5 deg, with a vernier permitting readings to be made to 0.1 deg. A small telescope was mounted in the tube that held the analyzing nicol and was focused upon a ⅛-in.-diameter hole, which formed a stop for the light beam as it emerged from the polarizer.

3. Preparation of Samples

The optical glasses tested are shown in table 1, together with their chemical compositions as computed from the raw materials in the batch. Column 4 of table 1 identifies the glass according to optical type, refractive index, and Abbe valve [12].

These glasses were made in clay pots holding from 1,000 to 2,000 lb of glass, depending on the type of glass. A 5-lb piece of high quality glass,[3] which was representative of the type of glass under investigation, was selected from each melt. A test specimen was cut from each piece of glass and annealed. During heat treatment, each specimen was enclosed in a metal box in order to eliminate temperature gradients. The specimen was supported on small bits of refractory material so that it was not in contact with any part of the metal. The glasses were heated to a temperature about 20 deg C below the deformation point [13], held at this temperature for several hours, and then cooled at a rate of 1 deg C/hr through the transformation region. Once through the transformation region, the glass was rapidly cooled to room temperature.

Each specimen of glass was annealed and then carefully ground to the shape of a rectangular block, the approximate dimensions being 3 cm by 3 cm by 10 cm. Two opposite faces 3 cm by 10 cm were

[3] High-quality glass—seed free, striae free, having a nominal index of refraction, and a nominal dispersion.

TABLE 1. *Relative stress-optical coefficient and compositions (computed from batch) of NBS optical glasses*

Specimen	C, brewsters, $\frac{10^{-13}\ cm^2}{dyne}$	Standard error of C	Glass type	Melt	Component oxides (weight %)									Other oxides	Specimen
					SiO_2	PbO	BaO	B_2O_3	Na_2O	K_2O	ZnO	As_2O_3	Sb_2O_3		
1	2.93	0.027	CF 529/516	8217	65.4	10.0	0.2	...	13.2	5.6	3.6	0.2	1.8		1
2	2.97	.029	F 5725/425	7841	55.1	31.7	1.0	.....	5.0	6.9	.....	.3	.....		2
3	3.18	.029	F 5795/410	7073	53.1	35.5	0.6	.....	0.4	9.6	.....	.3	0.5		3
4	2.98	.016	F 605/380		47.6	40.9	.....	.....	2.2	8.8	.....	.5	.....		4
5	2.77	.014	F 617/366	8853	45.6	43.2	.....	.....	4.6	6.1	.....	.5	.....		5
6	2.89	.031	F 620/362	8622	45.6	45.5	.....	.....	2.7	5.7	.....	.5	.....		6
7	2.65	.015	F 649/338	8865	41.2	51.1	.....	.....	0.7	6.5	.....	.5	.....		7
8	2.45	.026	F 666/324	7686	39.3	54.4	.....	.....	.....	6.0	.....	.3	.....		8
9	2.18	.020	F 689/309	8652	37.0	58.1	.....	.....	.....	4.6	.....	.3	.....		9
10	1.77	.010	F 720/293	8968	34.1	62.4	.....	.....	.....	3.2	.....	.3	.....		10
11	1.33	.013	F 754/277	8001	31.2	66.2	.....	.....	.....	2.3	.....	.3	.....		11
12	−1.16	.039	F 920/211	A2059	20.0	79.6	.....	.....	.....	0.4	.....	.....	.....		12
13	2.73	.026	BaC 541/599	8700	58.8	.....	19.9	3.8	2.8	10.3	4.1	.3	.....		13
14	2.56	.025	BaC 5725/574	8702	45.2	.....	28.7	5.8	1.8	7.0	7.5	.3	.7	Al_2O_3 3.0	14
15	2.65	.019	BaC 574/577	8573	47.4	.....	30.0	4.9	0.9	7.0	7.5	.3	.5	Al_2O_3 1.5	15
16	1.85	.012	BaC 6109/572	8462	38.2	0.2	42.9	6.7	.....	.....	4.2	.4	.2	Al_2O_3 4.9, CaO 2.3	16
17	1.83	.013	BaC 611/588	8621	38.3	.2	42.6	10.7	.....	.....	.....	.4	.2	CaO 4.5, Al_2O_3 3.1	17
18	2.03	.013	BaC 617/550	8890	37.3	1.4	44.8	4.4	.2	0.4	5.6	.3	.7	Al_2O_3 4.9	18
19	1.82	.018	BaC 620/600	7903	37.8	.....	44.2	11.3	.....	.....	.....	.3	.2	{CaO 3.6, BeO 2.3, ZrO_2 0.3.	19
20	2.95	.022	BaF 584/460	7631	49.8	18.8	13.4	.....	1.5	8.2	7.8	.5	.....	.....	20
21	2.35	.026	BaF 588/534		45.8	5.6	28.0	4.4	2.3	6.0	7.5	.4	.....	.....	21
22	2.84	.037	BaF 605/436	8610	45.7	23.3	14.3	.....	.....	8.2	8.1	.4	.....	.....	22
23	2.78	.016	LC 512/605	8691	71.9	.....	.....	5.0	14.7	5.0	.....	.....	1.2	CaO 2.2	23
24	2.76	.016	LC 523/586	8695	70.2	.....	.....	1.5	14.0	2.5	.....	.....	1.2	{CaO 9.4, Cl 0.7, SO_3 0.5.	24
25	2.66	.016	LC 528/580	7617	68.3	.....	.....	1.5	14.0	2.5	.....	.....	1.2	{CaO 11.3, Cl 0.7, SO_3 0.5.	25
26	2.75	.021	BSC 511/635	8713	68.8	.....	.....	8.5	7.8	14.7	.....	.2	.....	.....	26
27	2.81	.019	BSC 517/645	8843	66.3	0.5	.....	12.5	7.5	12.8	.....	.4	.....	.....	27

polished, in order to transmit the light beam. Attention is called to the fact that the length of the specimen was made three times its width to avoid end effects [14].

After annealing, grinding, and polishing, the residual strain was measured. An optical path difference of no more than 2 or 3 mμ/cm was observed. This nominal residual strain was presumed to remain constant during the tests. A zero correction was unnecessary as the relative stress-optical coefficient is determined from differences in applied load.

4. Method of Loading

The load was applied by means of a vertical shaft which supported a horizontal yoke, and suspended loading platform, as shown in figure 2. The shaft and the two vertical guides were machine polished to insure a smooth and close fit, thus allowing only vertical motion to the shaft. A ⅜-in.-diameter steel ball was seated in the center of a metal disk at both ends of the glass specimen. Seats were also made on the end of the shaft and the bottom steel support to accommodate the ball. When this assembly was inserted under the shaft, the axis of the shaft and glass coincided. By taping the glass near both ends, the specimen was centrally located within each disk. A light film of oil was placed at the glass and metal interface. This method has been described in a previous paper [15], and it has proved quite satisfactory in producing a uniform stress.[4]

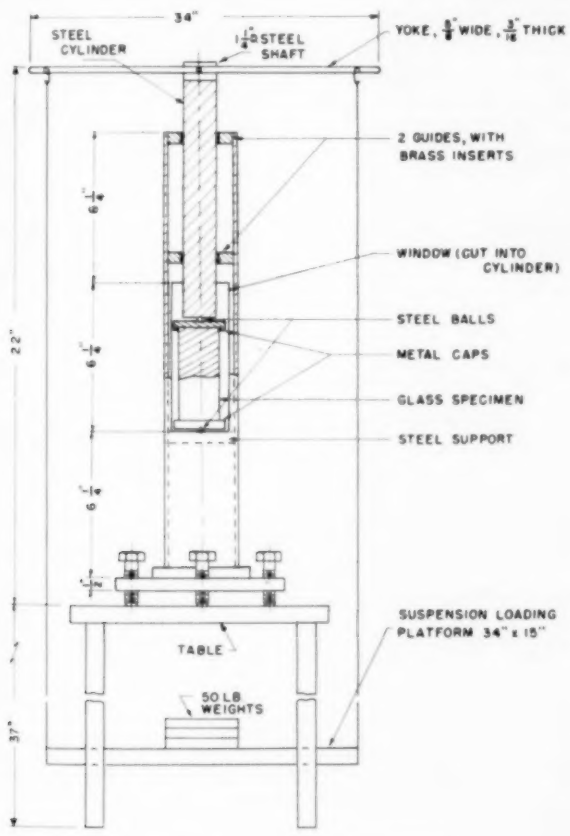

FIGURE 2. *Loading apparatus.*

By means of leveling screws and a bubble level, the steel cylinder was adjusted into a vertical position, making it possible to rest the glass on a horizontal surface. The glass, being then in vertical position, could be placed in alinement with the direction of force created by the load. This line of force established the directions of the planes of polarization of light transmitted by the glass.

To apply the stress, 50-lb weights were supplied by the Mass and Scale Section of the Bureau. Upon calibrating these weights, it was found that they were accurate to within 0.007 lb, which was felt to be more than satisfactory because it was desired to determine the values of the stress-optical coefficients only to three significant figures.

5. Procedure

Each part of the optical train was adjusted so as to be perpendicular to the light path. This was accomplished by noting the reflection of light from each surface and making certain that the reflected beam of light coincided with the incident beam.

It was necessary also to have some base point on the graduated circle of the analyzer in order to orient the polarizer and quarter-wave plate in 45-deg positions relative to the optic axes of the stressed glass. For this reason each specimen was loaded to 300 lb, and one of the optic axes was found by alternately rotating the polarizer and analyzer until a position of minimum intensity was reached. Extinction positions noted on the analyzer and polarizer could be reproduced to within ±0.1 deg of arc. Both axes were found in this manner, and a point midway between the two, as noted on the analyzer, was used as a base point for subsequent settings of the polarizer and quarter-wave plate. These elements then could be set to within ±0.1 deg. This method was felt to be satisfactory, considering the magnitude of errors that might possibly be introduced by missettings [11].

The birefringence produced in stressed glass may be used to ascertain the uniformity of stress distribution, as well as its magnitude. Before making any measurements, several of the specimens were loaded and examined in a broad beam of white light between sheets of Polaroid in a crossed position. With the aid of a sensitive red-tint plate it could be seen that the whole central portion of the specimen had a uniform color.

In making measurements, the glass was weighted with a tare consisting of the steel shaft, yoke, and loading platform, and the extinction position of the analyzer was noted. Then a 50-lb weight was added to the loading platform, and another extinction position noted. This process was repeated with 50-lb weight increments until the maximum load was 300 lb. Waiting about 5 min before readings,

[4] With this method of loading, the vertical thrust passes exactly centrally through the block, and it is a well-known principle in mechanics that at a sufficient distance from the point of application of a load, the stress system depends only on the statical resultant of the load.

the measurements were made in a darkened room so that the eye might be more sensitive to the intensity of the light beam viewed through the analyzer. The room was kept at a temperature of approximately 20° C.

It was noted that a specimen would exhibit the same extinction position before and after the application of the 300-lb load. This was checked with several glasses, and no difference could be detected outside the error of the instrument.

In investigating a particular specimen, 10 measurements were made for each extinction position, making a total of 70 measurements.

6. Results and Discussion

The results of this investigation are given in table 1, which lists the values of the relative stress-optical coefficient and their standard errors. The values were determined from the measurements in the following manner.

If Δw is the load increment in pounds, d the thickness of the specimen in inches, and b the width of the specimen in inches, we obtain

$$r=\frac{1.752C(\Delta w)d}{bd}, \tag{2}$$

where r is the retardation in angstroms, and C is the stress-optical coefficient in brewsters. The number, 1.752, is a conversion factor for the units employed.

As discussed in section 2, the retardation can also be expressed in terms of the angle through which the plane of polarization is rotated. The equation reads

$$r=\frac{2(\Delta y)\lambda}{360.0}, \tag{3}$$

where $2\Delta y$ is twice the rotation of the analyzer in degrees of arc and λ is the wavelength of the light in angstroms.

The angular rotation of the plane-polarized light is a linear function of the applied load. The increment in angular rotation can be represented by the relation

$$\Delta y=B(\Delta w) \tag{4}$$

from eq (2) and (3), where B is the slope of the straight line. It is appropriate to consider increments rather than accumulated total rotations, because, for each glass, the measurements corresponding to the various loads were all made on the same specimen, and consequently a cumulative effect may be expected in the errors of the accumulated rotation values. Errors in the optical measurements, on the other hand, are effectively reduced through the compensating effect of averaging 10 duplicate measurements at each load. A detailed statistical analysis shows that this reduced error in the optical measurement is negligible in comparison with the experimental errors due to the method of applying the load. Under these conditions, the correct least-squares estimate of slope B is obtained by averaging the five values of Δy, corresponding to the five consecutive 50-lb increments. From these five values it is also possible to calculate the precision of the evaluated slope. Each slope estimate was converted into a C value, expressed in brewsters, and the standard error of C was derived from that of the corresponding slope. Table 1 lists the C values and their standard errors. A measure of uncertainty (95% confidence interval) can be obtained for these values by considering the interval $C \pm$(2.8 times standard error).

As shown in table 1 most of the glasses studied in this investigation have values of stress-optical coefficient that are fairly close together, ranging from 2 to 3 brewsters. Two glasses in table 1, Nos. 16 and 17, vary only slightly in composition, and may be seen to have almost the same value of stress-optical coefficient, 1.85 and 1.82 brewsters, respectively.

Because optical glasses are in general made up of so many different chemical components, it is difficult to correlate changes in physical properties with a particular constituent. As the series of flint glasses consists principally of silica and lead oxide, it is interesting to note that, when the values of the stress-optical coefficient are plotted against percentage of lead oxide, a regular variation is indicated. This confirms the observations of other investigators, notably Pockels[5] [5] and Filon [6], whose results are shown in figure 3, together with the values obtained in this investigation. Furthermore, flint glass F920/211 is seen to depart from the general rule that glass in compression acts as a uniaxial negative crystal.

[5] Pockels determined the absolute changes in the refractive index of a stressed glass for light polarized, parallel, and perpendicular to the direction of force, and expressed his results by the coefficients p/r and q/r. With knowledge of these values, the relative stress-optical coefficient, C, may be calculated for purposes of comparison. This was done by Filon, and his results are shown in figure 3. Adams and Williamson also calculated C for Pockels' glasses and found that the results showed good agreement with their own determinations.

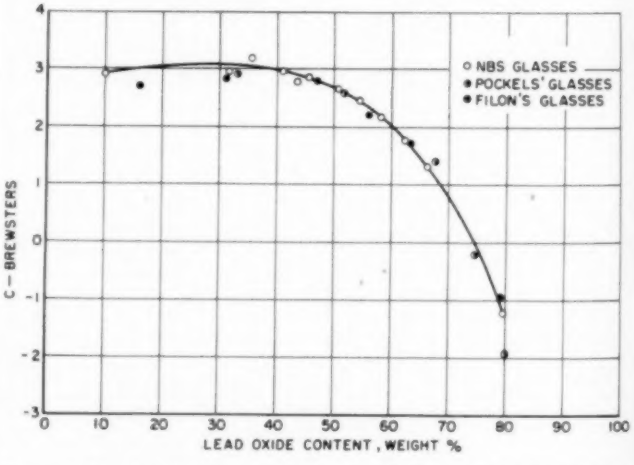

FIGURE 3. *Variation of the stress-optical coefficient with lead oxide content in flint glasses.*

Pockels [5] and Filon [6] also concluded that lowering the amount of B_2O_3 in a series of glasses decreased the relative stress-optical coefficient. It was impossible to verify this from the results of the present investigation because the glasses studied here were multicomponent and contained comparatively little boric oxide, the amount being, at most, only 12.5 percent.

The authors are deeply appreciative of the statistical analysis of the data by John Mandel and Mary N. Steel. They are also grateful to Joseph M. Nivert, Jr., for preparation of the glass specimens for this work.

7. References

[1] Sir David Brewster, Phil. Trans. (105), 60 (1815); Phil. Trans. (106), 156 (1816); Trans. Roy. Soc. Edinburgh **8,** 369 (1818).
[2] E. G. Coker and L. N. G. Filon, Treatise on photo-elasticity (Cambridge University Press, London, 1931).
[3] S. R. Savur, Phil. Mag. **50,** 453 (1925).
[4] L. N. G. Filon, A manual of photo-elasticity for engineers, p. 33–36. (Cambridge University Press, London, 1936).
[5] F. Pockels, physik Z. **2,** 693 (1901); Ann. Physik **7,** 745 (1902); **9,** 220 (1902); **11,** 651 (1903).
[6] L. N. G. Filon, Proc. Roy. Soc. **79,** 440 (1907); **83,** 572 (1910).
[7] L. H. Adams and E. D. Williamson, J. Wash. Acad. **9,** 609 (1919).
[8] K. Vedam, Proc. Indian Acad. Sci. [A] **31,** 450 (1950).
[9] Clemens Schaefer und Heinrich Nassenstein, Z., Naturforsch. [A] **8,** 90 (1953).
[10] H. R. Lillie and H. N. Ritland, J. Am. Cer. Soc. **37,** 466 (1954).
[11] R. W. Goranson and L. H. Adams, J. Franklin Inst. **216,** 475 (1933).
[12] ASTM standards on glass and glass products ASTM designation: C 162–52, page 68 (April 1955).
[13] F. W. Glaze, Optical glass at the National Bureau of Standards, NBS Circ. 469.
[14] M. M. Frocht, Photo-elasticity, vol. II, p. 30 (John Wiley & Sons, Inc., New York, N. Y., 1948).
[15] R. M. Waxler, Glass Ind. **34,** 258 (1953).

WASHINGTON, January 31, 1957.

Journal of Research of the National Bureau of Standards Vol. 59, No. 2, August 1957 Research Paper 2780

Physicochemical Studies of the Destructive Alkali-Aggregate Reaction in Concrete

Robert G. Pike and Donald Hubbard

In a further study of the alkali-aggregate reaction in high-alkali cements, 11 reactive and nonreactive experimental aggregates were examined by several procedures. On comparing the results of each method with the standard expansion-bar test, it appears that each property studied has some bearing on the expansion characteristics of each aggregate. For example: (1) The chemical durability as determined by the interferometer procedure was poor for the aggregates that showed excessive expansion, but not all aggregates that are shown to be chemically reactive by this procedure will cause expansion, (2) all aggregates are sufficiently hygroscopic to attract the water necessary for the reaction if other properties are also favorable, (3) surface electrical-resistance measurements confirm the hygroscopicity determinations; however, free ions in glasses may have considerably more effect on the surface resistance of certain glasses than do their hygroscopic properties, and (4) the uneven distribution of migratable ions between the aggregate surface and the outer phase offers a mechanism for the osmotic swelling of individual aggregate grains, with accompanying expansion in concrete members.

1. Introduction

In a previous publication [1] [1] concerning the mechanism of the destructive expansion of concrete structures caused by opaline and glassy silicate types of materials when used with high-alkali cements [2, 3, 4] there were included some data on the chemical durability of a few natural and synthetic aggregates. Those results, obtained with an interferometric procedure under controlled exposures of time, temperature, and *p*H, illustrated surface alterations of the aggregate materials during the incipient stages of attack. In light of the varied and unexpected dimensional changes found for various reactive and nonreactive aggregates, it became apparent that much remained to be learned about the chemical and physical nature of these and kindred materials before any completely acceptable picture of the destructive alkali-aggregate reaction could be formulated.

The present investigation was undertaken to gain further insight into the physicochemical principles operating in the alkali-aggregate reaction by extending the previous work on chemical durability to a broader range of aggregate materials. Further, in order to obtain a more comprehensive picture of the nature of these materials, their relative hygroscopicities, heterogeneous equilibria, electrical surface resistance, and reactivity in expansion bars were studied.

2. Experimental Techniques and Results

2.1. Techniques

For the sake of clarity, the techniques for each of the procedures are outlined briefly or covered by references in the sections where the results for each of the respective methods are presented and discussed.

[1] Figures in brackets indicate the literature references at the end of this paper.

2.2. Expansion Bars

The expansion of standard mortar test bars [5, 6] [2] brought about by 11 different aggregates when used in a high-alkali cement is shown in figure 1. The three forms of silica, viz, quartz (crystalline

[2] The expansion bars were prepared and measured according to the procedure of Mielenz and Witts [5]. A water to cement to standard Ottawa sand ratio of 0.4 to 1 to 2 was used, and the bars were then stored over water at 100° F, as described in a previous paper [1]. Six percent of Ottawa sand was replaced by the aggregate under test, using the size fraction passing a No. 50 and retained on a No. 100 U. S. Standard Sieve. This size gave maximum expansion with Pyrex, and 6 percent seemed a fair compromise between the expansion caused by the addition of 8 percent of Pyrex, as reported previously [1], and that caused by lower percentages of opal, as reported by other investigators [4, 8]. An analysis of the cement used is given in table 1. However, it should be kept in mind that the curves in figure 1 would be altered if the test conditions, such as percentage [4] or size [8] of aggregate, temperature of storage [9], and percentage of alkali [10], were changed.

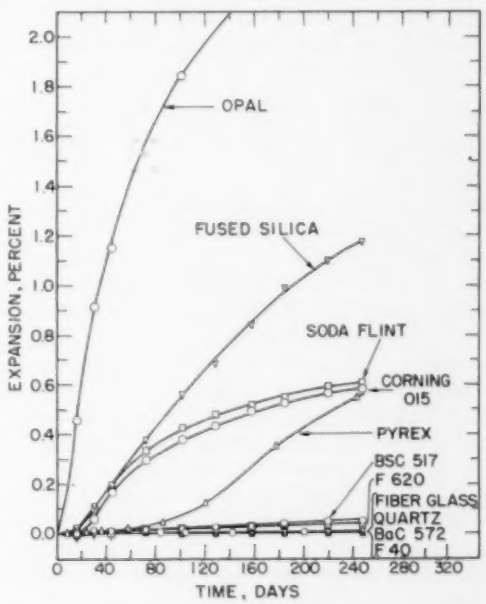

FIGURE 1. *Expansion of mortar bars aged over water at 100° F, made from high-alkali cement, and with 6 percent of the standard Ottawa sand replaced by various reactive and nonreactive aggregates.*

SiO_2), fused SiO_2 (glass), and opal (hydrous SiO_2), form an interesting series, ranging in activity from quartz with no abnormal expansion of the bars in 8 months, to opal with approximately 2 percent of expansion in 4 months, followed by mechanical failure of the specimens. Fused SiO_2 occupies an intermediate position, with an expansion far in excess of permissible tolerance [5]. Other aggregates besides quartz causing no appreciable expansion are F 40, BaC 572, and fiber glass type E. Pyrex 7740, the glass adopted as a standard reactive aggregate [6], is included for comparison.

The induction period, which appears in the curves for the reactive aggregates, can be partially attributed to the shrinkage that takes place during the early stages of the setting of cements. However, the great difference in the induction periods for different materials implies that the induction features are primarily characteristic of the individual aggregates. These composite characteristics are undoubtedly a function of the chemical durability and other chemical and physical properties of the materials and the storage environment.

2.3. Chemical Durability [3]

The varied chemical durabilities over an extended *p*H range, characteristic of the 11 aggregates evaluated in figure 1, are shown in figures 2, 3, 4, and 5.

The chemical-durability curves for the three forms of SiO_2 (quartz, fused SiO_2, and opal) are shown in figure 2. These three forms of silica have distinctive individual durability characteristics, with quartz showing no detectable alteration between *p*H 2 and *p*H 11.8. Over the same range, fused silica shows surface alteration (attack) only at alkalinities above *p*H 10, whereas opal exhibits dimensional changes over the entire *p*H range, with liberal swelling in the acid buffers and severe attack at *p*H 11.8. The relative order for destructive swelling of mortar bars by these three forms of silica is the same as for their relative chemical durabilities, with quartz the least and opal the most reactive.

In figure 3 are grouped the silicate aggregates that exhibit pronounced swelling over the acid range and well into the alkaline region, similar to opal. These three greatly dissimilar silicates (table 1), having the common characteristic of swelling, also cause conspicuous destructive expansion of mortar bars, as shown in figure 1. Continuing, in figure 4 are presented the glassy aggregates that showed unusual attack near neutrality by the buffers between *p*H 4 and *p*H 10, in contrast to the aggregates shown in figure 3, with extensive swelling over the same *p*H range. A glance at figure 1 reveals a pronounced difference for these groups in the expansion-bar test. For example, of those with the attack near *p*H 7, one (BaC 572) shows no destructive expansion, and

[3] The chemical durability of the various aggregates was determined by an interferometer procedure that has been particularly useful in the study of the chemical durability of optical glasses, voltage anomalies of the glass electrode, and in practical applications in various other fields [11, 12]. The procedure consists in observing the surface alteration of the specimen after exposure to Britton-Robinson universal buffer mixtures [13] for 6 hr at 80° C.

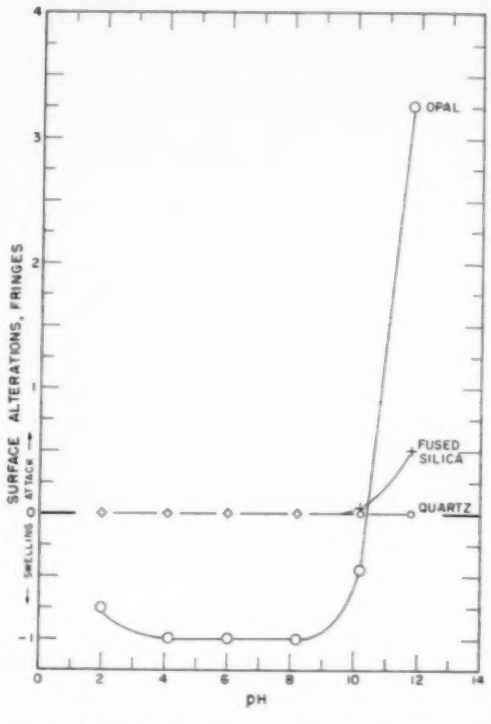

FIGURE 2. *Chemical durability (surface alteration) of three forms of silica.*

Exposure 6 hr at 80° C.

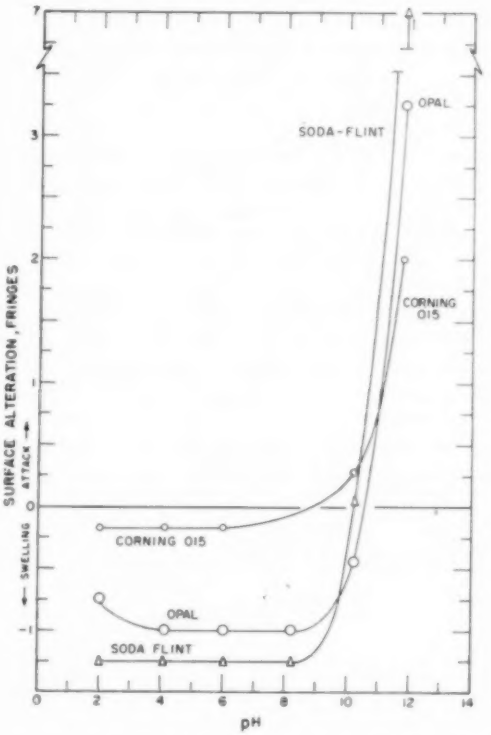

FIGURE 3. *Chemical durability (surface alteration) of three aggregates that exhibit swelling in the acid range.*

Exposure 6 hr at 80° C.

TABLE 1. *Chemical compositions*

Oxides	Corning 015 [a]	BaC 572 [b]	BSC 517 [b]	F 620 [b]	Soda flint [b]	Pyrex [c]	Fiber glass type E [d]	F 40 [b]	Opal [e]	Opal [f]	High-alkali cement
Na_2O	22	0.4	8.4	3.6	20	3.8					1.10
K_2O		7.7	11.8	5.2		0.4					0.09
CaO	6						16.0				63.3
BaO		30.8						30			
PbO				45.1	20						
ZnO		7.2	0.5								
B_2O_3		3.6	12.4			12.9	9.5				
As_2O_3		0.2	0.5	0.5							
Sb_2O_3		.4									
SiO_2	72	49.7	66.4	45.6	60	80.5	55	50	93.09	90.38	21.6
Al_2O_3						2.2	14.5		0.87	2.72	6.0
Fe_2O_3									.11	0.54	2.5
MgO							5.0				1.9
SO_3											2.3
TiO_2								20			
Ignition loss									5.40	5.32	1.1
Insoluble residue											0.2
HF residue [g]									1.51	4.30	

[a] Composition from references [1,11]. [b] Compositions of batch material. [c] Composition from C. J. Phillips, Glass, the miracle maker, p. 47. Pitman Publishing Corp., New York, N. Y. [d] Composition from reference [11]. [e] Selected clear pieces, used in all tests except expansion bars. [f] Run-of-mine grade, used in expansion bars. [g] The HF residue was fused and dissolved and R_2O_3 precipitated with NH_4OH and ignited. The Fe_2O_3 was determined in the ignited precipitate and the remainder of the R_2O_3 assumed to be Al_2O_3.

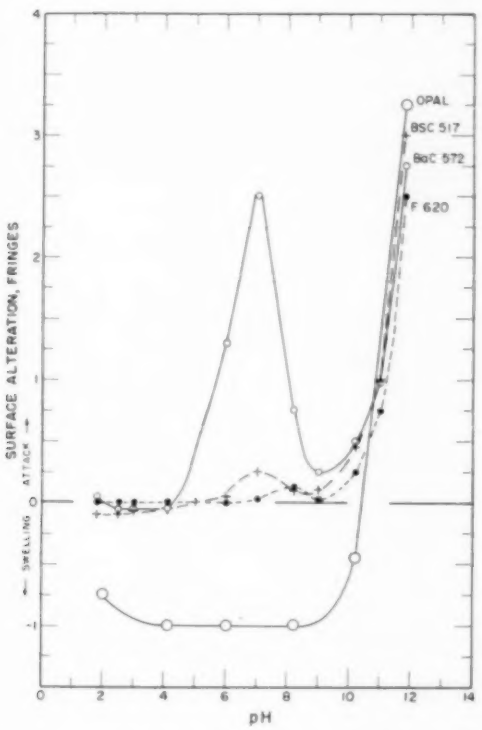

FIGURE 4. *Chemical durability (surface alteration) of three aggregates (optical glasses) showing unusual attack near neutrality.*

Data by Bernard R. Nebel.

the other two (BSC 517 and F 620) much reduced or delayed action.

An additional group of experimental aggregates is given in figure 5, in which the chemical durability of Pyrex 7740 glass, which serves as a standard reactive aggregate for testing high-alkali cements [6], is compared with F 40 and fiber glass (commercial type E). The latter two aggregates show attack in the acid region at *p*H 2, but are dissimilar in their reaction in the alkaline range, with F 40 being unaltered, whereas the fiber glass is severely attacked. These two aggregates, along with quartz and BaC 572, showed no destructive expansion of the test mortar bars. As F 40 and quartz are chemically resistant to attack by the high-alkaline buffers, their acceptable behavior in the mortar-bar tests is to be expected. The behavior of BaC 572 and the fiber-glass aggregates, with their poor chemical durability in the alkaline range, seems to be anomalous. However, these two exceptions furnish the most interesting and probably the most useful data of the entire series. For example, cross sections of the expansion bars reveal that BaC 572 and fiber-glass aggregates had not been attacked by the high-alkaline conditions [14] existing in the hydrated high-alkali cement. Thus, the inhibiting effect of saturated Ca $(OH)_2$ [15] from the cement, and certain individual constituents of the aggregates, such as barium and magnesium oxides, must be examined in future experiments.

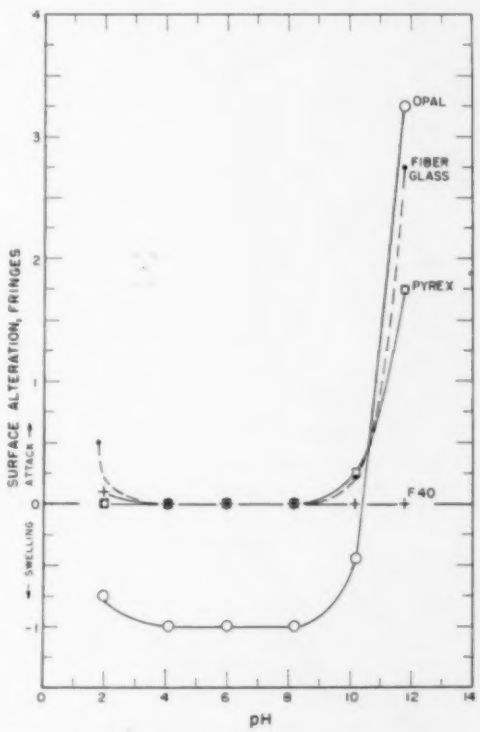

FIGURE 5. *Chemical durability of three special-purpose glasses.*

2.4. Hygroscopicity [4]

As the alkali-aggregate reaction cannot take place without the presence of water, and also because water is one of the chief constituents in the products resulting from the reactions, the relative hygroscopicities of the aggregate materials were determined. Figure 6 illustrates the results obtained for the 11 aggregates of figure 1, after 1 and 2 hr of exposure. Some of the groupings applicable to the chemical-durability data persist for the hygroscopicity in a superficial fashion. For example, the three forms of SiO_2 fall in the order, opal, fused SiO_2, and quartz, although the differentiation between fused SiO_2 and quartz is not very pronounced. The three chemically dissimilar aggregates, opal, Corning 015, and soda flint, characterized by swelling in the acid range, are also the three most hygroscopic materials of figure 6. Likewise, 6 of the 7 aggregates that caused unacceptable destructive expansion of mortar bars are found to be the most hygroscopic of the 11 materials tested, fused silica being the only destructive aggregate that does not conform. BaC 572, fiber glass, quartz, and F 40, the 4 nondestructive aggregates, are among the 5 least hygroscopic materials. The fact that fused SiO_2 constitutes such a glaring exception once again furnishes the most interesting data of the series and needs further study.

[4] The procedure for determining hygroscopicity was that reported in a previous publication [1], which consists in determining the change in weight of samples (water sorbed [16], ground to pass a No. 140 U. S. Standard Sieve) when exposed to the high humidity maintained by a saturated aqueous solution of $CaSO_4 \cdot 2H_2O$.

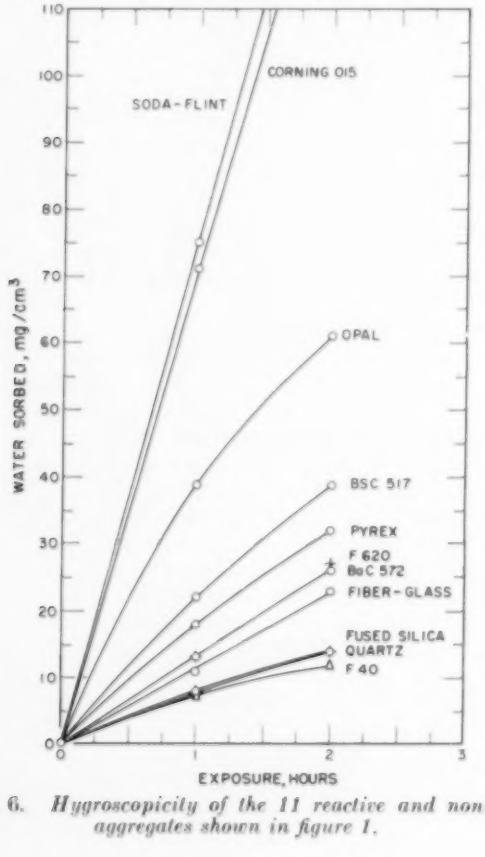

FIGURE 6. *Hygroscopicity of the 11 reactive and nonreactive aggregates shown in figure 1.*

2.5. Heterogeneous Equilibria [5]

The uneven distribution of migratable ions, as shown in figure 7, using excess $Ag(NH_3)_2^+$ as the indicator, reveals that the aggregate materials studied possess a negative nonmigratable ionic charge after leaching. Early inquiry into the destructive expansion of concrete structures caused by the presence of reactive aggregates, when used with high-alkali cement, revealed that osmotic forces were operative [3, 17]. In addition to differentiating between aggregate materials, these data also demonstrate that the frameworks of these materials (primarily silicates) behave as negatively charged nonmigratable ions. This condition is favorable for initiating and accelerating reaction within the silicate framework. The increased sodium ion concentration within the silicate framework over that in the ambient phase would reduce the solubility of $Ca(OH)_2$ so that it precipitates at the aggregate surface [14], inhibiting reaction there while the inner portion of the particle was being completely reacted and disintegrated as alkali silicates [1, fig. 14]. The destructive capacity of any aggregate would be partially determined by this heterogeneous equilibrative factor and by the chemical and physical nature of the reaction products.

The three forms of SiO_2 fall in their usual order of reactive and destructive capacity, with opal occupying the least, and quartz the most favorable position of the series.

[5] In the experiments on heterogeneous equilibria, the uneven distribution of the migratable ions $Ag(NH_3)_2^+$ and Br^- between the aggregate material and the ambient phase was determined by potentiometric titration of the excess Ag^+ ions remaining with the aggregate or the excess Br^- ions appearing in the ambient solution after the leached aggregate sample was treated with full-strength aqueous NH_4OH saturated with AgBr. The procedure consisted in treating 10 g of aggregate material (−50-, +140-mesh particle size) with 50 ml of the $Ag(NH_3)_2Br$ solution for 5 minutes, decanting and acidifying, followed by potentiometric titration, using Ag-AgBr and glass electrodes as the indicator and reference electrode, respectively. Standardized solutions of KBr or $AgNO_3$ (whichever the situation required) were used in the titration.

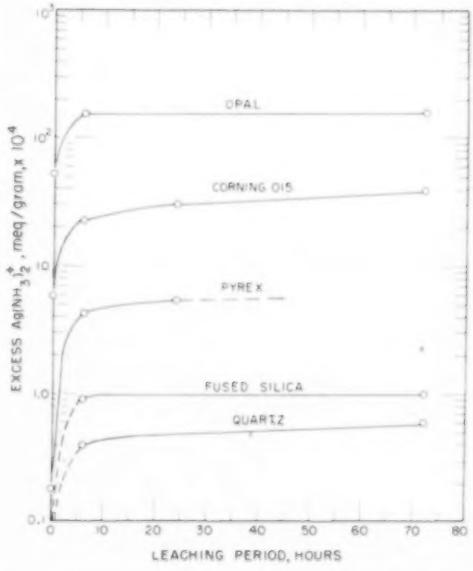

FIGURE 7. *Uneven distribution of migratable ions expressed as milliequivalents per gram of sample across the aggregate solution interface, after various periods of leaching at pH 4.1 at 80° C, using $Ag(NH_3)_2^+$ as the indicator ion.*

2.6. Surface Resistance [6]

Figure 8B shows the surface electrical resistance obtained for the same five aggregates whose heterogeneous equilibrium characteristics are given in figure 7. The surface resistances for the three forms of silica constitute a consistent series comparable with the heterogeneous equilibrium data, but the positions of the opal and Corning 015 aggregates are reversed. They follow, instead, the order of their hygroscopicity characteristics in figure 6. Thus, it appears that electrical surface-resistance measurements may give an indication of hygroscopicity. However, there are marked differences in the characteristics of the curves for these two types of data. The electrical-resistance data come to apparent acceptable equilibrium values for periods exceeding 2 hr, whereas the hygroscopicity curves (figs. 8A and 6) do not. In some cases, hygroscopicity values have continued to increase with the acquisition of water vapor until the weighing bottles have been filled to overflowing, as dictated by the lowered vapor pressure of aqueous solutions. On the other hand, electrical-resistance measurements give constant values characteristic of the aggregate material.[7]

Although the surface ohmic resistance and hygroscopicity of the aggregates might be expected to parallel each other, inspection of the results in figures 6 and 9 reveal reversals of position for several of the aggregates, and some of these even occupy different positions at different humidities. These latter reversals are undoubtedly determined by the nature of the hydrated and hydrolyzed reaction products following the sorption of moisture.

[6] The surface-resistance data were obtained by measuring with an eight-decade logarithmic ohmmeter [18] the resistance of a cell (fig. 10) containing a measured volume of powdered sample (−30, +50 U. S. Standard Sieve) when the cell was placed in the grid circuit and exposed to a controlled relative humidity. This special meter was necessary because the usual d-c megohm bridge caused excessive polarization, and the readings by the available a-c meters were vitiated by the capacity of the cell.

[7] This constant resistance can be attained much more rapidly at faster flow rates through the resistance cell.

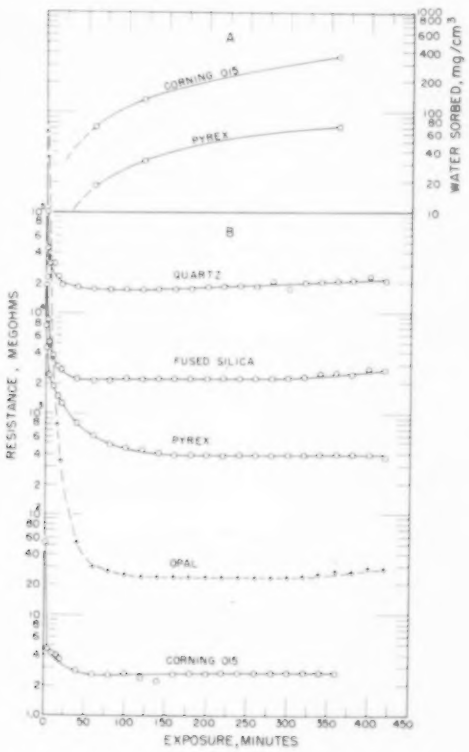

FIGURE 8. *Electrical resistance and water sorption of several aggregates.*

A. Typical hygroscopicity curves illustrating continued sorption of water with time of exposure; B, typical surface electrical resistance curves for five aggregates exposed to 98 percent relative humidity at flow rate of 0.5 liter per minute, illustrating an equilibrium state after 2 hr.

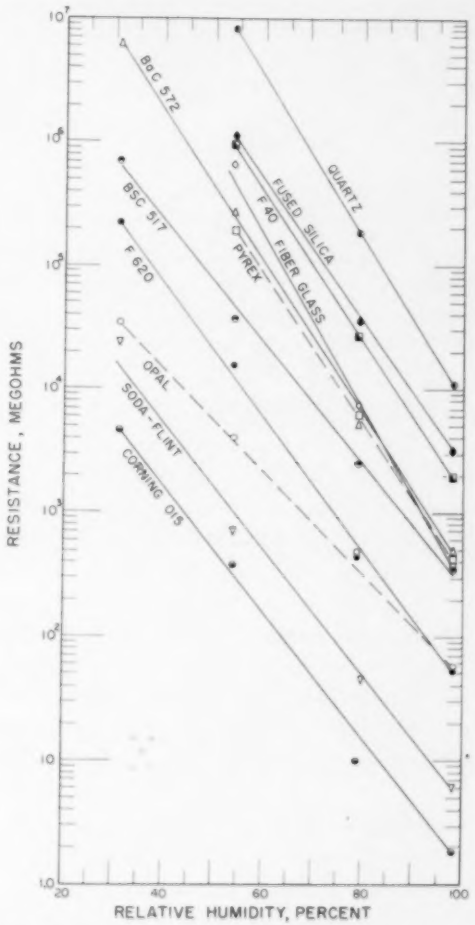

FIGURE 9. *Surface electrical resistance of 11 reactive and nonreactive aggregates at various relative humidities.*

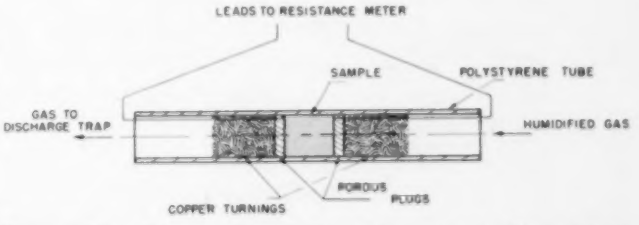

FIGURE 10. *Diagram of the cell used in measuring the resistance of aggregate samples while being exposed to controlled relative humidities.*

3. Conclusions

Although the properties studied and the procedures used lead to a broader understanding of the aggregate materials and of the part played by various physicochemical principles operative in the destructive expansion of concrete structures, it is evident that no single property was determined that can be used as a serviceability criterion for all materials.

The authors thank Given W. Cleek and S. B. Garfinkel for their assistance in the progress of this investigation, the former for furnishing experimental aggregate materials of special and interesting properties and the latter for designing and assisting in building the eight-decade logarithmic ohmmeter.

4. References

[1] Robert G. Pike, Donald Hubbard, and Herbert Insley, Mechanism of alkali-aggregate reactions, Proc. Am. Concrete Inst. **52,** 13 (1955).

[2] Thomas E. Stanton, Expansion of concrete through reaction between cement and aggregate, Proc. Am. Soc. Civil Engrs. **66,** 1781–1811 (1940).

[3] W. C. Hansen, Studies relating to the mechanism by which the alkali-aggregate reaction produces expansion in concrete, Proc. Am. Concrete Inst. **40,** 213–227 (1944).

[4] A. R. Alderman, A. J. Gaskin, R. H. Jones, and H. E. Vivian, Studies in cement aggregate reaction, Bulletins 229 and 256, Commonwealth Sci. and Ind. Research Organization, Australia (1947, 1950).

[5] Richard C. Mielenz and Leslie P. Witte, Tests used by Bureau of Reclamation for identifying reactive concrete aggregates, Am. Soc. Testing Materials, Proc. **48,** 1071–1103 (1946).

[6] Federal Specification, SS–C–208b, Cement: Portland-Pozzolan (1954).

[7] A. J. Gaskin, R. H. Jones, and H. E. Vivian, The reactivity of various forms of silica in relation to the expansion of mortar bars, Australian J. Appl. Sci. **6,** 78 (1955).

[8] Donald O. Woolf, Reaction of aggregate with low-alkali cement, Public Roads **27,** 50 (1952).

[9] H. E. Vivian, XVII: Some effects of temperature on mortar expansion, Australian J. Appl. Sci. **2,** 114 (1951).

[10] C. E. S. Davis, XVIII: The effect of soda content and of cooling rate of Portland cement clinker on its reaction with opal in mortar, Australian J. Appl. Sci. **2,** 123 (1951).

[11] Martin J. O'Leary and Donald Hubbard, Some properties of a glass used in paper manufacture, J. Research NBS **55,** 1 (1955) RP2599.

[12] Robert G. Pike and Donald Hubbard, An interferometer procedure applied to the study of the chemical durability of silicates, enamels, and metals, J. Research NBS **50,** 87 (1953) RP2394.

[13] H. T. S. Britton, Hydrogen ions I, 3d ed, p. 313 (D. van Nostrand Co., New York, N. Y., 1943).

[14] George Kalousek, C. H. Jumper, and J. J. Tregoning, Composition and physical properties of aqueous extracts from Portland cement clinker pastes containing added materials, J. Research NBS **30,** 215 (1943) RP1530.

[15] George Verbeck and Charles Gramlich, Osmotic studies and hypothesis concerning alkali-aggregate reaction, Am. Soc. Testing Materials, Proc. **55,** 1110 (1955).

[16] James W. McBain, The mechanism of the adsorption (sorption) of hydrogen on carbon, Phil. Mag. **18,** 916 (1909); Z. physik. Chem. **68,** 471 (1909).

[17] D. McConnell, R. C. Mielenz, W. Y. Holland, and K. T. Greene, Cement and aggregate reaction in concrete, Proc. Am. Concrete Inst. **44,** 93 (1947).

[18] Samuel B. Garfinkel, An eight decade logarithmic ohmmeter, Instrument Soc. Am. J. **3,** 54 (1956).

WASHINGTON, January 31, 1957.

Journal of Research of the National Bureau of Standards Vol. 59, No. 2, August 1957 Research Paper 2781

Insulated Loop Antenna Immersed in a Conducting Medium

James R. Wait

A solution is given for the fields of a circular loop in a conducting medium. The loop is assumed to have a uniform current, and it is enclosed by a spherical insulating cavity. The impedance of the loop is also considered. It is shown that the power radiated from the loop varies approximately as the reciprocal of the radius of the cavity for a specified loop current. Furthermore, if the cavity is electrically small, relative to the external medium, the radiation field is not significantly affected by the presence of the cavity.

1. Introduction

There has been some interest shown in recent years on the subject of radiating systems immersed in dissipative media [1 to 9].[1] Such a condition exists when transmitting antennas are located in sea water, buried beneath the ground, or surrounded by an ionized medium, such as the ionosphere. Most investigators have considered only the propagation aspects of the general problem. That is, attention was devoted only to the radiated field for a specified antenna current. An associated, and a usually much more difficult problem, is the calculation of the impedance of the antenna.

Tai [1], in an interesting analysis, showed that for a Hertzian electric dipole in a dissipative medium, infinite power is required to produce a finite field strength at some distant point in the medium. This difficulty is overcome when the dipole is placed in an insulated cavity. It has also been shown that a magnetic-dipole-type antenna was more efficient than an electric-dipole-type antenna [2, 5].

It is the purpose of the present paper to reinvestigate the problem treated before. Specifically, the impedance and fields are calculated for a circular loop with a spherical insulating cavity, all immersed in a homogeneous dissipative medium. In the previous analysis [5], the loop was represented as a magnetic dipole at the center of the cavity. It was implied that the dimensions of the loop were small compared to those of the cavity. In this sequel, these limitations are removed by treating the problem from another viewpoint.

In terms of spherical coordinates (r, θ, ϕ) the insulating cavity is defined by $r<a$ and has a dielectric constant, ϵ_0. The exterior homogeneous dissipative medium, $r>a$, has a dielectric constant, ϵ, and a conductivity, σ. The permeability, μ, of both regions is taken to be that of free space. The loop, for the moment, is considered to be a single turn carrying a uniform current, I. The coordinates of the loop are $\theta=\beta$ and $r=b$, so that the axis of the (circular) loop passes through the center of the spherical cavity (see fig. 1).

The dimensions of the cavity are taken to be very small compared to the wavelength, which suggests that a quasi-static approach to the problem should be adopted. As a consequence, the fields are a solution of Laplace's equation inside the cavity and a solution of the wave equation outside. Although it is not necessary to invoke the quasi-static assumption for the field calculation, it leads to the desired result in a direct fashion without becoming encumbered with a myriad of spherical Bessel functions. Furthermore, in any instance where the cavity was not small compared to the wavelength, the assumption of uniform current around the loop would be a poor one for a localized generator.

[1] Figures in brackets indicate the literature references at the end of this paper.

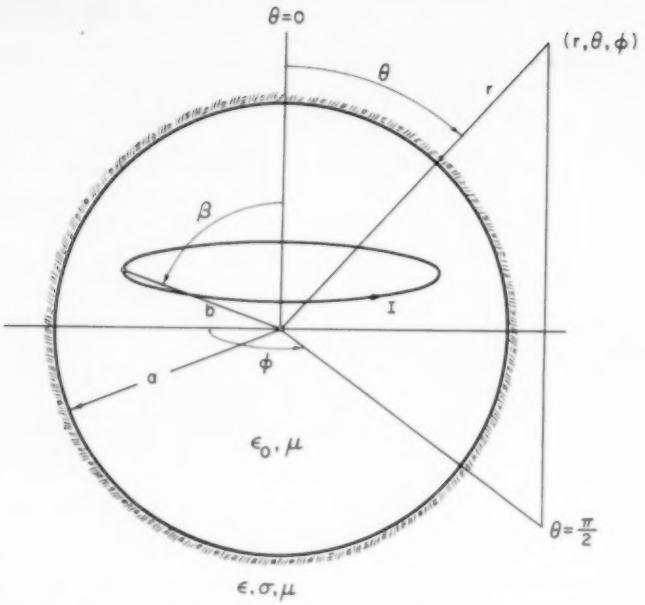

FIGURE 1. *Circular loop antenna in a spherical insulating cavity.*

The surrounding homogeneous dissipative medium is infinite in extent.

2. Formal Solution

In view of the polar symmetry of the stated problem, the usual vector potential, $\vec{A}$, has only an azimuthal component, A. The nonvanishing field components are then given by

$$E_\phi = -i\mu\omega A,$$

$$H_\theta = -\frac{1}{r}\frac{\partial(Ar)}{\partial r} \tag{1}$$

$$H_r = \frac{1}{r\sin\theta}\frac{\partial}{\partial\theta}(A\sin\theta).$$

The (quasi-static) form of the vector potential of the primary field of a circular loop in an insulating space can be expressed in terms of spherical harmonics (see appendix):

$$rA^p = \frac{I\sin\beta}{2}\sum_{n=1}^{\infty}\frac{b}{n(n+1)}\left(\frac{b}{r}\right)^n P_n^1(\cos\theta)P_n^1(\cos\beta) \tag{2}$$

for $r>b$, where P_n^1 is the associated Legendre function. To account for the spherical wall of the cavity, a secondary field, A^s, must be added. Because it is also a solution of Laplace's equation and is finite $r=0$, it must be of the form

$$rA^s = \frac{I\sin\beta}{2}\sum_{n=1}^{\infty}\frac{S_n b}{n(n+1)}\left(\frac{r}{b}\right)^{n+1} P_n^1(\cos\theta)P_n^1(\cos\beta) \tag{3}$$

for $r<a$, where S_n is an unknown coefficient.

The field in the external region is a solution of the wave equation, and furthermore the solution must give rise to outgoing waves at infinity. Therefore,

$$rA = \frac{I\sin\beta}{2}\sum_{n=1}^{\infty}\frac{T_n b}{n(n+1)}\frac{k_n(\gamma r)}{k_n(\gamma a)}P_n^1(\cos\theta)P_n^1(\cos\beta) \tag{4}$$

for $r>a$, where $k_n(z)$ is a spherical Hankel function defined by

$$k_n(z)=e^{-z}\sum_{m=0}^{n}\frac{(n+m)!}{m!(n-m)!(2z)^m}, \tag{5}$$

$\gamma=(i\mu\sigma\omega-\epsilon\mu\omega^2)^{1/2}$, and T_n is an unknown coefficient. The boundary condition at $r=a$ requires the continuity of E_ϕ and H_θ. The solution of the resulting algebraic equations leads to

$$S_n=\left[\frac{n+\alpha_n}{(n+1)-\alpha_n}\right]\left(\frac{b}{a}\right)^{2n+1} \tag{6}$$

and

$$T_n=\left[\frac{(2n+1)}{(n+1)-\alpha_n}\right]\left(\frac{b}{a}\right)^{n}, \tag{7}$$

where

$$\alpha_n=\left[z\frac{d}{dz}\log k_n(z)\right]_{z=\gamma a}.$$

When S_n and T_n are inserted into eq (3) and (4), the complete solution is obtained.

3. Discussion of Result

It is now of interest to investigate the influence of the cavity on the external fields. With this in mind, A, for $r>a$, is written in the form

$$rA=\frac{I\sin\beta}{2}\sum_{n=1}^{\infty}\frac{b}{n(n+1)}\frac{k_n(\gamma r)n!}{(2n)!}(2\gamma b)^n G_n\times P_n^1(\cos\theta)P_n^1(\cos\beta), \tag{8}$$

where

$$G_n=\left[\frac{2n+1}{(n+1)-\alpha_n}\right]\frac{(2n)!}{n!(2\gamma a)^n k_n(\gamma a)}. \tag{9}$$

It can be readily verified that $\lim_{\gamma a\to 0} G_n=1$. When this limiting form is inserted into eq (8), the resulting expression would be the field of a small loop in an infinite dissipative medium without any cavity. Specific values of G_n for finite γa are

$$G_1=\frac{3e^z}{3+3z+z^2} \tag{10}$$

and

$$G_2=\frac{15e^z}{15+15z+6z^2+z^3}, \tag{11}$$

where $z=\gamma a$. The value G_1 can be regarded as the ratio of the effective dipole moment for a loop in an insulated cavity to that of the loop without any cavity. It agrees with a result given previously [5] by a somewhat different method. G_2 is the corresponding ratio for the next higher multipole term. For most cases of practical interest, γa is somewhat less than unity, and the multipole terms are not important in the external region when γr is large compared to one. Furthermore, in this case

$$G_1=1+\frac{z^2}{6}+\ldots\cong 1,$$

and the external fields for a specified loop current are not dependent on the presence of the cavity.

Attention is now turned to the effect of the cavity on the impedance of the circular loop. The impedance of the loop in free space is denoted Z_0, which is assumed known. The impedance of the loop inside the cavity is then written

$$Z=Z_0+\Delta Z$$

where ΔZ is the incremental change due to the finite size of the cavity. ΔZ is the secondary electric field E_ϕ^s integrated along the circumference for a unit loop current. Therefore,

$$\Delta Z=i\mu\omega A^s\frac{2\pi b}{I} \tag{12}$$

$$=i\mu\omega \sin\beta(\pi b)\sum_{n=1}^{\infty}\frac{T_n}{n(n+1)}\left(\frac{b}{a}\right)^{2n+1}P_n^1(\cos\beta)P_n^1(\cos\theta), \tag{13}$$

where T_n is given by eq (7). The above expression is simplified somewhat in the important case where $|\gamma a|$ is small compared to unity, because then

$$T_n\cong-\frac{2}{(2n+1)(2n-1)}(\gamma a)^2 \tag{14}$$

neglecting terms containing $(\gamma a)^3$, $(\gamma a)^4$, etc. Furthermore, if $\theta=\beta=\pi/2$, it follows that

$$\Delta Z\cong\frac{(\mu\omega)^2(\sigma+i\omega\epsilon)S^2}{6\pi a}\sum_{n=1}^{\infty}\frac{6}{n(n+1)(2n+1)(2n-1)}\left(\frac{b}{a}\right)^{2n-2}$$

$$\cong\frac{(\mu\omega)^2(\sigma+i\omega\epsilon)S^2}{6\pi a}\left[1+\frac{1}{15}\left(\frac{b}{a}\right)^2+\frac{1}{70}\left(\frac{b}{a}\right)^4+\cdots\right], \tag{15}$$

where $S=\pi b^2$. When displacement currents are negligible (i. e., $\omega\epsilon\ll\sigma$) and $(b/a)^2\ll1$,

$$\Delta Z\cong\frac{(\mu\omega)^2\sigma S^2}{6\pi a}. \tag{16}$$

For a specified current, I, on the loop, the power supplied to the surrounding conducting medium is then given by

$$P\cong\frac{(\mu\omega)^2\sigma I^2S^2}{12\pi a}, \tag{17}$$

which agrees with a previous result [5] derived from energy considerations.

Although the preceding analysis refers to a single-turn loop, the results are directly applicable to a loop of N turns by replacing S by SN. The appropriate expression must also be used for Z_0, of course.

It would appear that power radiated from the loop for a specified current varies approximately as the reciprocal of the diameter of the cavity. This conclusion is not modified to any extent by the finite size of the loop in the cavity.

4. Appendix

It is well known that the vector potential can be obtained from a volume integration over the contained current. Furthermore, because the loop has a filamental uniform current with a component only in the ϕ direction, the vector potential has polar symmetry and has only a ϕ component A; it is given by the line integral

$$A^p=\frac{I}{4\pi}\int_0^{2\pi}\frac{\cos\phi_1}{R}\,b\sin\beta d\phi_1, \tag{18}$$

where ϕ_1 is the azimuthal coordinate for a point on the loop relative to the reference plane, and where

$$R^2=r^2+b^2-2rb\cos\Omega$$

and $\cos\Omega=\cos\theta\cos\beta+\sin\theta\sin\beta\cos\phi_1$. Now the factor $1/R$ is a solution of Laplace's equation and can be written in terms of spherical harmonics, as is well known [10].

$$\frac{1}{R}=\sum_{n=0}^{\infty}\sum_{m=0}^{n}\epsilon_m\frac{(n-m)!}{(n+m)!}P_n^m(\cos\theta)P_n^m(\cos\beta)\cdot\cos m\phi_1\begin{cases}b^n/r^{n+1}; & r>b\\ r^n/b^{n+1}; & r<b,\end{cases}\tag{19}$$

where $\epsilon_0=1$, $\epsilon_m=2$ $(m\neq 0)$, and where the P_n^m are the associated Legendre polynomials. On inserting the above expression for $1/R$, and utilizing orthogonality, eq (18) reduces to

$$A^p=\frac{I\sin\beta}{2}\sum_{n=1}^{\infty}\frac{P_n^1(\cos\theta)P_n^1(\cos\beta)}{n(n+1)}\begin{cases}(b/r)^{n+1}; & r>b\\ (r/b)^n; & r<b,\end{cases}\tag{20}$$

which is the desired result.

5. References

[1] C. T. Tai, Hertzian dipole immersed in a dissipative medium, Cruft Lab. Report No. 21 (Harvard University 1947).

[2] J. R. Wait, Transient electromagnetic wave propagation in a conducting medium, Geophysics **16,** 213 (1951); **18,** 138 and 971 (1953); see also Ph. D. Thesis, University of Toronto (March 1951).

[3] R. K. Moore, Theory of radio communication between submerged submarines (Ph. D. Thesis, Cornell University, 1951).

[4] J. R. Wait, The magnetic dipole on the horizontally stratified earth, Can. J. Phys. **29,** 577 (Nov. 1951).

[5] J. R. Wait, The magnetic dipole antenna immersed in a conducting medium, Proc. Inst. Radio Engrs. **40,** 1244 (Oct. 1952).

[6] J. R. Wait and L. L. Campbell, Fields of an oscillating magnetic dipole immersed in a semi-infinite conducting medium, J. Geophys. Research **58,** 167 (June 1953).

[7] R. H. Lien, Radiation from a horizontal dipole in a semi-infinite dissipative medium, J. Appl. Phys. **24,** 1 (Jan. 1953) (see a discussion of this paper by J. R. Wait, J. Appl. Phys. **24,** 958 (July 1953) in equation (6), V should be replaced by U).

[8] A. Banos and J. P. Wesley, The horizontal electric dipole in a conducting half-space, University of California, Marine Physical Lab., Pt. I, S10 Ref. 53–33, Sept. 1953, and Pt. II, S10 Ref. 54–31 (Aug. 1954).

[9] H. A. Wheeler, Fundamental limitations of a small V. L. F. antenna for submarines, Paper No. 14 (Symposium on V. L. F. Radio Waves, January 23–25, 1957, Boulder, Colo.).

[10] P. M. Morse and H. Feshbach, Methods of theoretical physics, vol. II, p. 1326 (McGraw-Hill Book Co., Inc., New York, N. Y., 1953).

Boulder, Colo., February 15, 1957.

Journal of Research of the National Bureau of Standards Vol. 59, No. 2, August 1957 Research Paper 2782

Noncrystal Ionic Model for Silica Glass

Leroy W. Tilton

A model was constructed of pentagonal rings of symmetrical tetrahedra so connected that all five silicons lie in one plane and all angles Si—O—Si approximate 180°. From an initial tetrahedron the rings extend in six directions to include its six edges, and in the resulting three-dimensional network each ring forms a common interface between dodecahedral cages which necessarily have fivefold symmetry. Such symmetry is incompatible with formation of a crystal lattice and thus the structure can be extended in three dimensions only to a very limited degree and with unavoidable stress and distortional strain. A stressed network cluster of such dodecahedral cages is here called a VITRON.

If the scale in this model for silica glass is taken as 1.6 A, from silicon to oxygen, the model is found to be in accord with other radial distances computed from diffraction data and the density is correct within 10 percent. The apertures of the pentagonal interfaces are of suitable size to explain data on the diffusion of noble gases through silica. Shared penta faces and intermittent oxygen bridges connect neighboring vitrons and constitute an interstitial tissue of relatively weakened structure that accounts for the observed low tensile strengths of silica glass and provides channels for viscous flow.

The proposed cages would be less pliable at low temperatures and so the interstitial tissues between vitrons should expand in volume on cooling. This "negative" expansion would counter the normal expansion and account for the known extremely small (net) expansivity of silica glass. The accompanying changes in strength and volume of the glass at its weakest places, the interstitial tissues, can account for a number of known "anomalies" in thermal behavior of silica glass with respect to its volume, compressibility, elastic moduli, and viscous flow.

The vitron concept reconciles the crystallite and the network theories of glass by proposing nuclei that cannot grow extensively and a distribution of localized stresses that may constitute an acceptable degree of randomness and provide effective modulations in continuity. This concept of definite but limited microregularity in structure suggests that other noncrystal symmetries should be studied for possible interest in other fields such as liquids and high polymers.

1. Introduction

Evidence from X-ray data shows that glasses and even liquids have some degree of ordered arrangement, although it definitely differs from that in crystals. Also, in studies of liquids and plastics it is recognized that limited ordered arrangements, often called "crystallinity," can exist without formation of macroscopic crystals. Under these circumstances two important theories of the glassy state have developed. The *crystallite* theory was stated by Randall and coworkers [1][1] in 1930. The presence of submicroscopic crystallites or crystalline nuclei in very large numbers in undercooled glasses was inferred, soon after the X-ray reports published by Clark and coworkers [2] in 1929, in order to account for the breadth of the observed diffraction rings. The acceptance of this idea proved difficult because many investigators found no evidence of a normal growth in the size of such crystallites under conditions that do promote growth whenever nuclei of crystals are known to be present.

The *network* theory resulted largely from the work of Zachariasen [3] and his coworkers in the field of chemical crystallography, and some associated ideas were more definitely formulated by Warren [4] and his coworkers in analyzing their X-ray data to establish interatomic distances and in interpreting the breadth of the diffraction rings from glass as contrasted with the well-defined rings from crystals. This continuous random network theory of glasses has been stimulating and fruitful in the field of inorganic glasses. A very limited degree of short-range order of arrangement of nearest neighbors and next nearest neighbors among the ions in glass is now definitely determinable by X-ray and electron diffraction, but the unbroken continuity and the very considerable randomness that is often assumed at longer distances seem incompatible with some experimental data.

W. A. Weyl [5] has considered that the network theory "in its present form" is not satisfactory to account for some existing data, and he wrote a paper "to show the need for a revision in our present approach to the constitution of glasses." In this paper he says: "One of the most important properties of glass, its mechanical strength, seems to resist all attempts to unveil its secrets"; again, "We have no plausible explanation yet for the thermal expansion of glasses as a function of their composition"; also, "It is customary to talk about 'flow units' in describing viscosity . . . about association-disassociation equilibria in any discussion of the effects which thermal history has upon the properties of glass. . . . Nobody, however, has yet given an accurate description of a 'flow unit' . . . nor presented a reasonable concept of the unit which disassociates. . . ."

Confining attention to the simple case of silica glass, one finds numerous and well-established data that characterize this material as unusual or even unique in respect to some of its properties, such as expansibility, compressibility, rigidity, and variations therein as effected by temperature and pres-

[1] Figures in brackets indicate the literature references at the end of this paper.

sure. These relationships have been discussed in detail by Babcock, Barber, and Fajans [6], who say, ". . . Use of the random network theory . . . has in general been unsuccessful in interpreting the properties of silicate glasses. . . ." Spinner [7], who measured elastic moduli at elevated temperatures, says: "It seems clear that . . . the usual picture of the structure of silica, as a random 3-dimensional network of SiO_4 tetrahedra, needs to be amended or modified to explain the various phenomena associated with the material."

Evidence of somewhat long-range order in silica glass was found by Melkonian [8], who wrote, "Fused quartz . . . was expected not to show microcrystalline interference effects because of its supposed lack of long-range crystalline structure. Thus, it was expected to show a transmission nearly independent of neutron energy and hence to be suitable for use as a secondary standard . . . . Fairly large interference effects are evident which make this particular sample useless as a secondary standard." In accord with this, Milligan, Levy, and Peterson [9], in their neutron-diffraction studies on vitreous silica, found 5 or 6 well-defined maxima and 4 or 5 others that were less well defined. Hoffman and Statton [10] used the low-angle scattering of X-rays in glass and found evidence of spacing in fused silica of 30 A or larger. In brief, there is evidence that the short-range order should be extended at the expense of longer-range randomness.

In order to study possible extensions of the accepted short-range order in simple silica glass, a three-dimensional model was constructed starting with silicon-oxygen tetrahedra connected at their corners by the sharing of their oxygens. This model, described in this paper, gives the correct density for silica glass within 10 percent, provided the scale is determined in accord with the established average distance of 1.6 A from silicon to oxygen as found [11] for silica and the silicates. It will be shown that the interatomic distances are in very good agreement with all radial distances computed from X-ray, electron, and neutron-diffraction data, and the apertures are of suitable size to explain Norton's [12] data on the diffusion of noble gases through silica.

The proposed model is a network of pentagonal rings of tetrahedra with 12-sided regular cavities, as in figure 1 (approximate diameter, locus of silicon centers, 8 A). It cannot grow extensively without peripheral tensional distortions that ultimately prevent further maintenance of the silicon-oxygen bonds. A cluster of such dodecahedral cavities or cages, such as shown in figure 2, is here called a VITRON, a new concept that may have application in other fields such as rheology and high-polymer studies where noncrystal order may be evidenced.

Aside from the fundamental conceptual difference between a vitron and a crystallite, the proposed model does in many respects accord well with the crystallite hypothesis. It is also essentially the network hypothesis with a modulation of its continuity,

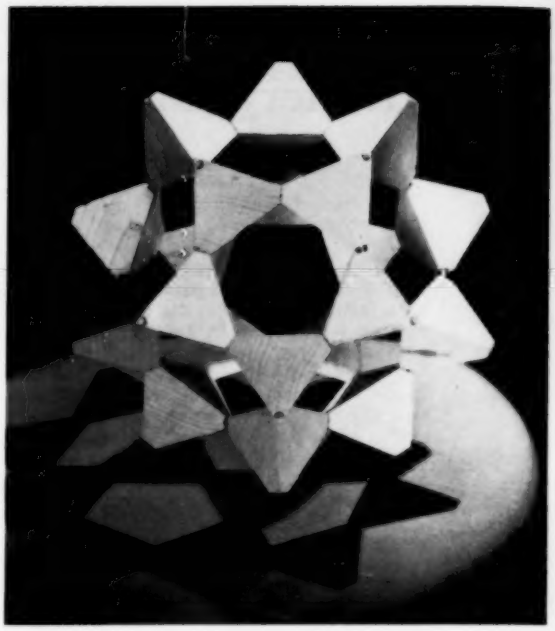

FIGURE 1. *View along fivefold axis of a single-element vitron constructed of 20 tetrahedra representing 20 silicon atoms at their centers and 30 oxygen atoms at their connected corners.*

(Twenty outer corners are available for attachments.) Only one-quarter of each Si and one-third of each (connecting) O belong to this cage as an element or unit of a larger vitron. In other words, 5 (SiO_2) constitute a single element or cage of a vitron on a continuum basis.

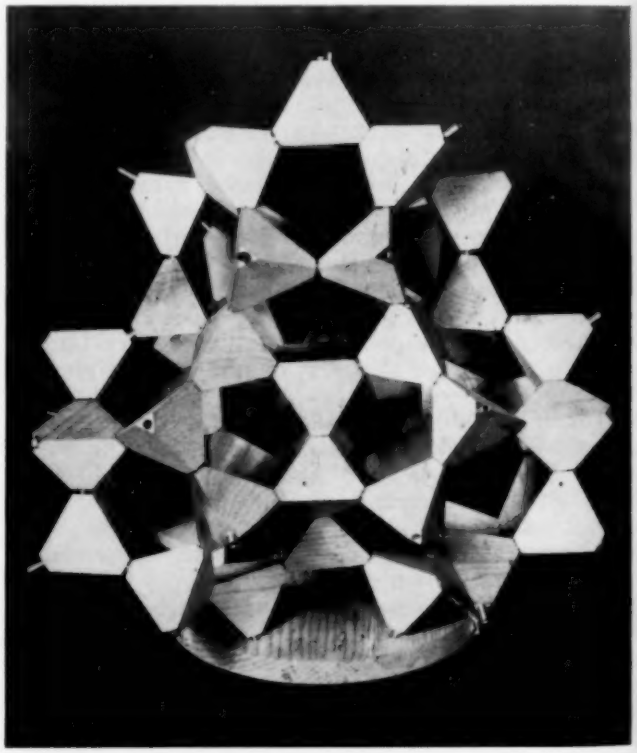

FIGURE 2. *Off-axis view of completed four-element vitron (type 4, tetrahedral).*

Coiled wire springs indicate extra O− charges and vacant tetrahedral corners indicate Si+ charges available for attachments to other vitrons by oxygen bridges. At center foreground is a reentrant three-face that can unite with another vitron presenting a convex three-face. See appendix.

a reduced randomness, and an added feature of localized stress distribution.

Partial unions and attachments between adjacent vitrons form interstitial channel tissues that are less regular and weaker than the intravitron structure. These tissues, together with the localized stress distributions within vitrons, are important in qualitative explanations of the peculiar effects of heat and pressure on the volume characteristics of silica glass; also in understanding viscous flow and conductance. Preliminary studies indicate that the proposed model will permit semiquantitative inferences concerning possible cavity-saturation limits for nonsilica that correlate with property-composition curves of solubility, chemical attack, volatilization, and specific volume for binary alkali-silicate glasses.

2. Pentagonal Dodecahedral Model

Silica glass is here considered to have a high-temperature arrangement of connected silicon-oxygen tetrahedra that has been cooled so quickly that the conditions at high temperature have been "frozen" by rapid increases in rigidity. It is therefore assumed that the connected tetrahedra will have minimum density, and this can obtain only if the bonds form angles Si–O–Si of 180° and the rings, if any, are circular and planar so that the tetrahedra can have maximum distention. (See fig. 3.) Under these circumstances, probability greatly favors the formation of pentagonal rings, as mentioned by Poncelet [13], because the interior angle of a regular tetrahedron is 109° 28′ and differs so little from 108°, the interior angle of a regular pentagon.

Growth of this structure of minimum density proceeds uniquely in 6 directions from an initial tetrahedron to form a network containing dodecahedral holes or cavities, each separated from its 12 somewhat-distorted neighboring cavities by 12 planar interfaces of very slightly stressed penta rings. An important property of this model is its many axes, 15 of twofold, 10 of threefold, and 6 of fivefold symmetry. Each of the 15 twofold axes makes an angle of 36° with each of its 4 neighbor axes, and similarly the 10 axes are equidistributed at angles of 41° 48′ and the 6 axes at 63° 26′. These features mean close relation to crystal symmetry and a high probability of approximate alinement of different portions of the structure even if separated by less well alined interstitial regions or tissues.

The most important property of this proposed model is its fivefold symmetry, which precludes formation of crystals. Just as penta tiles fail where hexagons succeed in covering a floor, so do regular penta dodecahedra fail to fill space completely and extensively. The interior dihedral angle of a dodecahedron is, however, 116.6°, and thus not far from 120°, which would be exactly right for filling space without stress and distortions. If one regular dodecahedron is attached or joined on each face to 12 like structures, none in the outer shell can touch any of its 5 neighbors. By radial compression these neighbors may meet and the requisite tangential tension in the peripheral bonds may not be excessive for the first shell. Further increase in cluster size by the addition of 32 cages in the second shell would require much higher tensions in the outermost bonds, and some defective attachments or broken bonds might result in order for bonds to hold elsewhere on the periphery. Thus the great strength of the silicon-oxygen bond is the factor that should cause, and yet automatically limit, the growth in size of

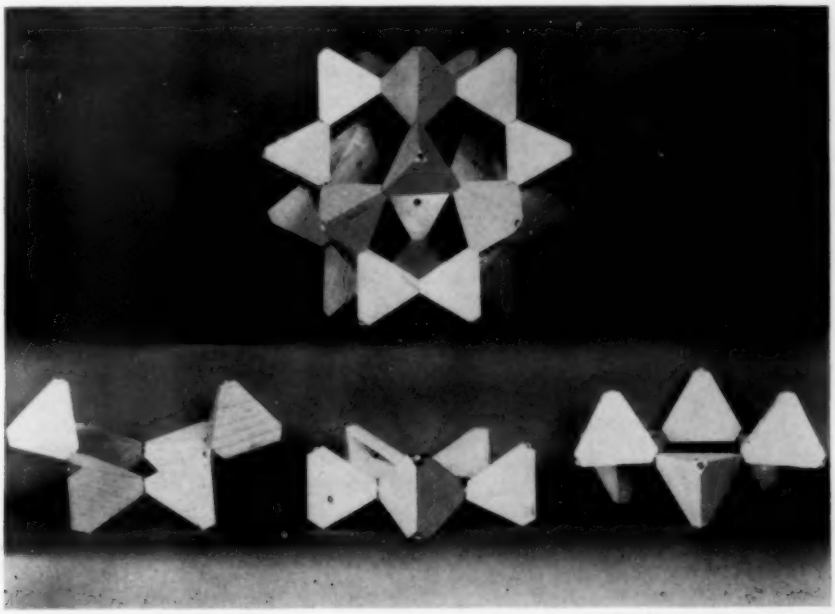

FIGURE 3. *View of regular pentagonal dodecahedral cage formed of planar pentagonal rings of tetrahedra as shown at lower center.*

The high-temperature low-density planar ring proposed for silica glass contrasts with the nonplanar hexagonal elemental rings in the denser silicas tridymite (left) and cristobalite (right).

vitrons. The automatically limited ability to grow, and a distribution of stresses localized and balanced within each vitron, are features that may distinguish a vitreous substance from a crystal.

Silicon ions are situated at each of the 20 vertices of a pentagonal dodecahedron, and oxygen ions at the midpoint of each of the 30 edges. An isolated unit of this sort would consist of 20 silicon atoms and 30 of oxygen with 20 plus charges, and thus be represented as $(Si_{20}O_{30})^{20+}$. A cluster of 7 such units is $(Si_{85}O_{145})^{50+}$ but it is decidedly nonspherical. With 13 such cages there is again an approximation to sphericity with a diameter of 20 A (see fig. 7). This 13-cage cluster can be represented as $(Si_{130}O_{230})^{60+}$, and the plus charges are distributed over the whole surface in 12 pentagonal groups. Upon addition of the next shell, consisting of 32 dodecahedral cages, to form a 45-cage cluster the diameter increases to 30 A and the formula is $(Si_{330}O_{620})^{80+}$. The plus charges indicate the degree of attachability of these vitrons to their neighbors through oxygen bonds. In addition, or alternately, they may actually unite or grow together with neighbors to limited extents, as further discussed in the appendix.

Figures 4, 5, and 6 (also 9 and 10) are helpful for visualizing the arrangement of atoms in the proposed model. With dimensions based on the average X-ray datum of 1.60 A for the Si-O distance (between centers), an element or cage can be inscribed in a sphere of 9 A diameter, and a sphere of 7 A diameter can be inscribed inside a cage. Only a central cage of a vitron can be truly regular and symmetrical. The surrounding cages must be deformed in order to contact their neighbors. Hence it is interesting to recall that Warren [14] estimated 8 A as the maximum dimension of the region of periodicity in fused quartz, and that Valenkov and Poray-Koshitz [15] estimated 12 A as the extent of perfect order, with surrounding regions of intermediate degree of order. Also, measurements on thermal conduction in glasses have made it possible, as shown by Kittel [50], to estimate 8 A as the mean free path distance over which plane elastic heat waves (phonons) may travel in silica glass at room temperatures before distortional scattering.

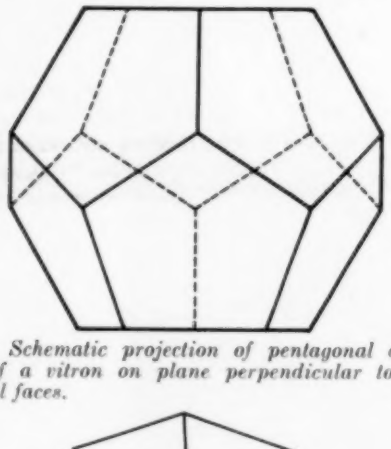

FIGURE 4. *Schematic projection of pentagonal dodecahedral element of a vitron on plane perpendicular to two of its pentagonal faces.*

FIGURE 5. *Schematic dodecahedral element viewed along one of its six axes of fivefold symmetry through pairs of opposite and parallel faces.*

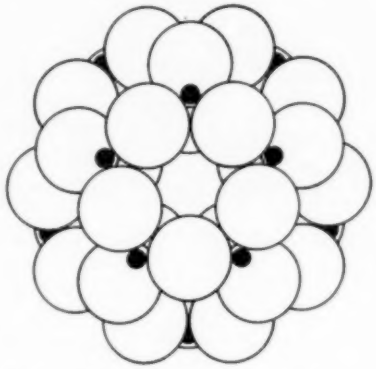

FIGURE 6. *Dodecahedral element viewed along one of its six axes of fivefold symmetry.*

Some outer atoms are omitted.

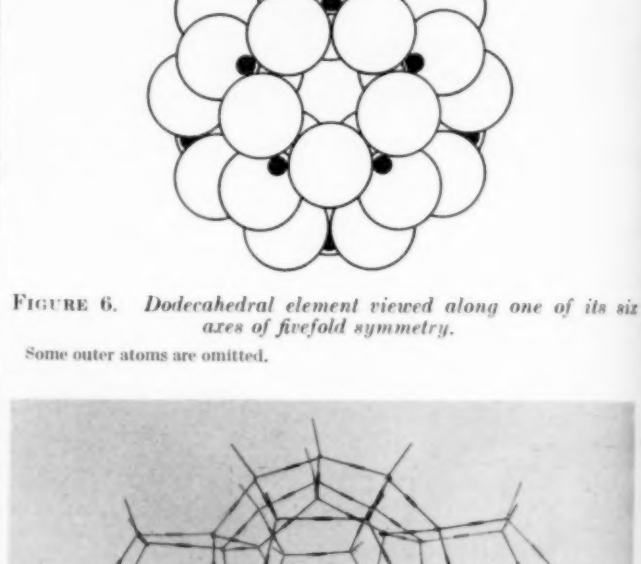

FIGURE 7. *View along one of 15 identical twofold axes of symmetry of a 13-element vitron (type 1, spherical).*

In this model a tetrahedron is represented by two wires bent at an angle of 109.5° and soldered at their symmetrical crossing to represent silicon. Oxygen is represented by friction-tight couplings. Two other axes of twofold symmetry lie normally to the line of sight.

3. Density of Vitreous Silica

On the basis of unlimited continuity of the proposed structure for silica glass (as if it were extensible without distortion from micro to macro proportions) there would be $5(SiO_2)$ per dodecahedral unit of volume, and the density is computed from the molecular weights and cage dimension as

$$d=\frac{5\times 60.06}{7.663Nl^3},$$

where N, Avogadro's number, is 6.023×10^{23} molecules per mole and l is the length of an edge of the dodecahedron expressed in centimeters. The volume of one dodecahedral cage is $7.663l^3$ cu A and the computed density of fused silica would be 1.949, 1.986, or 2.023 g/cm^3 according as $l/2$, the Si-O distance, is assumed from X-ray data as 1.61, 1.60, or 1.59 A. These densities are only 10 percent lower than 2.20, the density of silica glass from room temperatures to 1,400° C or higher.

Possibly such low values of the density of fused silica may be approximated in its liquid state at very high temperatures at or near vitron formation. However, the continuity above assumed cannot exist when silica is cooled, because of the noncrystal nature of its structure with fivefold symmetry and the distortions and fissuring inherent in the process of its macro-growth. The tensions induced in the outer bonds, as the vitrons grow in volume, probably lead to some tangential rarefactions and radial compressions as successive shells are built up on vitrons, and the net effect on the average density, not readily evaluated, may be densification mainly because of decrease in volume as the empty cages are flattened by slight changes in bond angles.

Aside from densification through such a decrease in the unit volumes of the outer and distorted cages of vitrons, there would be a variation in the effective density of vitrons according to their size. The *internal portion* of each elemental volume or cage contains $5(SiO_2)$ in 251 A^3, and the volume of the atoms is only about 95 A^3. *Outside* an isolated small vitron there may be almost as many atoms as inside. The outside atoms must project into interstitial or channel tissues and add proportionately more to the mass of the vitron than they do to its effective volume. A useful and attachable elemental unit volume to consider is $(Si_{10}O_{20})$ with 10+ and 10− associated charges. Such a unit with balanced charges is attachable to a like unit to form the attachable two-cluster vitron $(Si_{20}O_{40})^{15+,15-}$. The unit $(Si_{10}O_{20})^{10+,10-}$ has $5(SiO_2)$ inside and the same number outside its 251 A^3 limits. Considering this unit as a single-cluster vitron, the outside atoms would extend into the surrounding interstitial tissues, which must have a minimum thickness of 1.6 A (the Si-O distance). From the single-cage volume of 251 A^3 one computes the diameter of an equivalent sphere as 7.8 A, and 9.4 A would be the effective diameter of the one-cluster vitron including its minimum share of neighboring interstitial connective tissues. The computed maximum effective density is then 2.3, instead of 2.0

TABLE 1. *Characteristics of attachable [a] vitrons (clusters of dodecahedral elemental units of volume having balanced charges)*

Units in cluster	1	2	3	4	5	7	13	14	26	45	54
Type of cluster	Spherical Central cage	Ellipsoidal Central face	Cylindrical Central O	Tetrahedral Central Si	Cylindrical Central O	Ellipsoidal Central face	Spherical Central cage	Tetrahedral Central Si	Tetrahedral Central Si	Spherical Central cage	Tetrahedral Central Si
Type of center											
Formula	$(Si_{10}O_{20})^{10+,\ 10-}$	$(Si_{20}O_{40})^{15+,\ 15-}$	$(Si_{20}O_{35})^{15+,\ 15-}$	$(Si_{17}O_{32})^{20+,\ 20-}$	$(Si_{45}O_{90})^{25+,\ 25-}$	$(Si_{45}O_{120})^{25+,\ 35-}$	$(Si_{160}O_{280})^{20+,\ 20-}$	$(Si_{123}O_{242})^{34+,\ 34-}$	$(Si_{191}O_{382})^{34+,\ 38-}$	$(Si_{320}O_{680})^{40+,\ 40-}$	$(Si_{379}O_{758})^{38+,\ 38-}$
Interior:											
Si atoms	5	10	15	20	25	35	65	70	130	225	270
Weight of Si, g/N	140.3	280.6	420.9	561.2	701.5	982	1824	1964	3648	6313	7576
O atoms	10	20	30	40	50	70	130	140	260	450	540
Weight of O, g/N	160	320	480	640	800	1120	2080	2240	4160	7200	8640
Mass, g×10^{-24}	498.6	997	1496	1994	2493	3490	6482	6980	12963	22437	26924
Volume, A^3	251.2	502.4	753.6	1005	1256	1758	3266	3517	6531	11304	13565
Diam equiv sphere, A	7.8	9.9	11.3	12.4	13.4	15.0	18.4	18.9	23.2	27.8	29.6
Interstitial tissue:											
Si atoms	5	10	14	17	20	25	35	51	61	75	109
Weight of Si, g/N	140.3	280.6	393	477	561	701	982	1431	1712	2105	3059
O atoms	10	20	28	34	40	50	70	102	122	150	218
Weight of O, g/N	160	320	448	544	640	800	1120	1632	1952	2400	3488
Mass, g×10^{-24}	498.6	997	1396	1695	1994	2493	3490	5086	6083	7479	10869
Min effective vitron diameter, A	9.4	11.5	12.9	14.0	15.0	16.6	20.0	20.5	24.5	29.4	31.2
Min tissue volume, A^3	186	288	368	440	507	629	927	974	1446	2064	2325
Total mass, g×10^{-24}	997	1994	2892	3689	4487	5983	9972	12066	19046	29916	37783
Total volume, A^3	437	790	1122	1445	1763	2387	4193	4491	7979	13568	15890
Max vitron density	2.28	2.52	2.58	2.55	2.51	2.51	2.38	2.69	2.30	2.24	2.38

[a] Vitrons are attachable from unsaturated Si$^+$ of one vitron to O$^-$ on a neighboring vitron and are unitable whenever the tetrahedra in a face of one vitron can also serve as a face of an adjacent vitron.

as computed on the continuum basis. In other words, the interstitial tissues can be denser than the internal portions of vitrons, even if the bonds therein be fewer, less regular, or unconnected, because these tissues cannot share in the extreme degree of rarefaction in space that characterizes silica in dodecahedral structure.

The results of a study of vitrons of various sizes are given in table 1. It is considered that at the high temperatures of formation the vitrons grow simultaneously in situ throughout a melt and that smaller vitrons will grow in every sizable region that might otherwise remain undeveloped between larger vitrons. All these vitrons of various sizes and perhaps of somewhat irregular shapes can be actually, if imperfectly, united with neighbors at some common interfaces, and by multiple oxygen bridges across intervening channels can be more or less securely attached to each other.

It appears from table 1 that the maximum effective density exceeds the constant internal density of 2.0 by various amounts depending on the size of the vitron and the degree in which its shape approximates the sphericity assumed in the estimates. It will be evident that nonspherical clusters must have greater peripheral areas than assumed, and hence their estimated effective densities must be too high. However, there are several clusters for which the estimated maximum density is less than 10 percent above 2.20, the known density of silica glass. Further details concerning vitrons and their aggregation are given in the appendix.

4. Diffusion of Gases in Silica Glass

An important feature of a model for the network of glasses with high silica content is the minimum or limiting aperture through which atoms must pass when gases diffuse through glasses and when ions migrate under the influence of an electrical field.

Experiments concerning the diffusion of gases through glass may not, in general, be considered solely on a mechanical basis, as a process of the squeezing of molecules through molecular holes or cracks. The more reactive hydrogen diffuses slower than the inert helium when oxygen is present, but their rates are about the same in a solid without oxygen anions.

However, in the case of diffusion of noble gases it is probably valid to consider dimensions as much more important than chemical nature, and in seeking to understand the very marked diminution in the permeability of silica glass to argon, in comparison with that for neon, it seems tenable and sufficient to regard size only. As measured by Norton [12], the diffusion rate for neon with atom diameter 2.4 A, was found to be more than 100,000 times as high as the rate for argon, atom diameter 3.2 A. Figure 8 shows how well the penta faces of the elements of vitrons in silica are adapted to pass neon and smaller atoms such as deuterium, hydrogen, and helium, but obstruct argon, oxygen, and nitrogen, which have larger diameters.

Norton found, also, that the rates for helium at

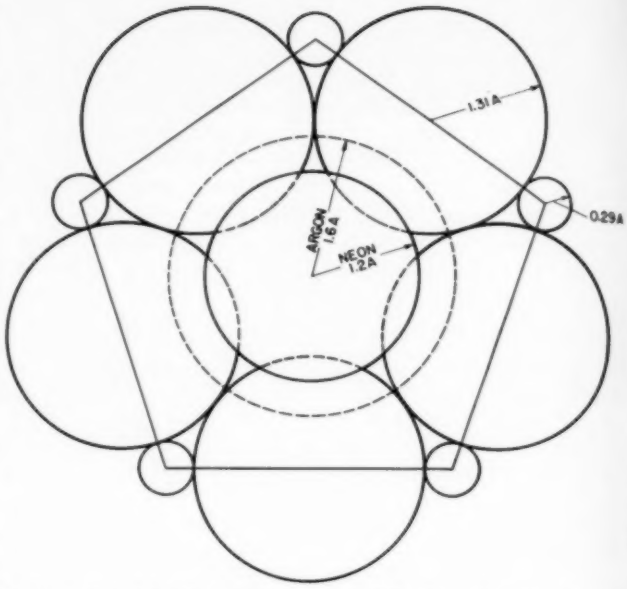

FIGURE 8. *Limiting aperture for diffusion of gases through silica glass.*

The clear aperture of the pentagonal faces of the vitron elements is comparable in diameter with the neon atom which is the largest that rapidly diffuses in quantity.

100° C are decreased by a factor of 1,000,000 as the percentage of modifiers is increased from glass to glass. It is here suggested that this difference is caused mainly by the physical presence of nonsilica packed inside the elemental cages of the vitrons. It does not seem necessary to look to the interstices between vitrons as the only channels for permeability in silica glass.

5. Radial Distribution of Atoms

All atoms in this model are found to be distributed in accord with published data on the radial distribution of atoms with respect to any one ion in vitreous silica. That is, for very short distances to their nearest neighbors both Si and O atoms are so situated that the arrangement is not distinguishable from that formerly assigned to high cristobalite. Warren [16] was a leader in applying the radial-distribution method to the analysis of X-ray diffraction patterns obtained from glasses. The concept of a random network required such treatment instead of the simpler computation of Bragg-*d* values as is done for crystals. Hartlief [17] also reported such distances for fused silica from X-ray data. More recently, neutron diffraction data for fused silica were treated in this manner by Milligan, Levy, and Peterson [9]; and Weber [18] et al. have reported similar unpublished data on two samples of silica glass, one of "high purity" made by the Corning Glass Company and another of "ordinary" quality. These experimental results are listed in table 2 for comparison with the atomic separations as computed from the model made by the writer. (The scale value of (Si-O) = 1.60 is, of course, assumed in the computations.)

TABLE 2. *Radial distribution of atoms in silica glass*

From O to:		From Si to:		Distances to neighbor atoms in angstroms						
				Proposed model	Neutrons			X-rays		
					Mulligan, Levy, & Peterson [9] 1951	Weber [19] 1954		Warren [16] et al. 1936	Hartlief [17] 1938	Norman [a]
No.	Kind	No.	Kind			Corning	"Ordinary"			
2	Si	4	O	1.60	1.58	1.56	1.56	1.62	1.7	1.64
6	O	----	----	2.60	2.56	2.62	2.71	[b] (2.65)	[b] (2.7)	2.67
----	----	4	Si	3.20	3.02	3.32	3.22	3.2	3.1	3.14
6	Si	12	O	4.00	4.0	3.94	.....	4.2	4.1	4.17
6	O	----	----	4.19	.....	4.46	.....	.....	.....	.....
3	Si	6	O	4.92						
12	O	----	----	4.99	5.1	5.08	.....	5.2	5.3	5.25
----	----	12	Si	5.18						
12	O	----	----	5.93	5.9	.....	.....	.....	.....	.....
12	Si	24	O	6.14						
12	O	----	----	6.79	6.6	.....	.....	.....	6.3	6.5
12	O	----	----	7.14						
6	Si	12	O	7.15						
12	O	----	----	7.3	7.4	.....	.....	.....	7.5	.....
----	----	24	Si	7.33						
12	Si	24	O	7.71						
12	O	----	----	8.04	.....	.....	.....	.....	.....	.....
3	O	12	Si	8.38	.....	.....	.....	.....	.....	.....
----	----	24	Si	8.4	.....	.....	.....	.....	.....	.....
6	Si	12	O	8.54	.....	.....	.....	.....	.....	.....
18	Si	----	----	8.6	.....	.....	.....	.....	.....	.....
----	----	4	Si	8.97	9.0	.....	.....	.....	.....	.....

[a] Read in 1956 from "uncorrected" curves in Prof. Warren's laboratory. A letter received from N. Norman of Oslo, Norway, just as this paper goes to press, lists his "uncorrected" and still unpublished values as 1.62, 2.62, 3.05, 4.08, and 5.02.
[b] Not resolved.

No attempt is made to compute the angle Si—O—Si from the diffraction data. The departure, α, of this angle from 180° might be estimated by means of the equation

$$\cos(\alpha/2) = (\text{Si-Si})/2(\text{Si-O}),$$

but the precision is much too low, and even for averages there must be residual error because the peak corresponding to the O-O distance of 2.6 A is usually imperfectly resolved, and that makes the reading for Si-Si systematically too low and the computed departures from 180° too large.

The proposed model agrees with the experimental data of table 2 somewhat better than does a random network model. A random orientation around bond axes soon leads to indefinite predictions of the radial distances. The first uncertain case is the oxygen to second-oxygen distance. For random orientation there are 18 oxygens that might be found anywhere within the range 4.2 to 5.2 A. The last fixed distance would be silicon to 12 second-silicons at 5.2 A. Thereafter 18 third silicons might vary from 4.9 to 6.5 A from an oxygen, and 36 third oxygens be found anywhere within the same limits of radii from any silicon. (Incidentally the uncertainties start with nearer neighbors and rapidly become much greater if values other than 180° be assumed for the angle Si—O—Si.) Weber [19] was evidently surprised to find only 6.9 instead of 18 oxygen atoms at 4.46 A from an oxygen, and he remarks, ". . . A random orientation of these outlying tetrahedra probably causes 1 oxygen of each 3 to be closer in yielding 6 as the number of oxygens at the O-2d O distance." In table 2 it will be seen that the proposed model predicts that 6 of these second oxygens should be found at 4.19 A and 12 of them at 4.99 A, very close to 3 other distances, so that only the high radial density near 5.1 to 5.3 A is noticed by most observers.

6. Planar Distribution of Atoms and Values of Bragg-*d*

Computations of values of Bragg-*d* are not usually made for glasses if it is assumed that their structure is random. When a considerable degree of order is assumed, it then becomes pertinent to consider such tests. In contrast with the simplicity of crystal spacings, those in this model are very numerous and multivalued. Within a single dodecahedron, which seems useful as a unit volume, one finds the atoms all distributable in 6 equivalent sets of 7 planes, each set perpendicular to one of the 6 axes of fivefold symmetry. Also, the same atoms are distributable in 10 sets of 11 planes, each set perpendicular to one of the 10 axes of threefold symmetry; and in 15 sets of 13 planes, each set perpendicular to one of the 15 axes of twofold symmetry. Figures 9 and 10 show how the atoms may be projected to locate these three different systems of planes.

Among the very numerous spacings of figures 9 and 10 there are many duplications, and one finds only 31 different possible values of plane separations for a single cage between limits of 0.8 and 4.5 A and

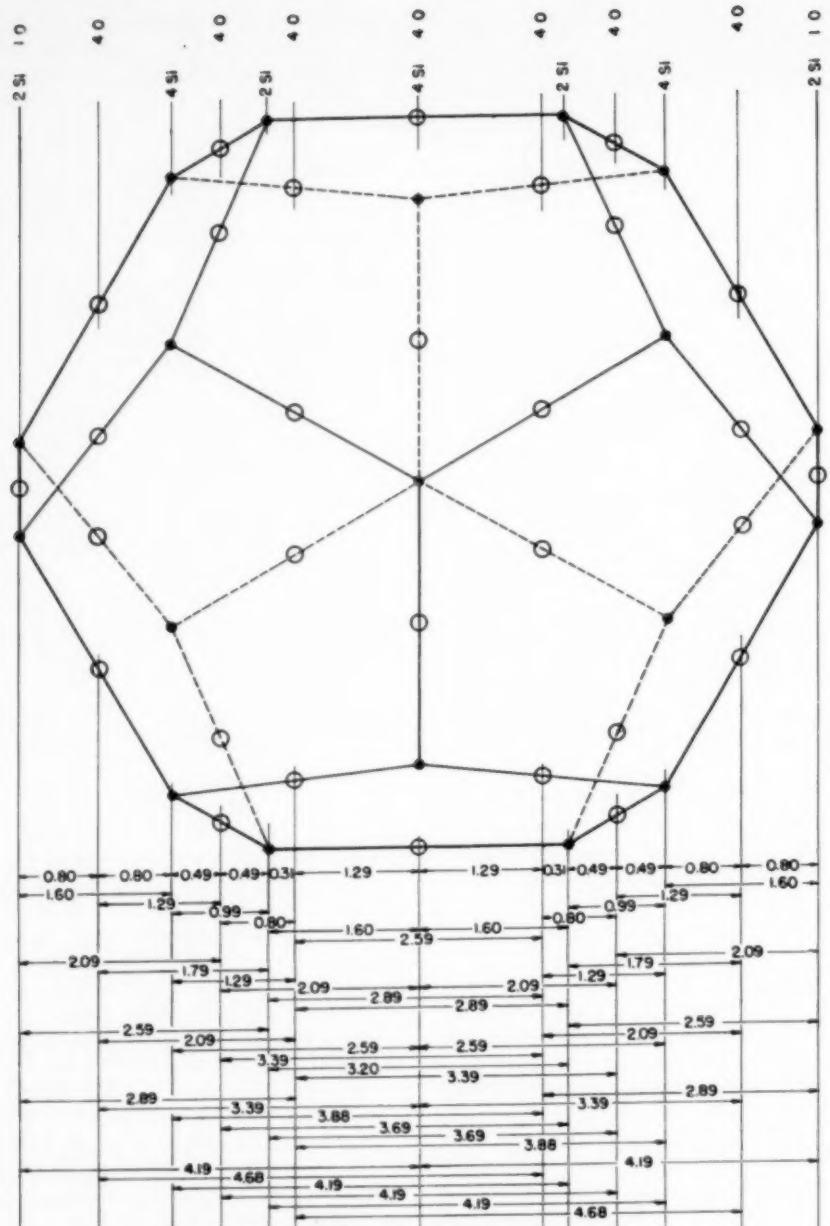

FIGURE 9. *Projection of atom centers of dodecahedral element on plane perpendicular to one of its 10 axes of threefold symmetry.*
The atoms are further projected to determine the spacing of 13 pseudo lattice planes perpendicular to the 15 twofold axes.

considering all three sets of projections. This can be compared with about 35 peaks (or indications thereof) that can be used for computing *d*-values from the curves of scattering of neutrons as found by Weber [18] for a sample that he labels as Corning fused silica; or 18 peaks for a sample called ordinary fused silica.

Because of the numerous atoms in intervening planes, no X-ray values of Bragg-*d* should be expected for plane separations exceeding about 3 A, as judged from analysis of the data in figures 9 and 10. Below 3 A it is estimated by a rough process of atom counting and weighting that about 10 *d*-values might be detected by X-ray and electron diffraction, and 6 or 7 are found from such data.

For vitron clusters, as wholes, there are some other possibilities which seem chiefly to be distorted values of the separations as shown in figures 9 and 10. An example is the *d*-value near 4.3 A that is not predicted from the model on the basis of a single element but is prominent in X-ray data. In clusters there takes place an overlapping of the vitron ele-

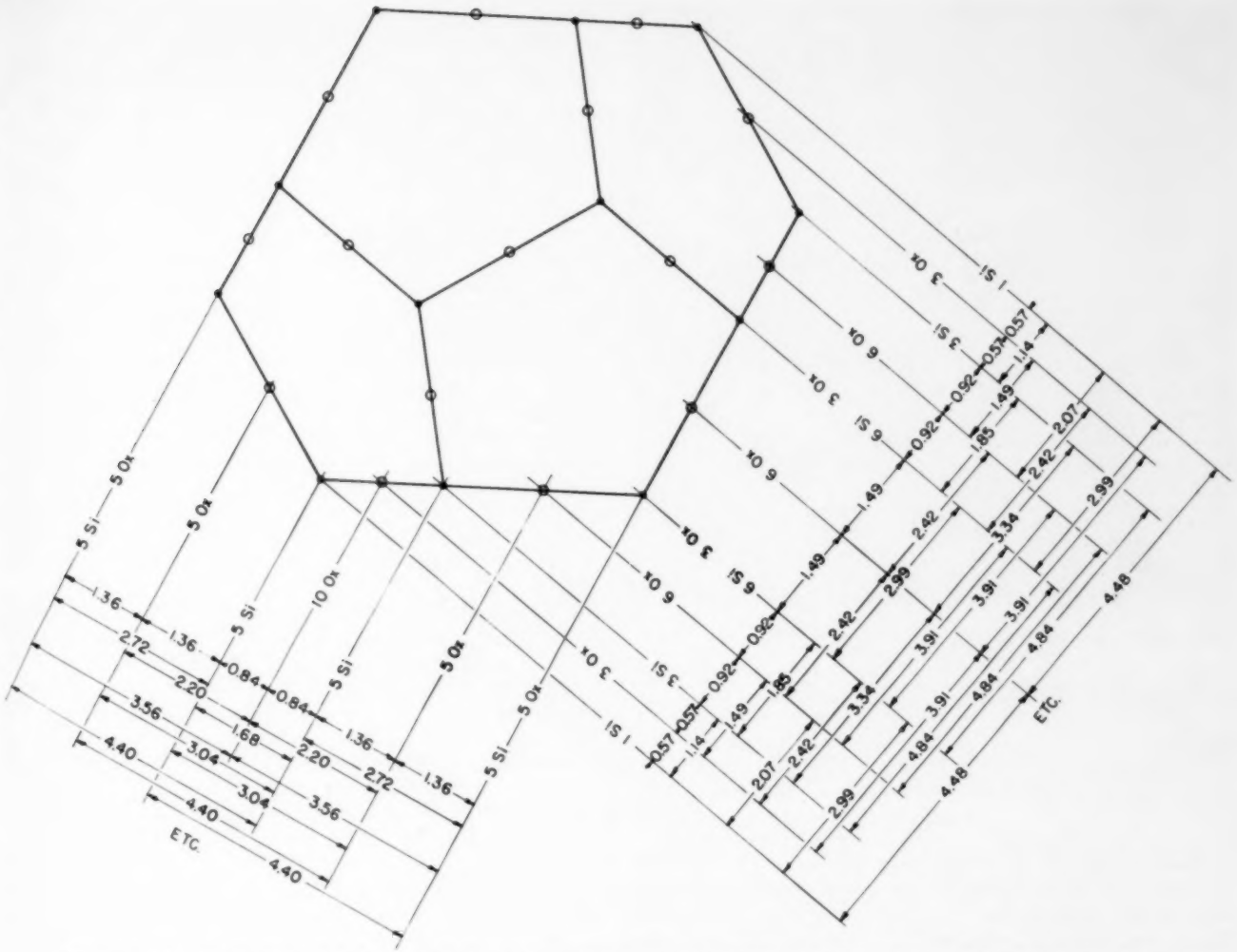

FIGURE 10. *Projection of dodecahedral element on plane perpendicular to one of its 15 axes of twofold symmetry.*

The atoms are further projected to determine sets of pseudo lattice spacings of 7 planes perpendicular to the fivefold axes and also spacings of 11 planes perpendicular to the threefold axes.

ments. An important case seems to be the overlapping of fivefold and twofold axes, and this was first noticed in a model of the 13-element vitron as viewed transversely to any of its fivefold axes. The distortions are such that approximate coincidence is forced for the 4.19 A separation along the twofold axes and the 4.40 A separation along the fivefold axes. The hybrid "planes" are curved with separation varying from 4.40 A along the principal fivefold axes of the whole vitron to 4.19 A at distances of something like 6 A from the principal axis (see figure 11).

In brief, because of the limit of precision in the experimental data one can say only that the number and values of Bragg-*d* separations predictable from the proposed model agree with the diffraction data about as well as the agreement among different experimenters or for different samples of silica glass. It is suggested, however, that the large number of these distorted pseudo planes has an important effect on the level of observed scatter and the general fuzziness of diffraction patterns.

7. Potential Flaws and Tensile Strength

The properties that may logically be inferred from the nature of vitrons, as they have been here defined and described, seem to offer interesting explanations of some of the unusual and not satisfactorily understood properties of silica. For example, in the testing of bulk specimens the actual tensile strength of fused silica (and other silica glasses) is only a fraction of the computed "cohesive" strength. The Griffith [20] crack theory is the usual "explanation," namely, that glass is completely riddled with flaws, but there seems to be no acceptable basis for the existence of the cracks. Stanworth [21] says that it seems as if the entire volume of glass may be permeated with cracks. Cox [22] considers some of the facts as suggestive of crack propagation in an elastic continuum after initiation by a flaw, but on the other hand finds that associated factors lead to an atomic view involving period and energy of vibration and size of ions in order to explain what may be "macroscopic manifestations of the discrete nature of glass."

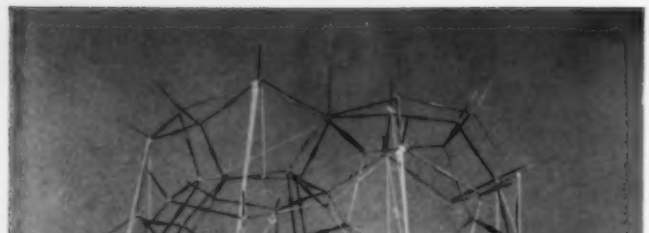

FIGURE 11. *View perpendicular to one of the 6 fivefold axes of symmetry of a 13-element vitron.*

Strings show locations of prominent curved or hybrid "planes" in which numerous ions are located. The separation of adjacent hybrid planes of like curvature is 4.4 A along the fivefold axes and 4.2 A along approximately parallel (secondary) twofold axes at distances of 6 A from such principal axes. A similar forced approximation to coincidence is found at right and left of center along the 15 axes of twofold symmetry, to which secondary fivefold axes are approximately parallel. These separations of 4.2 and 4.4 A are of interest because the most prominent diffuse ring commonly observed in both X-ray and electron diffraction patterns indicates a Bragg-*d* of 4.2 ±1 A.

According to the vitron concept, the intrinsic tensions of distortional origin cause weak peripheral bonds that provide a basis for incipient cracks, and there are fewer bonds per unit cross section in the interstitial connective tissues between vitrons than within them. This explains the low glass strength as compared to a medium having bonds of uniform strength uniformly distributed.

Murgatroyd [23] discussed the delayed elastic effects in glass and attributed the effects to gradual yielding of weak bonds. He proposed that the constitution of silicate glasses is such that the binding force between atoms varies from the maximum possible value to a relatively small value, and "regions occur where numerous bonds of the weakest type exist as neighbors." He concluded that "the low strength of massive glass is due to the numerous weak bonds it contains."

Murgatroyd also mentions the smallness of the difference in density between liquid silica glass and cristobalite, and points out that silica resembles a normal liquid in this respect. He observes that one way in which the great increase in fluidity may be accounted for is "the presence of regions of weak bonds interspersed amongst normally bonded groups of atoms."

On the basis of a continuous random network theory there is no satisfactory evidence that weak bonds would be sufficiently numerous to account for the very great discrepancies between theoretical cohesive strengths and maximum realized tensile strengths of glasses, and especially so for fused silica glass; but the vitron concept, with very numerous bonds that are seriously tensed and interstitial connective tissues where the bond density is low, seems definitely satisfactory in this respect.

Much of the testing of glass for breaking tensile strength has been done on fibers. The values obtained are higher than for tests on samples with large cross sections, and especially so if the fibers are drawn in approved manner and great care taken to avoid damage to their surfaces. If ambient conditions are favorable during drawing and if average results are plotted against diameter of cross section, or formation temperatures as was done by Otto [40], the curves can be extrapolated toward smaller diameter or higher temperature for somewhat higher estimates of the breaking strengths, which however, are still much below expectations from the computed cohesive strengths of 2.5 to 5×10^6 lb/in.^{2} for commercial glasses [39].

Considerable attention has been given to reasons for higher breaking strengths of fibers as compared with massive glass. Chilling should introduce compressions in the surface layers and increase breaking strengths to some extent but this effect must become less important as diameters are decreased because there must be interior compensating tensions. Orientation of structure into threadlike alinements, caused by the drawing process, has been much discussed, but Otto and Preston [48] found little difference in strengths whether by tensile or torsional tests; more recently Otto [40] and Brannan [49] have reported high values of strength on fibers that do not show anisotropy; and Goldstein and Davies [47] did not find anisotropy in silicate glass fibers although it was present in some others. Additional pertinent evidence has been presented by Lynch and Tooley [46], who find that their observed increases in strength (up to 62%) by down-drawing under increased load are not eliminated, although materially reduced, after abrasion of the surfaces of the fibers.

The idea of change in either statistical or spatial distribution of types of vitron is not analogous to elongational distortion of a given type of vitron. The stresses and distortions involved may, however, be smaller and thus union with neighbors may be improved. In any event the stress systems would necessarily be balanced on a vitron-volume level, and it would seem that vitrons at and near the surface could more easily meet the requirements for strong unions and attachments with neighbors because of less exacting three-dimensional requirements. This would mean a maximum of strong intervitron connections in all directions near the surface, and a progressively smaller proportion of strong connections inside until the distance from the surface becomes large compared to the vitron size.

8. Effects of Localized Stresses on Extensive Properties and Elastic Moduli Above Room Temperatures

The unusual extensive and elastic properties of silica glass have been so well discussed by Babcock, Barber, and Fajans [6] that some details and many references will be omitted here. In order to explain these peculiar relationships those authors suggest the coexistence of two or more different ionic structures in equilibrium in ratios that vary with temperature and pressure. Also, they consider that the low-temperature heat capacity, as well as infrared and Raman spectra, may "indicate the coexistence of relatively weak and strong forces."

An experimental curve showing the temperature variations in the modulus of rigidity of fused silica indicates strong thermal variations in stresses within the components of its structure. This modulus decreases from 2° K to a minimum near 65° K, rises to a maximum near 880° C, and then has an extremely rapid decrease near 1,020° C [24]. It will be noticed that the minimum near 65° K coincides with the minimum for Young's modulus of silica glass, the maximum at 880° C is somewhat higher than the similar maximum for Young's modulus (not far from a broad weak minimum in expansion coefficient), and at 1,020° C the lower limit of the annealing range has been reached where viscosity approximates 10^{14} poises and localized differences in stress are not maintained indefinitely.

It is here suggested that the localized stress systems consist of (1) intratetrahedral attractive and repulsive forces that promote and maintain angular symmetry within the tetrahedra, and (2) the tensed Si—O—Si bonds that make and maintain contact between tetrahedra through the oxygen bridges—contacts that cannot exist without internal distortion in the tetrahedra.

As hot glass cools toward the critical lower limits of the annealing range, the strain response to stress has become decidedly time dependent. For silica glass in particular (free from the complication of modifiers) the repulsive and attractive forces within tetrahedra increase and maintain greater symmetry therein at the expense of greater tensions in the Si—O—Si bonds between tetrahedra. This necessitates more regular and symmetrical dodecahedra which can obtain only if some connections are broken and interstitial tissues or fissures are extended or widened. This is confirmed by the marked decrease in activation energy of flow (slope of $\log_{10}\eta$ versus $1/T$) for silica glass at temperatures below its annealing range where viscosity increases very slowly above $\log_{10}\eta = 13$.

After the initial rapid increase in cohesive forces during cooling near 1,020° C has produced increases in the moduli there are slower progressive changes or relaxations in the balanced internal stress systems of vitrons that produce marked but gradual decreases in the moduli but have very little effect on volume. In respect to volume the normal contractions of the units of structure are nearly offset by the expanded channels between vitrons over a long range in temperature. Although these contractions permit some readjustments and relaxations of stresses in the tetrahedra that in turn check the initially excessive fissuring effect, there is still progress in the fissuring (because of increased attraction and consequent increased symmetry within the tetrahedra) so that interstitial (intrachannel) cohesion can decrease slowly and the concurrent increase in intravitron cohesion be negated by the mere existence of the weaker channel interstices.

From the above discussion it is evident that the net coefficients of thermal expansion of silica glass can be very small and nearly constant between 1,000° C and room temperatures. Furthermore it is clear that these net coefficients at increased pressure should be larger because the negative components caused by stress-induced fissuring would be correspondingly suppressed by the increase in pressure.

The analysis given also suggests that the compressibility of silica glass should be abnormal and increase with pressure because the tensed bonds in and near the interstitial or channel tissues should aid the applied pressure and do so more effectively as and until the atoms approach their equilibrium positions. This has indeed been observed up to pressures near 36,000 kg/cm^2 where Bridgman [25] found that the abnormal increases in compressibility ceased abruptly and were then followed by decreases, in a normal manner, at higher pressures.

According to the automatically-limited-growth feature of the vitron theory, and to the extent that Bridgman's pressures are equivalent to hydrostatic pressures, his 36,000 kg/cm^2 applied radially to each vitron would seem to substitute directly for a radial compression previously produced or maintained indirectly by tangential tensions of $(36{,}000/\sigma)$kg/cm^2, where σ is Poisson's ratio which is near 0.16 for silica glass at room temperatures. Such tangential tensions of 225,000 kg/cm^2 or 3.2×10^6 lb/in.^{2} are in very reasonable agreement with estimates of theoretical cohesive strength. Shand [39], for example, gives 2.5 to 5×10^6 lb/in.^{2} for common commercial glasses, and thus this abnormal compressibility observed by Bridgman seems quantitatively to confirm the writer's inference (section 2, above) that vitron growth is limited by the strength of the Si—O—Si bonds.

Moreover it will be realized that the compression produced by a given pressure should be lower at increased temperatures because the process of fissure closing by applied pressures is then applicable only to the lowered level of fissuring that can exist at the higher temperatures. This accords with observations and measurements by Birch and Dow [26] from room temperatures to 400° C on fused silica and a Pyrex glass.

9. Internal Friction and Elastic Constants at Low Temperatures

A study of thermal effects on elastic moduli at low temperatures invites consideration of the internal friction evidenced by the attenuation of ultrasonic waves observable from 2° to 190° K and having very broad maxima near 30 to 50° K depending on the frequencies used (60 kc to 20 Mc/sec).

Such friction effects are very small in quartz and observable only with care. In fused silica they were observed by Marx and Sivertsen [38], by McSkimin [36], and by Fine et al. [37] before their more detailed observation and discussion by Anderson and Bömmel [24]. Fine's data show minima in Young's modulus, torsion modulus, and Poisson's ratio near 65° K and a very broad maximum in compressibility near 65° K. The Anderson and Bömmel data show a minimum in rigidity at 65° K for 66 kc and near 75° K for the 20-Mc curve. The last named authors find that the temperature and frequency behavior suggest a structural relaxation with a distribution of activation energy averaging 1,030 cal/mole. Further they find that the absorption is largely due to a shear elastic wave and therefore to a mechanism that does not primarily tend to cause fluctuations in density; and that the relaxation strength is small, only a fraction of all particles contributing, as shown by the small increase (about 3%) in shear modulus from the minimum value to that at 4° K.

For discussing these results in relation to vitron theory it is convenient to start near room temperatures where there is a noticeable decrease in coefficient of thermal expansion. This may mean merely that the rate of expansive fissuring has fallen definitely below that of normal contraction and continues so until minimum volume is reached near 190° K. Here the above described internal friction begins very gradually to be detectable by attenuation of acoustic waves, and the compressibility after remaining relatively constant over an interval of ±75° near room temperatures resumes an abnormal climb as temperatures are lowered. It is here suggested that because of continuous and gradually increasing intravitron contraction some of the bonds yield in and near the interstitial channels between vitrons. This would provide limited numbers of less well bound oxygen for the sort of transverse vibrations visualized by Anderson and Bömmel, and do so in ever increasing number until the whole process is checked by the near contacts and strong repulsive forces at very low temperatures. Apparently lower temperatures are necessary to check the absorbing vibrations than those required to start closure of the fissures and decrease compressibility. At the lowest temperatures of observation it will be noticed that the rigidity increases and compressibility decreases as is normal on approaching absolute zero. The greater slopes on the low-temperature side of all of these curves may indicate that a normal balance between repulsive and attractive forces is effectively reached at the temperatures of their respective maxima or minima near 65° K.

10. Vitron Theory and Heat Treatments

According to the theory of intrinsically stressed vitrons, after fused quartz is repeatedly heated and cooled in treatments that reach 900° or 1,000° C, these repeated heat treatments should slightly reduce the localized stresses present within the vitrons and result in small volume changes at a given room temperature as compared with previous measurements at the same temperature. Such changes should be unidirectional (expansions) and permanent, that is not reversible by subsequent heat treatments in comparable temperature ranges. Considerable evidence of this has been found in the course of annealings and in measurements of the thermal expansion [42] of vitreous silica. Possibly some effects of this sort should be considered in connection with the results published by Saunders and Tool [43] on Pyrex glasses.

Such irreversible heat effects, or effects reversible only after more fundamental heat treatments at much higher temperatures, should be less and less evident as the nonsilica content of glasses is increased, and they were not of noticeable magnitude in the results reported by Tool [44] and associates on glasses other than Pyrex.

At very high temperatures in liquid silica the stresses incident to vitron growth produce strains and distortions easily, and there is no rigidity of tetrahedral structure sufficient to resist the tendency for dodecahedra to unite and fill space with a minimum of interstices. Upon cooling and approach to the solidification region, even slight trends toward greater symmetry within tetrahedra lessen the pliability of dodecahedra, create a few broken bonds, and in general form or widen interstitial tissues or fissures. This expansive effect may exceed the normal contractive effect and yield a small net negative coefficient of expansion such as was observed by Douglas and Isard [27] between 1,000° and 1,500° C. Small spheres of vitreous silica had previously been quenched by Salmang and von Stoesser [28] from high temperatures into water and they had announced the existence of a minimum density for this glass between 1,200° and 1,800° C.

These positive changes in density of silica glass with increase of temperature in and above its annealing or "transformation range" are very small, say $+1\times10^{-5}$/deg C, and contrast with negative values of from -16 to -46×10^{-5}/deg C that were found by Tool [44] for various silicate glasses in their annealing ranges. These larger and negative changes are attributable, according to the writer, almost entirely to the silica network but the cause may be very different. It is suggested by the writer [45] that there is an inherent temperature dependence of the silicon-oxygen-silicon bond angle that is locked in a semi-invariant or metastable state in pure fused silica, but is free to operate in silicate glasses in proportion as they contain modifiers. The result is a limited, temperature dependent, and reversible degree of folding or collapse of the network structure.

11. Specific Volumes of Soda Silicate Glasses

A useful feature of vitron theory is the degree in which it may be quantitatively applied in studies of the properties of simple binary glasses as functions of composition. Applications of the vitron concept to specific volume, viscosity, volatilization, and electrical resistivity of glasses are being made and data on infrared spectra are being studied. It is found that the proposed ideas accord with many such data for fused silica and for simple alkali-silicate glasses. These results will be given in another paper with emphasis on property-composition curves.

However, one such application to binary glasses can be readily summarized here. Since the number of cages in R_2O silicate glasses is proportional to $S/5$ (where constituent proportions $R+S=1$), it follows that the proportions of R_2O corresponding to integral numbers of cations per cage, R_h, are readily computed as $R=R_h/(R_h+10)$. At such integral steps or degrees of saturation (and supersaturation) of the cages it seems probable that some evidences of changes in rate might be found on curves of property versus composition. Huggins [35] has already studied existing data of volume-composition curves for soda-silicate glasses as published by Glaze [41] et al., and found evidence of special points at Si to O ratios of 0.437, 0.40, 0.38, 0.36, 0.345, and 0.333 which are now found to correspond precisely to values of 3, 5, 6, 8, 9, and 10 for R_h according to vitron theory. This good agreement between vitron theory and the results by Huggins from his investigation is shown in further detail in table 3.

TABLE 3. *Application of vitron theory to specific volumes of soda-silicate glasses*

Molar composition		Holes $S/5$	Cations per cage R_h	Special ratios of silicon to oxygen		
				Computed from vitron model	Found by Huggins	
Na_2O	SiO_2				1940	1954
0.00	1.00	0.200	0	0.50	0.50	0.50
.091	0.909	.182	1	.476		
.167	.833	.167	2	.454		
.231	.769	.154	3	.435	.435	.437
.286	.714	.143	4	.417		
.333	.667	.133	5	.400	.40	.40
.375	.625	.125	6	.385		(.375)
.411	.589	.118	7	.371		
.444	.556	.111	8	.357	[a](.364)	(.357)
.474	.526	.105	9	.345	.345	
.500	.500	.100	10	.333	(.333)	.333
etc.						
.630	.370	.074	17	.270	.27	

[a] Ratios in parentheses were less prominent or seem to be given less weight by Huggins.

12. Concluding Remarks

Study of this model for silica glass emphasizes two pertinent characteristics. First, it has a type of order with many axes and numerous and varied spacings of quasi lattice planes that cannot grow into a sizable crystal, and second, it has distortions and stresses and consequent curvature of the lattice planes. Because it has been shown that this model is consistent with known data on density, differential diffusion of gases, interatomic distances, low tensile strength, unusual thermal and pressure effects on volume, internal friction at low temperatures, and specific volumes of soda-silicate glasses, a new concept should be considered for general study of the glassy state: A small stressed cluster of definitely arranged but slightly distorted elemental groups or cages (such as pentagonal dodecahedra) that in turn are composed of smaller and more nearly regular stable structural units (such as tetrahedra), all of which as a system tends to form at high temperatures in a melt and have an approximate but not exact noncrystal symmetry (such as fivefold) and thus be capable of limited but not extensive continuous growth. Such a cluster may appropriately be called a VITRON in order to distinguish it definitely from a crystallite, which can increase in size without limit. Among the member ions and in connective tissues between the vitrons there will exist a wide distribution of bond strengths and some variation in angles between valence directions that can account not only for a range of melting points but for similar phenomena indicative of ranges in activation energies. The known high energy of dissociation of SiO_2 linkages (106 kcal/mole, an energy which is many times the mean energy of agitation at most industrial temperatures), indicates that vitrons are not necessarily completely broken up into tetrahedra even at temperatures far above fusion.

It would seem that the vitron concept should be welcomed by those who still regard a modified crystallite theory with favor. It is not difficult to visualize these very small submicroscopic vitrons (say 1 to 54-cages, approximately 9 to 30 A in total diameter) partially united to each other through common faces and also connected by other Si—O—Si bonds or "oxygen bridges," similar to those that unite the tetrahedra within a vitron, and thus forming a structure approximately filling space with intervening connective tissues that vary in width with temperature and degree of existing localized stresses. Considering their various multiple axes, the vitrons could, almost by chance, be positioned to present more or less equivalent orientations regardless of intervening tissues or fissures. This simple but fundamental concept of connected vitrons introduces more than short-range ordered arrangement and thus something that proponents of the crystallite theory have demanded. A quantitative interdistribution of stresses between elements of a vitron, and perhaps between vitrons, helps to explain the remarkable continuity of properties as a function of temperature through, during, and even above the melting range—something that, according to Peychès [29], a mere distribution of sizes and shapes does not satisfactorily explain.

Also, the intrinsic properties of a vitron, including numerous lattice planes, a distribution of stresses among its members, and curvature of the lattice planes, can account for much of the observed

broadening of diffraction rings without large percentages of voids such as the crystallite theory seemed to require.

The network theory is modified and strengthened by the vitron concept because the existing troublesome requirement for first-order randomness in the network is thereby eliminated—a randomness that is not entirely compatible with some of the well-established properties of glasses and is being challenged by electron and neutron diffraction data which evidence greater order than did X-ray data. Further, the idea of unbroken continuity is replaced by the much more useful concept of a quasi-discrete or modulated continuity.

In addition, the vitron concept readily diverts excessive attention from the old idea that glass is *merely* supercooled liquid. Thus it accords well with certain thermodynamical and other considerations that seem to have led Parks and Huffman [30], and later Berger [31], to suggest that glass is a fourth state of matter resembling but definitely differing from the crystalline state rather than a twilight zone intermediate between liquids and crystals. Because in some respects the glassy state differs so very little from the crystalline state, it has always been difficult to accept as fully satisfactory the undercooled liquid ideas or to account for the stability and reproducibility of definite degrees of major disorder in networks in the absence of coercive fields. An important difference between the present vitron concept and Berger's ideas, as usually understood, is that the vitron or glassy state forms at very high temperatures in the melt rather than at or near annealing or softening temperatures.

The vitron concept of stressed clusters of cages having a dodecahedral arrangement of pentagonal rings of slightly deformed tetrahedra, may be applicable to other than silicate glasses. For boric oxide glass with boron in four-coordination state, it can be shown that a reasonable density is given by such an arrangement starting with nearest-neighbor distances to accord with X-ray evidence.

In the broader field of glasses in general, it is possible that the vitron concept (with other noncrystal symmetries) may open new vistas for study and investigation. Perhaps it will suggest comparable concepts relating to the constitution of liquids and solutions. Particularly in the field of rheology, it may prove useful and possibly it may relate to crystallinity in the field of high polymers. It would seem that some writers have felt the need for and referred to somewhat similar concepts. Machatschki [32] speaks of "precrystalline" arrangements; Debye and Menke [33] describe a "quasi-crystalline" arrangement instead of a disordered atomic distribution in liquid mercury; and Matossi [34] infers that in fused silica there are regions of distorted order separated by places of still greater lattice distortion. Aside from an investigation of its possible applications, the idea seems to call for a mathematical study of the various classes of symmetry that are adapted to noncrystal-forming arrangements of matter in space, with a degree of periodic order and regularity roughly comparable to but much more limited than those found in crystals.

13. Appendix

13.1. Union and Attachment Between Vitrons

Some possibilities concerning the growth and uniting of clusters, or vitrons, may warrant examination in more detail. Consider a sphere inscribed in a regular pentagonal dodecahedron. It can be surrounded by 12 equal spheres tangent to the first on each of the 12 pentagonal faces to form a cluster of 13 spheres of which only the central sphere touches more than one other. In the next shell one may add 12 spheres along diameters through the 12 of the first shell and also 20 on diameters through the inner sphere and through the 20 apices of the original polygon. The cluster is now composed of 45 spheres. This is a packing that is regular but uniquely referable to only one definite center.

In this type of packing of rigid incompressible spheres or cages the density decreases toward the periphery because of voids between cages as the cluster grows. If the cages are *deformable*, however, there can be a small but limited growth of such a system with sufficient distortion of cages in the outer shells to close the interstices and form a cluster approximating uniform density. In the case of dodecahedrons of silicon and oxygen, the chemical bond between these elements is very strong and these are the forces that tend to maintain vitron structures after their formation at high temperatures. The extent to which they can be maintained is, however, definitely limited. Important possibilities in this type of vitron are clusters of 1, or 13, or 45 dodecahedra.

In grouping dodecahedral elements to form vitrons one can arrange them, as just described, around (1) a central elemental volume, (2) a common face of 2 elements, (3) a common edge of 3 elements, or (4) a common apex of 4 elements. The first type permits the nearest approach to spherical clusters. The second is perhaps the least spherical; it can lead to chain structure. The third can manifest a cylindrical tendency; also it seems adapted to sheet or laminated structure. The fourth is somewhat tetrahedral but the surfaces and edges of the whole cluster are so decidedly curved that sphericity is approximated as the vitron grows.

In studying these types of arrangement, the characteristics of attachable and unitable vitrons were computed for several more or less spherical clusters consisting of from 1 to 54 elements of volume. The results are summarized in table 1. In addition to the tabulated characteristics of vitrons in table 1, there are other factors that affect their degree of union or attachability. The single element as tabulated can unite any two clusters each of which has one free penta face. There are other useful reduced single elements such as $(Si_9O_{18})^{9+,9-}_{2F}$ which can be joined by union to 2 adjacent penta faces, as presented by a 2-cluster, to form a 3-cluster; and $(Si_8O_{16})^{8+,8-}_{3F}$

which is unitable to 3 adjacent faces, as presented by a 3-cluster, to form a 4-cluster vitron, etc.

A dual element as tabulated can unite with one single element as reduced for adjacent-2-face attachability and to one single element reduced to adjacent-3-face attachability, to form a 4-element cluster as tabulated; that is $1(Si_{20}O_{40})+1(Si_9O_{18})+1(Si_8O_{16})=1(Si_{37}O_{74})^{20+,\,20-}$. A reduced dual element that is unitable to two adjacent faces is $(Si_{19}O_{38})^{19+,\,19-}_{2F}$.

A triple element cluster as tabulated presents 3 convex 4-faces, or 2 reentrant 3-faces plus 3 convex 2-faces, and can unite clusters presenting correspondingly opposite combinations of penta faces.

The tabulated 4-element vitron can, among other possibilities, be intermediate (that is form or grow) between 4 clusters each presenting a reentrant 3-face.

The 5-element vitron can unite or have attached to it 2 small clusters each with reentrant 3-face plus 3 small clusters each with reentrant 2-face.

The 7-element cluster might unite or have attached to it 5 small clusters each with reentrant 2-face.

The 13-cluster vitron is very nearly spherical. It is directly and fully unitable through its 12 free faces; or it can accept unions simultaneously at 8 of the 20 places where it has reentrant 3-face combinations. A few oxygen connections are also available.

The 14-element vitron presents 12 places of reentrant 4-face and a few opportunities for connectibility through oxygens; or it presents convex 2-face possibilities of union in 6 places, together with added attachability through oxygens.

The 26-element vitron is directly unitable on each of 12 faces and has added attachability through oxygen.

The 45-element vitron is the largest of the spherical or element-center type that has been studied. It is directly unitable through each of 12 penta faces and also attachable through 20 oxygens at places equally distributed over the vitron surface.

The 54-element tetrahedral vitron is unique among those in table 1 in that it presents no penta faces for union with other vitrons. All connections must be through oxygen at 4 triple edges, 12 double edges, and 12 single edges.

13.2. "Unit Cell" of Vitreous Silica

The symmetry within vitrons of limited size has different aspects for the different arrangements. For type 1 clusters with a central element there is a center of symmetry and the whole vitron has, basically, all of the axes that were mentioned in section 2 in describing a dodecahedral element (see fig. 7); also there are quasi-reflecting planes similar to those for single elements. It is useful, in attempting to discuss the concept of a "unit cell" for vitreous silica, to note that it is possible to select 3 mutually perpendicular axes running through oxygen atoms and intersecting at the center of an element. As one travels along any of these orthogonal axes of a type 1 cluster, one proceeds 4.19 A from origin to first oxygen, and 4.91 A further to first silicon, then orients 90° around the axis and proceeds 4.91 A to second oxygen, and then 4.19 A to center of second elemental cage. The second element, however, is at 90° with the element of origin and one must repeat the four above-mentioned steps to arrive at an element center apparently identical with the origin (but in reality at 180° therewith). In other words the unit cell in the sense used in crystallography might seem to be 36.4 A on each edge, if the structure could grow to such an extent. Such a cell would contain 960 SiO_2. Apparently, one-eighth of this cell with edge of 18.2 A and containing 120 SiO_2 might be representative of the structure if suitable orientations and inversions are made.

The estimate of a unit cell just given does not seem satisfactory, however, because along axes parallel to, but somewhat displaced from, the principal axes the repeat distances are not always 36.4 A. Other repeat distances of 14.26 and 24.34 A are easily found.

If vitrons of type 4 with silicon as a center are considered, it is obvious that there are four axes equally distributed in space and making angles of 109° 28′ with each other as in a tetrahedron. Along any of these axes of a cluster of type 4, one proceeds 1.60 A from origin to first oxygen, 1.60 A to first silicon, 8.97 to second silicon, then orients 60° around the axis and proceeds to repeat these 3 steps in the same order to arrive at a silicon apparently identical with the origin (but in reality at 120° therewith). The apparent repeat distance is 24.34 A.

The vitron of type 3 with a common edge and oxygen at its center, has a principal axis with a repeat distance of 24.34 A, numerically equal to that just found for the tetrahedral axes of type 4 vitrons. Perpendicular to the principal axis there are three axes at 120° with each other. Along each of these the repeat distance is 36.4 A, numerically equal to that found for the orthogonal axes of type 1 vitrons.

More complicated is the vitron of type 2 with center in a face. Here one has a principal axis and 2 groups of 5 axes each in the plane of the central or common face. Along the principal axis, perpendicular to the central face, one proceeds 7.13 A to the center of the opposite face, then orients 36° and proceeds 7.13 A to a face center that appears as did the origin (but in reality at 72° therewith). The apparent repeat distance is 14.26 A. For one group of 5 axes, through the 5 oxygens of the central face, the repeat distance is 36.4 A; and for the other group, through the 5 silicons, the repeat distance is also 36.4 A.

The repeat distance of 36.40 A along a two-fold axis through an element center (type 1) must be multiplied by 2 to reach an element center identical with the origin in true orientation; the repeat distance of 24.34 A along a three-fold axis through a silicon center (type 4) must be multiplied by 3 to reach a silicon identical with the origin in true orientation; and the repeat distance of 14.26 A along a five-fold axis through a face center (type 2) must be multiplied by 5 to reach a face center identical with the origin in true orientation. The average of these 3 estimates gives the true repeat distance for

the proposed structure of vitreous silica along any of its multiple axes as 72.4 A and the corresponding cell would contain 7680 SiO_2. This can be interpreted as the size of the unit cell of vitreous silica that would be found *if* the structure were capable of growing to such an extent.

14. References

[1] J. T. Randall, H. P. Rooksby, and B. S. Cooper, Z. Krist. **75,** 196 (1930); Nature **125,** 458 (1930).
[2] C. W. Parmelee, G. L. Clark, and A. E. Badger, J. Soc. Glass Technol. **13,** 285, 290 (1929).
[3] W. H. Zachariasen, J. Am. Chem. Soc. **54,** 3841 (1932).
[4] B. E. Warren, Z. Krist. **86,** 349 (1933); **89,** 481 (1934); J. Am. Ceram. Soc. **17,** 249 (1934); Phys. Rev. **45,** 657 (1934).
[5] W. A. Weyl, J. Soc. Glass Technol. **35,** 421 (1951).
[6] C. L. Babcock, S. W. Barber, and K. Fajans, Ind. Eng. Chem. **46,** 161 (1954).
[7] Sam Spinner, J. Am. Ceram. Soc. **39,** 113 (1956).
[8 Edward Melkonian, Phys. Rev. **76,** 1749 (1949).
[9] W. O. Milligan, H. A. Levy, and S. W. Peterson, Phys. Rev. **83,** 226 (1951).
[10] L. C. Hoffman and W. O. Statton, Nature **176,** 561 (1955).
[11] W. L. Bragg, The structure of silicates (Leipzig, 1930).
[12] F. J. Norton, J. Am. Ceram. Soc. **36,** 96 (1953).
[13] E. Poncelet, Verres et Réfractaires **2,** 208 (1948).
[14] B. E. Warren, J. Appl. Phys. **8,** 645 (1937).
[15] N. Valenkov and E. Poray-Koshitz, Nature **137,** 273 (1936).
[16] B. E. Warren, H. Krutter, and O. Morningstar, J. Am. Ceram. Soc. **19,** 202 (1936).
[17] G. Hartlief. Z. anorg. u. allgem. Chem. **238,** 368 (1938).
[18] R. M. Delaney, P. J. Persiani, and A. H. Weber, Technical Report No. 1—Research Program on the Neutron Diffraction Study of the Structure of Glasses. November 1, 1954. Dept. of Army Project 5B99–01–004.
[19] Weber, et al, Table IV, p. 33 of Report cited in literature reference No. 18.
[20] A. A. Griffith, Trans. Roy. Soc. (London) [A] **221,** 163 (1920).
[21] J. E. Stanworth, Physical properties of glass, p. 82 (Oxford, Eng. 1950).
[22] S. M. Cox, J. Soc. Glass Technol. **32,** 128 (1948).
[23] J. B. Murgatroyd, J. Soc. Glass Technol. **32,** 291 (1948).
[24] F. Horton, Trans. Roy. Soc. (London) [A] **204,** 407 (1905); O. L. Anderson and H. E. Bömmel, J. Am. Ceram. Soc. **38,** 126 (1955).
[25] P. W. Bridgman, Am. J. Sci. **237,** 7 (1939).
[26] F. Birch and R. B. Dow, Bull. Geol. Soc. Amer. **47,** 1235 (1936).
[27] R. W. Douglas and J. O. Isard, Nature **175,** 747 (1955).
[28] H. Salmang and K. von Stoesser, Glastech. Ber. **8,** 479 (1930).
[29] Ivan Peychès, Verres et Réfractaires **8,** 181 (1954).
[30] G. S. Parks and H. M. Huffman, Science **64,** 364 (1926).
[31] E. Berger, Zeits. techn. Physik **12,** 344 (1931).
[32] F. Machatschki, Radex-Rundschau.p. 76 (Radenthein, Austria, 1952).
[33] P. Debye and H. Menke, Physik. Z. **31,** 797 (1930).
[34] F. Matossi, Z. tech. Phys. **18,** (12), 585 (1937).
[35] M. L. Huggins, J. Opt. Soc. Amer. **30,** 421 (1940); J. Phys. Chem. **58,** 1145 (1954).
[36] H. J. McSkimin, J. Appl. Phys. **24,** 988 (1953).
[37] M. E. Fine, H. Van Duyne, and Nancy T. Kenney, J. Appl. Phys. **25,** 402 (1954).
[38] J. W. Marx and J. M. Sivertsen, J. Appl. Phys. **24,** 81 (1953).
[39] Errol B. Shand, J. Am. Ceram. Soc. **37,** 572 (1954).
[40] Wm. H. Otto, J. Am. Ceram. Soc. **38,** 123 (1955).
[41] F. W. Glaze, J. C. Young, and A. N. Finn, BS J. Research **9,** 799 (1932) RP507.
[42] W. Souder and P. H. Hidnert, Sci. Papers NBS **21,** 21 (1926) S524.
[43] J. B. Saunders and A. Q. Tool, BS J. Research **11,** 807 (1933) RP626.
[44] A. Q. Tool, L. W. Tilton, and J. B. Saunders, J. Research NBS **38,** 519 (1947) RP1793.
[45] L. W. Tilton, J. Soc. Glass Technol. **40,** T338 (1956).
[46] E. D. Lynch and F. V. Tooley, J. Am. Ceram. Soc. **40,** 107 (1957).
[47] M. Goldstein and T. H. Davies, J. Am. Ceram. Soc. **38,** 223 (1955).
[48] W. H. Otto and F. W. Preston, J. Soc. Glass Technol. **34,** T63 (1950).
[49] R. T. Brannan, J. Am. Ceram. Soc. **36,** 230 (1953).
[50] Charles Kittel, Phys. Rev. **75,** 972 (1949).

WASHINGTON, MARCH 20, 1957.

U. S. GOVERNMENT PRINTING OFFICE: 1957

THE NATIONAL BUREAU OF STANDARDS

The scope of activities of the National Bureau of Standards at its headquarters in Washington, D. C., and its major field laboratories in Boulder, Colorado, is suggested in the following listing of the divisions and sections engaged in technical work. In general, each section carries out specialized research, development, and engineering in the field indicated by its title. A brief description of the activities, and of the resultant publications, appears on the inside of the front cover.

WASHINGTON, D. C.

Electricity and Electronics. Resistance and Reactance. Electron Devices. Electrical Instruments. Magnetic Measurements. Dielectrics. Engineering Electronics. Electronic Instrumentation. Electrochemistry.

Optics and Metrology. Photometry and Colorimetry. Optical Instruments. Photographic Technology. Length. Engineering Metrology.

Heat and Power. Temperature Physics. Thermodynamics. Cryogenic Physics. Rheology. Engine Fuels. Free Radicals Research.

Atomic and Radiation Physics. Spectroscopy. Radiometry. Mass Spectrometry. Solid State Physics. Electron Physics. Atomic Physics. Neutron Physics. Nuclear Physics. Radioactivity. X-rays. Betatron. Nucleonic Instrumentation. Radiological Equipment. AEC Radiation Instruments.

Chemistry. Organic Coatings. Surface Chemistry. Organic Chemistry. Analytical Chemistry. Inorganic Chemistry. Electrodeposition. Gas Chemistry. Physical Chemistry. Thermochemistry. Spectrochemistry. Pure Substances.

Mechanics. Sound. Mechanical Instruments. Fluid Mechanics. Engineering Mechanics. Mass and Scale. Capacity, Density, and Fluid Meters. Combustion Controls.

Organic and Fibrous Materials. Rubber. Textiles. Paper. Leather. Testing and Specifications. Polymer Structure. Plastics. Dental Research.

Metallurgy. Thermal Metallurgy. Chemical Metallurgy. Mechanical Metallurgy. Corrosion. Metal Physics.

Mineral Products. Engineering Ceramics. Glass. Refractories. Enameled Metals. Concreting Materials. Constitution and Microstructure.

Building Technology. Structural Engineering. Fire Protection. Air Conditioning, Heating, and Refrigeration. Floor, Roof, and Wall Coverings. Codes and Specifications. Heat Transfer.

Applied Mathematics. Numerical Analysis. Computation. Statistical Engineering. Mathematical Physics.

Data Processing Systems. SEAC Engineering Group. Components and Techniques. Digital Circuitry. Digital Systems. Analog Systems. Application Engineering.

Office of Basic Instrumentation. **Office of Weights and Measures.**

BOULDER, COLORADO

Cryogenic Engineering. Cryogenic Equipment. Cryogenic Processes. Properties of Materials. Gas Liquefaction.

Radio Propagation Physics. Upper Atmosphere Research. Ionospheric Research. Regular Propagation Services. Sun-Earth Relationships.

Radio Propagation Engineering. Data Reduction Instrumentation. Modulation Systems. Navigation Systems. Radio Noise. Tropospheric Measurements. Tropospheric Analysis. Radio Systems Application Engineering.

Radio Standards. High Frequency Electrical Standards. Radio Broadcast Service. High Frequency Impedance Standards. Calibration Center. Microwave Physics. Microwave Circuit Standards.

Recent Publications of the National Bureau of Standards

Journal of Research of the National Bureau of Standards, Volume 58, No. 6, June 1957 (RP2762 to RP2767 incl.). 60 cents. Annual subscription $4.00.

Technical News Bulletin, Volume 41, No. 6, June 1957. 10 cents. Annual subscription $1.00.

Basic Radio Propagation Predictions for September 1957. Three months in advance. CRPL–D 154. Issued June 1957. 10 cents. Annual subscription $1.00.

Circulars

C581. Metrology of gage blocks. $1.50.

C582. Worldwide occurrence of sporadic *E*. $3.25.

C583. X-ray attenuation coefficients from 10 kev to 100 Mev. 35 cents.

Available from the Superintendent of Documents, U. S. Government Printing Office, Washington 25, D. C. (foreign postage, one-fourth additional).

UNIVERSITY OF MICHIGAN
GENERAL LIBRARY
DOCUMENTS DIVISION
1276 ANN ARBOR MICH

U
GOVERNMENT PRINTING OFFICE
DIVISION OF PUBLIC DOCUMENTS
WASHINGTON 25, D. C.

OFFICIAL BUSINESS

PENALTY FOR PRIVATE USE TO AVOID PAYMENT OF POSTAGE, $300 (GPO)

Journal of Research of the National Bureau of Standards Vol. 59, No. 2 August 1957

Contents

		Page
A problem in self-heating of a spherical body. S. M. Genensky.	RP2773	79
Properties of arsenic sulfide glass. Francis W. Glaze, Douglas H. Blackburn, Jerome S. Osmalov, Donald Hubbard, and Mason H. Black.	RP2774	83
Thermal conductivity of beryllium oxide from 40° to 750° C. David A. Ditmars and Defoe C. Ginnings.	RP2775	93
A self-balancing direct-current bridge for accurate bolometric power measurements. Glenn F. Engen.	RP2776	101
Some observations on hydrated monocalcium aluminate and monostrontium aluminate. Elmer T. Carlson.	RP2777	107
Turbidity and viscosity measurements on some cationic detergents in water and in sodium chloride solutions. Lawrence M. Kushner, Willard D. Hubbard, and Rebecca A. Parker.	RP2778	113
Relative stress-optical coefficients of some National Bureau of Standards optical glasses. Roy M. Waxler and Albert Napolitano.	RP2779	121
Physicochemical studies of the destructive alkali-aggregate reaction in concrete. Robert G. Pike and Donald Hubbard.	RP2780	127
Insulated loop antenna immersed in a conducting medium. James R. Wait.	RP2781	133
Noncrystal ionic model for silica glass. Leroy W. Tilton.	RP2782	139

[A list of recent NBS publications is given on page 3 of the cover.]

For sale by the Superintendent of Documents, U. S. Government Printing Office, Washington 25, D. C. Price 60 cents (single copy). Subscription price: $4.00 a year; $1.25 additional for foreign mailing.

UNITED STATES GOVERNMENT PRINTING OFFICE, WASHINGTON 1957